DISSERTATION

Crosstalk between cholangiocytes and liver macrophages upon liver injury

Wechselwirkungen zwischen Cholangiozyten und Lebermakrophagen bei Leberschädigung

zur Erlangung des akademischen Grades

Doctor medicinae (Dr. med.)

vorgelegt der Medizinischen Fakultät

Charité – Universitätsmedizin Berlin

von

Hanyang Liu

Erstbetreuung: Prof. Dr. med. Frank Tacke

Datum der Promotion: 29. 11. 2024

Table of Contents

List of Figures 5
List of Tables 8
List of Abbreviations 9
Abstract (English) 11
Abstract (German) 13
1. Introduction 15
1.1. Chronic liver diseases in a multicellular perspective 15
1.2. Cholangiocyte pathobiology 17
1.3. Roles of cholangiokines in hepatic microenvironment 19
1.4. Hepatic macrophages in liver homeostasis and injury 20
1.5. Interactions between cholangiocytes and liver macrophages 22
1.6. *In vitro* approaches to dissect cellular interactions in the biliary niche 24
2. Hypothesis 26
3. Materials and methods 27
3.1. Materials 27
3.1.1. Animals and primary cells 27
3.1.2. Human samples 27
3.1.3. Cell line and organoid-derived (Od) cells 27
3.1.4. Equipment/supplies 28
3.1.5. Chemicals and proteins 28
3.1.6. Solutions 29
3.1.7. Kits 33
3.1.8. Cell dyes 33
3.1.9. Antibodies/magnetic beads/LEGENDplex beads 33
3.1.10. Primers 36
3.2. Methods 38
3.2.1. Primary cell isolation 38
3.2.1.1. Mouse liver perfusion and digestion 38
3.2.1.2. Mouse primary hepatocyte isolation 39
3.2.1.3. Mouse primary hepatic stellate cell isolation 39
3.2.1.4. Magnetic cell sorting 40
3.2.1.5. Peripheral blood mononuclear cell (or CIC) isolation 41
3.2.1.6. Mouse MoMF isolation 42
3.2.2. Mouse cholangiocyte organoid culture 42
3.2.3. Cell treatment 42
3.2.3.1. THP-1 cell activation 42
3.2.3.2. Cell injury induction 42
3.2.3.3. Macrophage stimulation 43
3.2.4. Gene interference assay 43
3.2.5. Quantitative real-time PCR assay 43
3.2.6. Immunohistochemistry (IHC) 44
3.2.6.1. IHC – horseradish peroxidase (HRP) approach 44

3.2.6.2. IHC – immunofluorescent staining 45
3.2.6.3. IHC – multiplex immunofluorescent staining 46
3.2.7. Immunocytochemistry (ICC) 46
3.2.8. Live cell staining 46
3.2.9. Transcriptome analysis 47
3.2.10. Bioinformatic analysis 47
3.2.11. Image analysis 47
3.2.12. Co-culture experiments 48
3.2.12.1. Co-culture using conditioned medium 48
3.2.12.2. Co-culture using compartmented chambers 48
3.2.12.3. BoC experiments 48
3.2.13. Flow cytometry 49
3.2.15. Statistical analysis 50
4. Results 51
4.1. ORM2 upregulation as a hallmark of intrahepatic cholangiocyte injury 51
4.2. ORM2 is differentially expressed in hepatocytes and cholangiocytes upon injury 52
4.3. ORM2 mobilizes monocytic accumulation in the biliary niche in liver 54
4.3.1. Administration of ORM2 enhances the gene expression of monocyte signatures in mouse liver 54
4.3.2. Upregulation of ORM2 is associated with monocytic accumulation towards ductular reaction 55
4.3.3. *Orm2* gene interference on cholangiocytes 57
4.3.4. Biliary niche-on-a-chip (BoC) system recapitulates monocyte attraction by cholangiocyte-derived ORM2 57
4.3.5. Biliary niche-on-a-chip (BoC) system recapitulates influences of cholangiocyte-derived ORM2 59
4.3.6. Micro-coculture chamber system recapitulates influences of cholangiocyte-derived ORM2 60
4.4. ORM2 induces liver macrophage reprogramming 63
4.4.1. ORM2 induces transcriptome alterations of liver macrophages 63
4.4.2. ORM2 increases liver macrophage phagocytic functions 65
4.4.3. ORM2 enhances lipid intake in liver macrophages 65
4.4.4. ORM2 induces cellular stress processes in liver macrophages 66
4.5. ORM2-activated macrophages influence their microenvironment in the biliary niche 67
4.5.1. ORM2 enhances inflammatory cytokine secretion by liver macrophages 67
4.5.2. ORM2-activated macrophages influence BECs 68
4.5.3. ORM2-activated macrophages promote fibrogenesis driven by HSCs 70
4.5.4. ORM2-activated macrophages exacerbate cell stress and ORM2 production in Hepatocytes. 71
4.5.5. ORM2-activated macrophages induce transcriptome alterations of BECs, HSCs and hepatocytes. 72
4.6. ORM2 reprograms liver macrophages through ITPR2-dependent calcium pathway 73
4.6.1. ORM2 enhances calcium pathway in liver macrophages 73
4.6.2. ORM2 activates calcium pathway through ITPR2 74

4.6.3. ORM2 regulates macrophage phagocytosis through ITPR2 76
4.6.4. ORM2 enhances macrophage lipid metabolism through ITPR2 77
4.6.5. ORM2 induces macrophage cellular stress through ITPR2 78
5. Discussion 80
6. References 88
7. Statutory Declaration 97
8. Curriculum Vitae 98
9. List of publications 99
10. Acknowledgements 102
11. Statistician's certificate 103

List of Figures

Figure 1. Ductular reaction and cholangiokines in the hepatic microenvironment…….19

Figure 2. Macrophages mediate inflammation in the hepatic microenvironment…….21

Figure 3. Driving hypothesis: cholangiocyte-derived ORM2 influences biliary niche via liver macrophage activation……...25

Figure 4. Biliary niche-on-a-chip modeling strategy……48

Figure 5. ORM2 is upregulated in intrahepatic ductular cells upon liver injury…….51

Figure 6. ORM2 production is increased in cholangiocytes but decreased in hepatocytes upon acute *in vitro* injury……..52

Figure 7. Administration of ORM2 enhances monocyte-associated gene signatures in mouse livers……54

Figure 8. Upregulation of ORM2 is associated with monocytic accumulation towards ductular cells…….55

Figure 9. siRNA transfection suppresses *Orm2* gene expression in cholangiocytes……..56

Figure 10. Cholangiocyte-derived ORM2 exacerbates monocyte accumulation in the BoC……..57

Figure 11. Cholangiocyte-derived ORM2 exacerbates fibrogenesis but attenuates cell proliferation in the BoC……59

Figure 12. Cholangiocyte-derived ORM2 suppresses the growth of cholangiocytes but promotes fibrogenesis of HSCs in presence of liver macrophages……61

Figure 13. ORM2 induces potent transcriptome alterations in liver macrophages……63

Figure 14. ORM2 favors macrophage phagocytosis……64

Figure 15. ORM2 influences macrophage lipid metabolism……65

Figure 16. ORM2 induces macrophage cell stress processes……...66

Figure 17. ORM2 induces significant secretome alterations of macrophages……67

Figure 18. ORM2-activated macrophages exacerbate BEC stress and ORM2 production……68

Figure 19. ORM2-activated macrophages promote fibrogenesis mediated by HSCs……70

Figure 20. ORM2-activated macrophages exacerbate cell stress and ORM2 production in Hepatocytes……71

Figure 21. ORM2-activated macrophages alter gene expression of key markers on BECs, HSCs and Hepatocytes……...72

Figure 22. ORM2 enhances calcium pathway in liver macrophages…...73

Figure 23. ITPR2 mediates the calcium-dependent functional effects of ORM2 on liver macrophages……74

Figure 24. ORM2 regulates macrophage phagocytosis through ITPR2...75

Figure 25. ORM2 enhances macrophage lipid metabolism through ITPR2……...76

Figure 26. ORM2 induces macrophage cell stress through ITPR2……...78

Figure 27. Graphical abstract……...……84

List of Tables

Table 1. List of equipment and supplies……27

Table 2. List of chemicals and proteins…….....27

Table 3. List of solutions……..…….....28

Table 4. Composition of the EGTA buffer……29

Table 5. Composition of the liver digestion buffer……30

Table 6. Composition of the GBSS/A buffer…….30

Table 7. List of kits……...32

Table 8. List of cell dyes used in this study……...32

Table 9. Antibodies/magnetic beads/LEGENDplex beads……...33

Table 10. Primer sequences used for gene expression analyses……35

List of Abbreviations

Act	Actin
Adam11	ADAM metallopeptidase domain 11
ALD	alcohol-associated liver disease
AML	acute myeloid leukemia
APAP	acetaminophen/paracetamol
APP	acute phase protein
BA	biliary atresia
BEC	biliary epithelial cell
BoC	biliary niche-on-a-chip
BT	biliatresone
CALM	calmodulin
CCK-8	cell counting kit-8
CCL	CC-chemokine-ligand
CCL_4	carbon tetrachloride
CCR	CC-chemokine-receptor
CD	cluster of differentiation
CDCA	chenodeoxycholic acid
CFP	cyan fluorescent protein
CIC	circulating immune cell
CK	cytokeratin
CSF	colony stimulating factor
CXCL	chemokine (C-X-C motif) ligand
CXCR	chemokine (C-X-C motif) receptor
DAMP	danger-associated molecular pattern
DEG	differentially expressed gene
DR	ductular reaction
EGTA	ethylene glycol-bis(β-aminoethyl ether)-N,N,N′,N′-tetraacetic acid
FBS	fetal bovine serum
FFAs	free fatty acids
FFPE	formalin-fixed paraffin-embedded
GEO	Gene Expression Omnibus
GBSS	Gey´s balanced salt solution
HBSS	Hanks' balanced salt solution
Hepatocyte	hepatocyte
HepPar1	hepatocyte paraffin 1
HRP	horseradish peroxidase
HSC	hepatic stellate cell
IBA1	ionized calcium binding adaptor molecule 1, also named AIF1
ICAM-1	intercellular adhesion molecule-1
ICC	immunocytochemistry
IHC	immunohistochemistry

IGF	Insulin-like growth factor
IL	Interleukin
IFN	Interferon
ITPR2	Inositol 1,4,5-Trisphosphate receptor type 2
KC	Kupffer cell
LoC	liver-on-a-chip
LPS	Lipopolysaccharide
LSEC	liver sinusoidal endothelial cell
MACS	magnetic-activated cell sorting
MASLD	metabolism dysfunction-associated steatotic liver disease
MASH	metabolic dysfunction-associated steatohepatitis
MoMF	monocyte-derived macrophage
MMP	Matrix metalloproteinase
MP	Macrophage
NGS	normal goat serum
Od	organoid-derived
ORM2	Orosomucoid 2
PAMP	pathogen-associated molecular pattern
PBC	primary biliary cholangitis
PBMC	peripheral blood mononuclear cell
PBS	phosphate-buffered saline
PFA	Paraformaldehyde
PMA	phorbol 12-myristate 13-acetate
PSC	primary sclerosing cholangitis
scRNA	single-cell RNA
siRNA	small-interfering RNA
TGF	transforming growth factor
TIM4	T-cell membrane protein 4
TNF	tumor necrosis factor
TRPV1	transient receptor potential vanilloid 1
YG beads	yellow green beads
ZO-1/TJP1	tight junction protein 1

Abstract (English)

Background

Liver diseases lead to more than two million deaths yearly worldwide, accounting for 4% of global deaths. Upon liver injury, cholangiocytes may promote ductular reaction (DR) by acquiring migratory properties and a de-differentiated phenotype. Notably, DR has been considered as an essential hallmark in a variety of liver diseases. Furthermore, reactive cholangiocyte-released mediators (termed cholangiokines) have been characterized to play major roles in portal fibrogenesis and to regulate cellular crosstalk in the portal area niche. The present work aimed at elucidating cellular crosstalk between cholangiocytes and macrophages upon liver injury as well as their potential relevance in liver disease progression.

Methods

To explore the key cell communication mediators released by cholangiocytes during liver injury, bioinformatics analysis was conducted on publicly available and our own transcriptome datasets. Immunohistochemistry and immunocytochemistry were performed to evaluate the distribution and protein levels of the candidates. Multiple mouse strains' (wild-type, *Mdr2*$^{-/-}$, Act CFP and Act DsRed) liver and blood as well as healthy human blood samples were collected for primary cell isolation and co-culture experiments. Recombinant mouse and human Orosomucoid 2 (ORM2), biliatresone and bile acids were used for *in vitro* stimulation. Cell phenotypic marker expression and cytokine release were measured by flow cytometry. Bulk RNA sequencing was performed on mouse liver macrophages to reveal transcriptome alterations. Small-interfering RNA transfection was used to knock down *Orm2* or *Itpr2* expression in cholangiocytes.

Results

ORM2 was screened out to be one of the most strongly induced secretory factors expressed by mouse-derived intrahepatic cholangiocytes under acute bile duct injury. Accordingly, cholangiocytes exhibited a strong upregulation of *Orm2* upon *in vitro*

stimulation. Furthermore, ORM2 induced monocyte recruitment and profound transcriptome alterations in liver macrophages, associated with the increase of pro-inflammatory cytokine secretion and expression of cell stress-related genes. Furthermore, ORM2-activated macrophages exacerbated cell stress and *Orm2* expression in both cholangiocytes and hepatocytes and promoted fibrogenesis in hepatic stellate cells. Finally, mechanistic experiments determined that ORM2 regulated liver macrophage functions via an ITPR2-dependent calcium pathway.

Conclusions

This study demonstrates that cholangiocyte-derived ORM2 induces liver macrophage reprogramming via an ITPR2-dependent calcium pathway in response to acute and chronic biliary injury, mediating a remodeling of the immune biliary niche.

Abstract (German)

Hintergrund

Lebererkrankungen verursachen weltweit mehr als zwei Millionen Todesfälle pro Jahr, was 4 % der weltweiten Todesfälle entspricht. Nach einer Leberverletzung können Cholangiozyten die duktuläre Reaktion (DR) fördern, indem sie wandernde Eigenschaften und einen entdifferenzierten Phänotyp annehmen. Die Die DR ist ein wesentliches Merkmal bei einer Vielzahl von Lebererkrankungen. Kürzlich wurde festgestellt, dass reaktive, von Cholangiozyten freigesetzte Mediatoren (so genannte Cholangiokine) eine wichtige Rolle bei der portalen Fibrogenese spielen und den zellulären Crosstalk in der Nische des Portalbereichs regulieren. Daher zielt die vorliegende Arbeit darauf ab, den zellulären Crosstalk zwischen Cholangiozyten und Makrophagen bei Leberschädigung und deren potenzielle Relevanz für die Leber aufzuschlüsseln.

Methoden

Um den Schlüsselfaktor zu untersuchen, wurde eine bioinformatische Analyse öffentlich zugänglicher und firmeneigener Transkriptom-Datensätze durchgeführt. Immunhistochemie und Immunzytochemie wurden durchgeführt, um die Verteilung der Zellen und ihrer Marker zu verstehen. Mehrere Mausstämme (Wildtyp, Mdr2-/-, Act CFP und Act DsRed), Leber- und Blutproben sowie gesundes menschliches Blut wurden für primäre Zellisolierungs- und Co-Kulturexperimente gesammelt. Für die In-vitro-Stimulation wurden rekombinantes Orosomucoid 2 (ORM2) von Maus und Mensch, Biliatreson und Gallensäuren verwendet. Die Expression phänotypischer Marker und die Zytokinfreisetzung wurden mittels Durchflusszytometrie gemessen. An Mäuselebermakrophagen wurde eine Massen-RNA-Sequenzierung durchgeführt, um Transkriptomveränderungen aufzudecken. Die Expression von *Orm2* oder *Itpr2* in Cholangiozyten wurde durch Small-Interfering-RNA-Transfektion ausgeschaltet.

Ergebnisse

ORM2 erwies sich als einer der am stärksten induzierten sekretorischen Faktoren, die von intrahepatischen Cholangiozyten der Maus bei akuter Verletzung der Gallenwege exprimiert werden. Dementsprechend zeigten die Cholangiozyten eine starke Hochregulierung von *Orm2* bei In-vitro-Stimulation. Darüber hinaus induzierte ORM2 die Rekrutierung von Monozyten und starke Transkriptomveränderungen in Lebermakrophagen, die mit erhöhten Sekretion proinflammatorischer Zytokine und Expression zellstressbezogener Gene einhergingen. Darüber hinaus verstärkten ORM2-aktivierte Makrophagen den Zellstress und die Expression von Orm2 sowohl in Cholangiozyten als auch in Hepatozyten und förderten die Fibrogenese in hepatischen Sternzellen. Schließlich wurde in mechanistischen Experimenten festgestellt, dass ORM2 die Funktionen der Lebermakrophagen über einen ITPR2-abhängigen Kalziumweg reguliert.

Schlussfolgerungen

Diese Studie zeigt, dass ORM2 aus Cholangiozyten infolge akuter und chronischer Gallengangsschädigungen eine Umprogrammierung von Lebermakrophagen auslöst, die über einen ITPR2-abhängigen Kalziumweg vermittelt wird, und somit eine Umgestaltung der biliären Immunzell-Nische herbeiführt.

1. Introduction

1.1. Chronic liver diseases in a multicellular perspective

The liver is the largest internal organ, playing a fundamental role in maintaining metabolic homeostasis in the human body. This organ serves as an indispensable metabolic factory responsible for gut-derived nutrient metabolism, essential protein synthesis and blood detoxification from endogenous and exogeneous harmful substances. Therefore, the liver is constantly exposed to toxic compounds, metabolic stress and gut-derived stimuli [e.g., pathogen-associated molecular patterns (PAMPs), microbial-derived antigens]. Thus, it is particularly prone to injury(1-3).

Liver epithelial cell injury plays a pivotal role in the panorama of diverse liver diseases that pose a formidable challenge to the structural and functional integrity of this vital organ(4). The spectrum of disorders ranges from viral hepatitis, alcohol-associated liver diseases (ALD) and non-alcoholic fatty liver diseases [now termed Metabolic dysfunction-associated steatotic liver diseases (MASLD)] to autoimmune hepatitis, each posing a unique threat to hepatic homeostasis(5-9). At the epicenter of these diseases, hepatocytes, the primary functional units of the liver, represent the center of attention of a complex interplay notably involving cell injury processes (e.g., oxidative stress), inflammation and fibrosis(10). The intricate mechanisms of liver injury involve a sophisticated involvement of immune cells, through cell-cell interaction mediators such as cytokines shaping the trajectory of disease progression. As liver injury persists, it may evolve into more advanced stages, culminating in conditions such as cirrhosis, with far-reaching implications for systemic health(11). Liver cirrhosis is a consequence of chronic insults, marked by exacerbated liver injury and exaggerated activation of repair mechanisms such as fibrosis and inflammation. Cirrhotic livers can irreversibly progress to decompensation-associated complications, while 1-4% patients with liver cirrhosis will develop hepatocellular carcinoma, all indicating a poor prognosis(12). The latest evidence shows that liver cirrhosis causes approximately 1 million deaths, making up to 50% of liver disease-associated deaths and 3.5% of total deaths globally.

Treatments that aim at curing the underlying liver diseases can prevent or, in some cases, reverse cirrhosis progression. However, liver transplantation, though it faces serious issues such as donor shortages and allergic responses, is currently the only effective therapy for patients with end-stage cirrhosis(13). A thorough understanding of both the similarities and the discrepancies that characterize liver injury in distinct liver conditions is essential for the development of effective therapeutic strategies. These strategies should aim not only to prevent or ameliorate the relentless progression of liver injury, but also to preserve the central functions of this vital organ.

In the wide range of liver physiological and disease-driving mechanisms, cellular interactions play a pivotal role. The liver is constantly exposed to various insults that can trigger a cascade of cellular responses. Hepatocytes, the predominant cell population (around 80%) of the liver, are at the forefront of these interactions(14). Upon injury, these resilient cells engage intricate signaling pathways to adapt their metabolism or initiate repair processes, while chronic damage-associated signaling cascade activation leads to progressive reactions (e.g., inflammation and fibrosis). In addition, non-parenchymal cells such as hepatic macrophages, hepatic stellate cells (HSCs) and liver sinusoidal endothelial cells (LSECs) actively orchestrate immune responses and tissue repair. Moreover, circulating immune cells (CICs), holding a key role as the immune system's frontline responders, are rapidly mobilized and accumulate in injured liver areas, thereby modulating the inflammatory microenvironment(15, 16). In general, lymphocytes (e.g., T and B cells) are markedly recruited upon liver injuries, especially in viral hepatitis and biliary diseases(17), whereas myeloid cells (e.g., monocytes, macrophages, and dendritic cells) are broadly involved in diverse liver diseases, mediating inflammation, fibrosis, and metabolism(18). The interplay among these different cell types, governed by a complex network of molecules and cytokines, determines whether the organ can regenerate successfully or be subject to chronic dysfunction. For instance, it was reported that in a choline-deficient and ethionine-supplemented (CDE) mouse model, infiltrated monocytes could promote progenitor cell expansion and liver regeneration via secreting tumor necrosis factor (TNF)-α(19).

Another report determines that monocyte-derived macrophages (MoMFs) can promote ductular reaction (DR) dependent on TWEAK without injury involvement(20). Additionally, our laboratory previously proved that CXC chemokine receptor (CXCR) 6-expressing innate lymphocytes orchestrated liver injury through interleukin (IL)-17 secreting monocytes(21). Understanding these intricate cellular interactions is crucial for developing successful therapeutic strategies to mitigate the effects of liver injury and promote effective regeneration.

1.2. Cholangiocyte pathobiology

Although cholangiocytes are relatively limited in number in the liver (making up 3 – 5% of total cells), they play fundamental roles in bile modification and transport. Cholangiocytes, also termed biliary epithelial cells (BECs), are polarized epithelial cells lining the intrahepatic and extrahepatic bile ducts. Cholangiocytes are responsible for key metabolic functions, including the control of the bile flow through their cilium system as well as bile composition through bicarbonate secretion, thus maintaining ductal homeostasis, and mediating biological crosstalk between the intra- and extra-ductal environments. In particular, the umbrella composed of cholangiocyte-secreted bicarbonate is believed to exert fundamental functions to protect cells from cytotoxic molecules(22). To date, cholangiocyte biology is currently not characterized in most studies. However, emerging evidence has shown that cholangiocytes actively participate in liver regeneration and in the hepatic microenvironment regulation both at healthy status and upon liver injuries(22, 23). In particular, obstructed or impaired bile efflux from the liver that frequently occurs in cholangiopathies such as primary biliary cholangitis (PBC), primary sclerosing cholangitis (PSC), and biliary atresia (BA) consequentially results in the accumulation of toxic bile, thereby provoking biliary injury and disturbing the biliary microenvironment, in addition to having a broader impact on hepatocytes(24).

Cholangiocytes have been categorized in two subpopulations that are classically referred to as small or large cholangiocytes. Large cholangiocytes typically line the

large branches of the biliary tree and form more complex structures than small cholangiocytes(25). Simultaneously, large cholangiocytes engage in bile secretion, while small cholangiocytes are prone to proliferate and exhibit functional plasticity in diseases(26-28). In addition, cholangiocytes are directly involved in the repair and regeneration of the biliary epithelium in response to injury or disease. Therefore, a thorough understanding of the sophisticated molecular mechanisms that regulate cholangiocyte biology is crucial to developing targeted therapies for hepatobiliary diseases.

During homeostasis, cholangiocytes undergo a small amount of apoptosis and senescence, processes which are replenished by newborn cells. When stimulated by exogenous (e.g., toxic bile, PAMPs) or endogenous [e.g., damage-associated molecular patterns (DAMPs), cytokines] stimuli, cholangiocytes are susceptibly disturbed, leading to cell death, and the remaining BECs may then engage in proliferation or senescence and adopt a secretory phenotype, forming the injury-repair switch(29, 30). Consequently, persistently damaged cholangiocytes mobilize immune cell accumulation and inflammatory reaction, resulting in variable pathological consequences, including excessive inflammation and fibrogenesis in portal areas, as evidenced from studies on patients and animal models under diverse liver disease conditions(25). Moreover, despite numerous ongoing debates, damage-activated cholangiocytes or reactive ductular cells are believed to contribute to liver regeneration through intense proliferation, migration and differentiation re-programming, while self-renewed cholangiocytes mostly exhibit immature characteristics, forfeiting the biliary functions (e.g., bile modification, bile flow maintenance)(31-34). Such complex pathological processes driven by reactive cholangiocytes are termed ductular reaction (DR)(35). DR has been identified in almost all metabolic liver diseases, including MASLD/metabolic dysfunction-associated steatohepatitis (MASH), ALD and viral hepatitis, together with cholestatic liver diseases, including PBC, PSC, and BA(36, 37). Excessive DR, with its active cytokine secretion, may act as an initiator of inflammatory cascades, fibrogenesis and irregular cell growth, promoting inflammation, cirrhosis and

carcinogenesis(34).

1.3. Roles of cholangiokines in hepatic microenvironment

The finely tuned interplay between proliferation, differentiation and trans-differentiation of hepatocytes, progenitor cells and cholangiocytes accompanies and defines DR. Nonetheless, more than regenerative potentials, activated cholangiocytes notably exert marked secretory phenotypes, harboring diverse cytokine secretion. Hence, cholangiocyte-derived cytokines, named cholangiokines, can significantly influence the surrounding microenvironment by modulating immune cell recruitment and mesenchymal cell migration(29). According to our current understanding, the cholangiokine production is associated with cholangiocyte statuses, resulting from inflammation, infection, and metabolic dysregulations during various liver diseases(38, 39). As mediators between intra- and extrahepatic ductal environments, cholangiocytes can recognize and react to a variety of PAMPs, DAMPs and microorganism metabolism-byproducts from liver and gut mostly via Toll-like receptors, leading to injury-shaped activated phenotypes(40, 41).

Fundamentally, cholangiokines can initiate immune cell accumulation in the biliary niche to promote an inflammatory environment. Accumulating evidence from patients and animal models under cholangiopathy conditions has demonstrated that a broad spectrum of pro-inflammatory cytokines [e.g., IL-1β, IL-8, IL-6, the chemokine (C-C motif) ligand (CCL)-2, TNF-α, INF-γ, TGF-β, CXCL-1, -8 and -16] released by reactive cholangiocytes attract and activate circulating immune cells, thereby inducing inflammation in portal areas(29). Taken together, cholangiokines play a crucial role in hepatic immunomodulation. However, a precise understanding of this cholangiocyte-driven inflammation and its implications for the whole organ is needed to evaluate the relevance of portal area-based inflammatory mechanisms. The roles of cholangiokines in the portal area microenvironment were reviewed in our previously published paper (**Figure. 1**)(29).

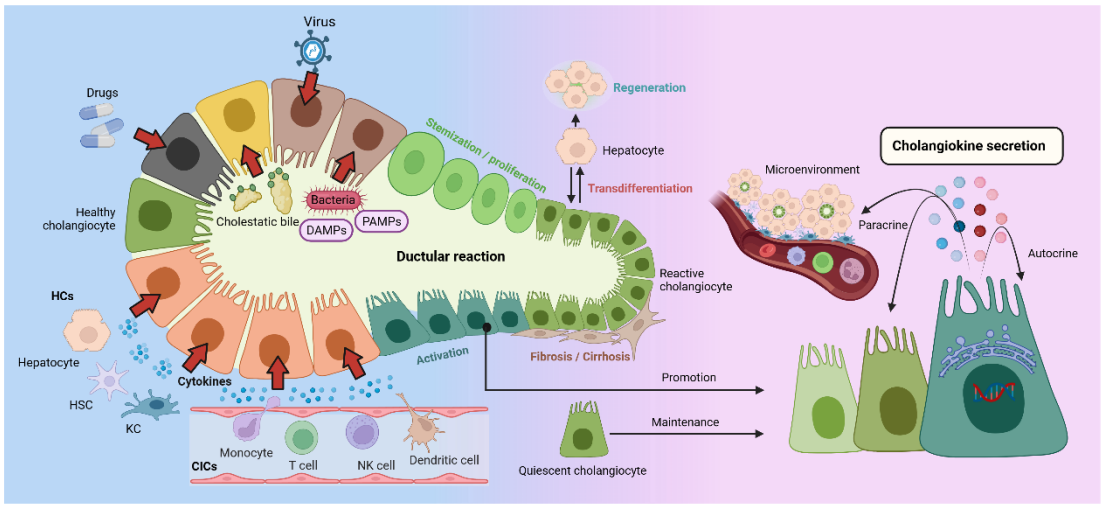

Figure 1. Ductular reaction and cholangiokines in hepatic microenvironment. Adapted from the author's published review(29).

1.4. Hepatic macrophages in liver homeostasis and injury

The liver harbors the highest proportion of macrophages among all solid organs. In a healthy mouse liver, it is estimated that 20-40 macrophages are present for every 100 hepatocytes(42). These liver macrophages play important roles in maintaining homeostasis for both the liver and the entire body. Their functions include scavenging microbial products in the blood coming from the intestines, sensing disruptions in liver tissue integrity, and acting as key sentinels initiating or suppressing immune responses as necessary(43, 44). Recent research has shed light on their origin, polarization, and functions, revealing their diverse roles in both healthy and pathological conditions(45, 46).

Kupffer cells (KCs) were first described by Wilhem von Kupffer in 1876 and later identified as liver-resident macrophages. KCs are the most represented cells in the liver macrophage pool and play a vital role in maintaining homeostasis by clearing PAMPs from the bloodstream, originating from both systemic and gut sources(47). They also contribute to the sensing of tissue injury by recognizing DAMPs. This recognition leads to their activation and the release of various cytokines and chemokines that foster an inflammatory environment in injured liver areas. For instance, DAMPs and PAMPs can

enhance the secretion of IL-1 via regulating Toll-like receptors in hepatic macrophages(41). Of note, differing from KCs, infiltrating macrophages or MoMFs are circulating bone marrow-derived myeloid cells with less self-sustaining and proliferating capacities. These infiltrating macrophages are mostly immunogenic and undergo functional differentiation in response to signals from the local microenvironment. During hepatic inflammation, MOMFs infiltrate the liver, giving rise to a distinct population of hepatic macrophages with unique functionalities compared to resident KCs(48).

Both infiltrating monocyte-derived macrophages and resident macrophages exhibit a plastic phenotype influenced by the local microenvironment. Hepatic macrophages are potential therapeutic targets due to their central roles in liver diseases(15, 49, 50). Approaches to reducing monocyte influx could include targeting chemokines (such as CCL-2), chemokine receptors [such as the chemokine (C-C motif) receptors CCR1, CCR2, and CCR5], or growth factors and their receptors [such as the colony stimulating factor 1 (CSF1) and CSF1R]. Such interventions hold promise for preventing the progression of liver fibrosis or the initiation of hepatocellular carcinoma (HCC)(51). On the other hand, macrophages secrete mediators involved in tissue repair [e.g., insulin-like growth factor (IGF), and matrix metalloproteinase (MMP)] in liver disease conditions, including mouse models with paracetamol (APAP)-induced acute liver injury or carbon tetrachloride (CCl_4)-induced liver fibrosis(52, 53). The contradictory roles of liver macrophages during disease conditions were reviewed in our previously published paper (**Figure. 2**)(54).

The development of potential therapies depends on a comprehensive understanding of the mechanisms governing macrophage polarization and fate. However, the explicit mechanisms that govern hepatic macrophage-centralized cellular interactions remain unclear.

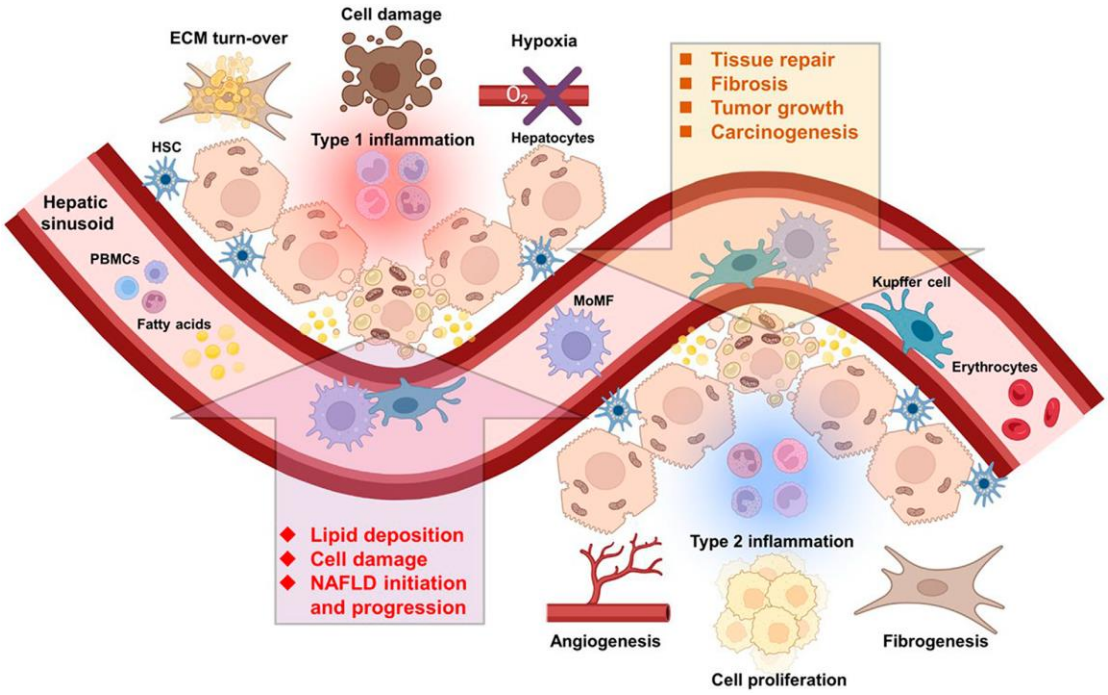

Figure 2. Macrophages mediate inflammation in the hepatic microenvironment. In accordance with diverse phenotypes, liver macrophages can regulate both type 1 and type 2 inflammation processes, thereby either provoking cell damage or promoting tissue repair. Adapted from the author's published review(54).

1.5. Interactions between cholangiocytes and liver macrophages

In this thesis, we hypothesize that the interaction between cholangiocytes and liver macrophages is a critical aspect of hepatic homeostasis and immune regulation. Cholangiocytes line the bile ducts and communicate bidirectionally with liver macrophages, including KCs and MoMFs(55). Under healthy conditions, cholangiocytes participate in immune surveillance by detecting disruptions in the liver [e.g., PAMPs and DAMPs], in turn expressing adhesion molecules (e.g., ICAM-1) and releasing signaling molecules (e.g., CCL-2, Immunoglobulin A, TNF, IL-1β, IL-6, and IL-8) that attract and modulate the activity of CICs (including MOMFs)(56). Conversely, macrophages regulate cholangiocyte function by releasing cytokines and chemokines in response to PAMPs and DAMPs(48, 57). For example, pro-inflammatory macrophages secrete TNF-α that upregulates the expression of αvβ6 integrin and transforming growth factor (TGF)-β1 on epithelial cells(58). Therefore,

αvβ6 integrin is believed to potentially promote DR and carcinogenesis(59, 60). Emerging studies have reported that liver macrophages can modulate inflammation at the early phase of liver injuries, via secreting inflammatory factors such as IL-1β, TNF, CCL2, and CCL5(61). Consequently, MoMFs fundamentally respond to the 'call' from liver macrophages, arriving in the liver in a short time (e.g., peaking at 3 hours after acute intrahepatic BEC injury(59)). Studies have pointed out that circulating monocytes are dispensable for renewing the liver macrophage pool in homeostasis, while the massive infiltration of MoMFs appears to be a critical phenomenon during liver injuries(48, 62). Excessive macrophage activities constitute the main characteristic of liver inflammation, facilitating liver disease progression. On the other hand, macrophage-derived cytokines, likely TGF-β and PDGF, can modify portal areas by activating HSCs, which in turn fuel liver fibrosis(16, 63). Notably, though to a minor extent, some studies have demonstrated the participation of lymphocytes in liver injury. For example, B cell inflammation plays a critical role in promoting hepatic fibrosis in response to injury(51, 64, 65). Our most recently published study indicated that T cells orchestrated liver injury via the CCR7-CCL21 axis in an acute liver failure patient cohort(66). However, little is known about the explicit effects of immune cells in biliary pathology, in particular DR.

Of note, DR-associated inflammation plays a significant role in the progression of liver diseases, acting as both a provoker and an alleviator(35). For instance, it was elucidated that T-helper 17 cells were remarkably accumulated around cholangiocytes according to the observation of a PSC patient's liver samples(67), while a recent study determined that cholangiocytes facilitate pathogenic T-helper 17 cell differentiation and liver disease progression via the regulation of cluster of differentiation (CD)100(68). On the other hand, our laboratory and other research groups established a positive and direct correlation between cholangiocytes and monocyte populations in the liver during MASLD and cholangiopathies(69, 70). Additionally, our previous study revealed the crosstalk between cholangiocytes and monocytes during acute biliary injury. Bile duct repair relies on integrin-αvβ6 expression by regenerating BECs, which is also involved

in the accumulation of $CCR2^+$ MoMFs and the regeneration of cholangiocytes(59). Nonetheless, the mechanisms of bile duct injury repair and cholangiocyte-immune cell interactions are complex and, more importantly, their impact on liver disease progression is still not fully understood.

1.6. *In vitro* approaches to dissect cellular interactions in the biliary niche

To date, studies on liver diseases have markedly relied on various animal models (e.g., rodents and zebrafish), which can effectively recapitulate *in vivo* features(71). Indeed, traditional *in vitro* models are inadequate for replicating hepatic cell functions and interactions. Therefore, understanding liver disease pathophysiology requires models that mimic both functions and multicellular interactions. In recent decades, multiple approaches (e.g., monolayer culture, organoid culture, multicellular coculture) have been developed for tackling these challenges(72-75). The LoC technology offers a reliable alternative for the preliminary investigation of disease-driving mechanisms(76, 77). Through microfluidic perfusion, multiple cell types which constitute the liver can be co-cultured, allowing for a more accurate modeling of early disease-driving events. This technology also enables the simulation of physiologically relevant stresses, including mechanical and shear stresses(78, 79). This innovative approach has practical applications in studying the pathophysiology of various liver conditions, such as drug-induced liver injuries, ALD, MASLD/MASH, and infectious liver diseases, thereby significantly promoting therapeutic development(80, 81). Moreover, LoCs can be interconnected with other organ-on-a-chip systems to enable a comprehensive understanding of the intricate interactions between the liver and multiple organs (e.g., gut and liver)(82, 83). As this technology advances, LoCs have the potential to significantly contribute to the development or pre-screening of therapeutic drugs for liver diseases. This highlights the importance of ongoing research and development in the field of organ-on-a-chip technology for advancing our understanding and treatment of liver-related conditions.

A tailored microfluidic LoC model equipped with immune cell circulation based on

multiple primary cell types (hepatocytes, HSCs, KCs, LSECs and CICs) was established in our laboratory and implemented for recapitulating inflammation and cellular interactions upon liver injury(84). This LoC model provides the capability to study the liver microenvironment for diverse purposes or disease conditions, and additionally inspires its implementation in further liver disease conditions. In particular, to study the mechanisms of DR processes upon liver injury, it is essential to dissect multicellular interactions and inspect key factors. For this purpose, a biliary niche-on-a-chip (BoC) was developed based on the LoC model, including cholangiocyte-macrophage crosstalk together with HSCs, endothelial cells and CICs.

2. Hypothesis

The scientific objective of this dissertation was to understand interactions between cholangiocytes and liver macrophages upon liver injury, and to provide novel evidence for the intricate DR processes, which promisingly open a door to develop targeted therapies against liver disease progression.

In accordance with previous and our own preliminary studies, a group of cytokines was identified that potentially regulate the hepatic microenvironment upon biliary injury(59, 85). Notably, the acute phase protein (APP) family stands out as a promising influencer in DR, not only at the early phase but also throughout disease progression. Additionally, ORM2 (Orosomucoid 2) could serve as a key regulator produced by injured cholangiocytes, based on transcriptome evidence.

Therefore, it was hypothesized that ORM2 holds a crucial role in mediating DR-associated disease-driving mechanisms, via regulating macrophage functions and influencing the microenvironment within the biliary niche. A diagram of the hypothetical mechanisms explored in this dissertation is shown below (**Figure. 3**).

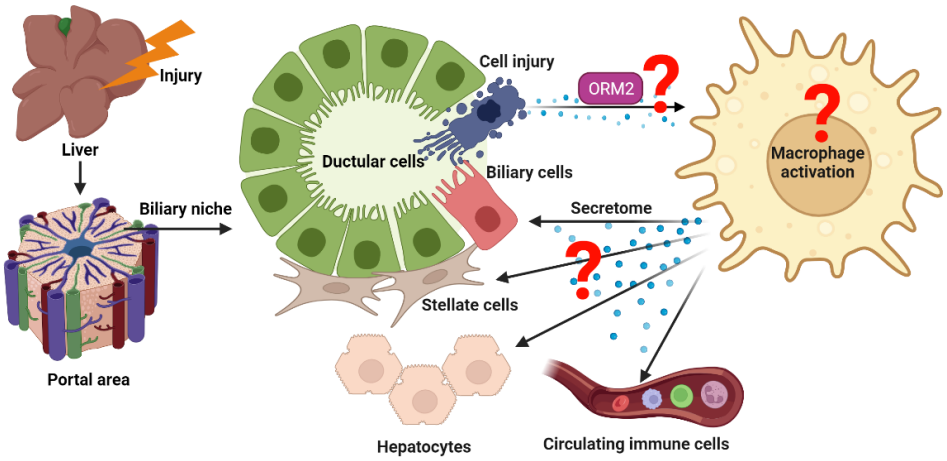

Figure 3. **Driving hypothesis**. It was hypothesized that upon biliary injury, cholangiocyte-derived ORM2 could (can) activate liver macrophages, thereby influencing multiple cell types in the biliary niche.

3. Materials and methods

3.1. Materials

3.1.1. Animals and primary cells

C57BL/6J wild-type mice (18- to 24-week-old), fluorescent reporter transgenic (actin-dsRed and actin-CFP in a B6 genetic background) and MDR2 knock-out mice were obtained from the Research Institutions for Experimental Medicine (FEM) of the Charité – Universitätsmedizin Berlin and sacrificed using prior isoflurane overdose as a primary cell source in this study. All animal procedures were approved by the appropriate State Office for Health and Social Affairs, Berlin (Registration number: T-CH 020/22, G 0243/ 19).

3.1.2. Human samples

The human study was conducted in accordance with the Declaration of Helsinki, and the protocol was approved by the Ethics Committee of the Charité-Universitätsmedizin Berlin (Project EA2/091/19). Formalin-fixed paraffin-embedded (FFPE) human liver tissues were obtained from BioIVT, Capital Biosciences, Discovery Life Sciences, and TriStar under Institutional Review Board and Ethics Committee approvals, and TriStar under Institutional Review Board and Ethics Committee approvals. The human blood samples utilized in this study were provided by healthy volunteers with informed written consent.

3.1.3. Cell line and organoid-derived (Od) cells

THP-1 (ATCC TIB-202) was purchased from the American Type Culture Collection (Virginia, USA). The purity, contamination, mycoplasma screen and genetic features were assessed and validated by the provider. Further phenotypic characterizations along the course of the project validated cell identity. Cholangiocyte organoids were developed based on mouse ($MDR2^{-/-}$)-derived primary cholangiocytes ($EpCAM^{+}$). The

organoid cultivation method was adapted from the literature(86). Then, Od-cholangiocytes were obtained by dissociating organoids.

3.1.4. Equipment/supplies

Equipment and supplies that were used in this study are listed in **Table. 1**.

Table 1. List of equipment and supplies

Description	Manufacturer	Catalog No.
70-µm strainer	Corning	352350
8-well cell culture chamber	Sarstedt	94.6170.802
AccuSpin 1R Centrifuge: Refrigerated	Thermo Fisher	4168
Blood vessel clamp and scissors	Fine Science Tools	18039-45
Bottle-top filter	Corning	431161
Falcon tubes - 15 mL	Corning	352095
Falcon tubes - 50 mL	Corning	352070
IV catheter	JELCO	22G IV
InkJet Plus Microscope Slides	Thermo Fisher	12-550-109
Microfluidic biochips	Dynamic42 GmbH	BC002
MS columns	Miltenyi	130-042-201
Perfusion pump and tubing	Ismatec REGLO digital	MS-CA-4/12–100
QuadroMACS Separator	Miltenyi	130-091-051
Sterican® Standard Cannulas	B Braun	4657519
Sterile filter for syringe, 0.22 µm	Millipore	SLGP033RB
Sterile Petri dishes, 100 mm and 10 mm	Corning	70165
Sterile Petri dishes, 12-, 24- and 96-well	Costar	2531
Sterile pipettes - 10 mL	Thermo Fisher	170356N
Sterile pipettes - 25 mL	Thermo Fisher	170357N
Sterile pipettes - 5 mL	Thermo Fisher	170366N
Syringes - 20 mL	BD	300296
Syringes - 5 mL	BD	309050

3.1.5. Chemicals and proteins

Chemicals and proteins that were used in this study are listed in **Table. 2**.

Table 2. List of chemicals and proteins

Description	Manufacturer	Catalog No.
2-APB	Sigma-Aldrich	100065
Albumin from bovine serum, BSA	Sigma-Aldrich	A9430
Biliatresone, BT	Axon Medchem	AXON 2867
Calcium chloride dihydrate, CaCl2·2H2O	Sigma-Aldrich	C7902

Chenodeoxycholic acid, CDCA	Thermo Fisher	C9377
Collagenase type 4	CellSystems	LS004186
D-(+)-Glucose	Sigma-Aldrich	G8270
DNase I	Roche	10104159001
EDTA	Sigma-Aldrich	E9884
EGTA	Sigma-Aldrich	E4378
HEPES	Sigma-Aldrich	H4034
Magnesium chloride hexahydrate, MgCl2·6H2O	Sigma-Aldrich	930970
Magnesium sulfate heptahydrate, MgSO4·7H2O	Sigma-Aldrich	230391
Nycodenz	Accurate Chemical	1002424
Oleic acid, OA	Sigma-Aldrich	O1008
Palmitic acid, PA	Sigma-Aldrich	P0500
Paracetamol, APAP	Sigma-Aldrich	BP371
Paraformaldehyde, PFA	Sigma-Aldrich	158127
Phorbol 12-myristate 13-acetate, PMA	Sigma-Aldrich	P8139
Potassium chloride, KCl	Sigma-Aldrich	P9333
Potassium phosphate monobasic, KH_2PO_4	Sigma-Aldrich	60229
Protease	Sigma-Aldrich	P5147
Sodium bicarbonate, NaHCO3	Sigma-Aldrich	S5761
Sodium chloride, NaCl	Sigma-Aldrich	S3014
Sodium Phosphate monobasic monohydrate, NaH2PO4·H2O	Thermo Fisher	S369
Sodium phosphate, Na2HPO4	Sigma-Aldrich	S9763
Human recombinant ORM2	Bio-mol	156190.5
Mouse recombinant ORM2	BIZOL	LS-G14265-50

3.1.6. Solutions

3.1.6.1. Solutions (premade)

Commercialized solutions that were used in this study are listed in **Table. 3.**

Table 3. List of solutions

Description	Manufacturer	Catalog No.
Acetic acid solution, CH3CO2H	Sigma-Aldrich	45754
BD Pharm Lyse™ Lysing Buffer (10×)	BD	555899
Citrate buffer antigen retrieval	Thermo Fisher	AP-9003-500
Collagen I, rat tail	Thermo Fisher	A1048301
Dulbecco's phosphate-buffered saline, DPBS	Gibco	14190144
Ethanol solution 70 %	Thermo Fisher	15542393
Fetal bovine serum, FBS	Gibco	A4736201
Hanks' Balanced Salt Solution, HBSS	Gibco	24020117
Image-iT FX signal enhancer	Thermo Fisher	I36933

Isoflurane	CP-pharma	798-932
Lipofectamine™ RNAiMAX	Thermo Fisher	13778100
Lipopolysaccharide (LPS) Solution (500X)	Sigma-Aldrich	00-4976-93
Lysing buffer (10×)	BioLegend	420301
Normal goat serum, NGS (10%)	Thermo Fisher	50062Z
PBS-10×	Life Technologies	10010-23
Percoll-100%	Sigma-Aldrich	P1644
Phosphate-buffered saline, PBS	Gibco	70011044
Primary hepatocyte maintenance supplements	Gibco	CM4000
Tris-EDTA buffer-10×, pH9.0	Novus Biologicals	NB900-62085
Triton X-100 solution	Sigma-Aldrich	93443
Universal SYBR Green Fast qPCR Mix	ABclonal	RK21203
VectaMount AQ aqueous mounting medium	Vector	H-5501
William's E medium	Gibco	W1878-500ML

3.1.6.2. Solutions (homemade)

Protocols for preparing the solutions or buffers used in this study are described below.

1) EGTA buffer: Prepare the solution by dissolving the components of the recipe given below in 1 L of ddH_2O. Adjust the pH to 7.4 and filter the solution through a 0.2-μm bottle-top filter. The constituted solution can be stored at 4°C for up to 6 months.

Table 4. Composition of the EGTA buffer.

Reagent	**Final concentration (mg/L)**
NaCl	8,000
KCl	400
$NaH_2PO_4 \cdot H_2O$	88.17
Na_2HPO_4	120.45
HEPES	2,380
$NaHCO_3$	350
EGTA	190
D-(+)-Glucose	900

2) Enzyme buffer: Prepare the solution by dissolving the components of the recipe given below in 1 L of ddH_2O. Adjust the pH to 7.4 and filter the solution through a 0.2-µm bottle-top filter. The ready-to-use solution can be stored at 4°C for up to 6 months.

Table 5. Composition of the liver digestion buffer

Reagent	Final concentration (mg/L)
NaCl	8,000
KCl	400
$NaH_2PO_4 \cdot H2O$	88.17
Na_2HPO_4	120.45
HEPES	2,380
$NaHCO_3$	350
$CaCl_2 \cdot 2H_2O$	560

3) GBSS/A buffer: Prepare the solution by dissolving the components of the recipe given below in 1 L of ddH_2O. Adjust the pH to 7.4 and filter the solution through a 0.2-µm bottle-top filter. The constituted solution can be stored at 4°C for up to 6 months.

Table 6. Composition of the GBSS/A buffer

Reagent	Final concentration (mg/L)
KCl	370
$MgCl_2 \cdot 6H_2O$	210
$MgSO_4 \cdot 7H_2O$	70
Na_2HPO_4	59.6
KH_2PO_4	30
Glucose	991
$NaHCO_3$	227
$CaCl_2 \cdot 2H_2O$	225

4) GBSS/B buffer: Add 8 g/L NaCl into 1 L of GBSS/A buffer as described above to make GBSS/B buffer. Adjust the pH to 7.35 – 7.4 and filter the solution through a 0.2-μm bottle-top filter. The constituted solution can be stored at 4°C for up to 6 months.

5) Digestion buffers: Prepare the solution by dissolving the components of the recipe given below. The buffers need to be freshly made for each experiment. Filter the buffer with a 0.22-μm filter before use.

   a) Digestion buffer I: Dissolve 4.4 U collagenase type 4 in 50 mL enzyme buffer.

   b) Digestion buffer II: Dissolve 4.4U collagenase type 4, 40 μg DNase I and 4.5 mg pronase in 50 mL enzyme buffer.

6) DNase I solution: Dissolve 100 mg in 100 mL PBS to make 1 mg/mL solution.

7) Percoll-50% solution: Dissolve 10.8 mL Percoll-100% and 1.2 mL 10X-PBS in 14.5 mL 1×-PBS to make Percoll-50% solution. Mix it thoroughly.

8) Nycodenz solution: Dissolve 4.94 g nycodenz in 15ml GBSS/A buffer and filter it through a 0.22-μm filter. Adjust the solution volume to 17ml. Optional: Add phenol red to indicate gradient layers.

9) Magnetic-activated cell sorting (MACS) buffer: Dissolve 250 μg BSA and 37.2 μg EDTA in 50 mL DPBS. Filter it through a 0.22-μm filter. The constituted solution can be stored at 4°C for up to 2 weeks.

10) Collagen-coating buffer: Dissolve 660 μL collagen-I in 50 mL DPBS containing 0.12% acetic acid. Filter it through a 0.22-μm filter.

11) Blocking buffer: 5% normal goat serum and 0.3% Triton-X in DPBS.

12) Antibody buffer: 1% BSA and 0.3% Triton X in DPBS.

13) FFA solution: Dissolve PA or OA in DPBS containing 1% BSA - the ratios of PA and OA in the FFA mixture can be adjusted for different purposes. The final working FFA concentration is 30 mM.

14) Blocking buffer: Respectively dilute NGS and TritonX-100 into the DPBS to make 5% NGS and 0.3% Triton X-100 as final concentrations.

15) Antibody buffer: Respectively dilute BSA and TritonX-100 into the DPBS to make 1% BSA and 0.3% Triton X-100 as final concentrations.

3.1.7. Kits

The kits that were used in this study are listed in **Table. 7**

Table 7. List of kits

Description	Manufacturer	Catalog No.
Amplified kit	Vector	DK-1488
cDNA synthesis kit	ABclonal	RK20400
Cell counting kit-8, CCK-8	MCE	HY-K0301
Fluoresbrite® YG Carboxylate Size Range Kit I	Polysciences	563794
Fluo-8 Calcium Assay Kit - Medium Removal	Abcam	ab112128
Horseradish peroxidase (HRP) kit	Vector	MP-7401
RNeasy micro kit	QIAGEN	74004

3.1.8. Cell dyes

Information on cell dyes is listed in the table below.

Table 8. Cell dyes used in this study

Name	Manufacturer	Catalog No.
Zombie NIR™ Fixable Viability Kit	BioLegend	423105
Hoechst 33342	Thermo Fisher	62249
DAPI	Thermo Fisher	D21490
BODIPY 505/515	Thermo Fisher	D3921
CellMask plasma membrane stain kit	Thermo Fisher	C37608
Apoptosis/ Necrosis Assay Kit	Abcam	ab176749
Senescence Green Detection Kit	Thermo Fisher	C10850
DAB Substrate Kit	Abcam	ab64238
Haematoxylin	Sigma-Aldrich	1092492500

3.1.9. Antibodies/magnetic beads/LEGENDplex beads

Information on the antibodies, magnetic beads for cell sorting and LEGENDplex beads for cytokine measurement that were used in this study is listed below in tables.

Table 9. Antibodies/magnetic beads/LEGENDplex beads

Primary antibodies for IHC/ICC

Description	Manufacturer	Catalog No.	Clone	Host species
CYP450-2E1	Abcam	ab28146	Polyclonal	Rabbit
Cytokeratin-19	DSHB	TROMA-III	RIgG2a	Rat
CD68	Abcam	ab237968	FA-11	Rat
LYVE1	Abcam	ab14917	Polyclonal	Rabbit
Collagen-I	Abcam	ab270993	EPR24331-53	Rabbit
CD3	Abcam	ab16669	SP7	Rabbit
CD11b	Abcam	ab133357	EPR1344	Rabbit
CD45R (B220)	BioLegend	103202	RA3-6B2	Rat
CLEC4F	R&D	MAB2784	370901	Rat
Cytokeratin-7	Abcam	ab181598	EPR17078	Rabbit
IBA1	VWR	100369-764	Polyclonal	Rabbit
MPO	Abcam	ab208670	EPR20257	Rabbit
PCNA	Abcam	ab29	PC10	Mouse
PDGF-Rβ	Abcam	ab32570	Y92	Rabbit
ORM2	Thermo Fisher	PA5-119322	Polyclonal	Rabbit
ITPR2	ABclonal	A19320	Polyclonal	Rabbit
CALM1/2/3	ABclonal	A1185	Polyclonal	Rabbit
CD36	Abcam	ab133625	EPR6573	Rabbit
TIM4	Abcam	ab47637	Polyclonal	Rabbit
Ki67	Abcam	ab16667	SP6	Rabbit

Secondary antibodies

Description	Manufacturer	Catalog No.	Host species
Mouse IgG, Alexa Fluor 555	Cell Signaling	4409S	Goat
Mouse IgG, Alexa Fluor 647	Cell Signaling	4410S	Goat
Rabbit IgG, Alexa Fluor 647	Cell Signaling	4414S	Goat
Rabbit IgG, Alexa Fluor 750	Thermo Fisher	A-21039	Goat
Rat IgG, Alexa Fluor 488	Cell Signaling	4416S	Goat
Rat IgG, Alexa Fluor 647	Cell Signaling	4418S	Goat

Description	Manufacturer	Catalog No.	Clone	Host species
CD11b Monoclonal Antibody (M1/70), eFluor™ 450	Invitrogen	48-0112-82	M1/70	Rat
Brilliant Violet 421™ anti-mouse CD4 Antibody	BioLegend	100437	GK1.5	Rat
Brilliant Violet 711™ anti-mouse CD8a Antibody	BioLegend	100747	53-6.7	Rat
FITC anti-mouse Ly-6G Antibody	BioLegend	127605	1A8	Rat
CD45 Monoclonal Antibody (30-F11), Alexa Fluor™ 532	Invitrogen	58-0451-82	30-F11	Rat

PE anti-mouse CD115 (CSF-1R) Antibody	BioLegend	165003	W19330C	Rat
PE/Cyanine5 anti-mouse CD19 Antibody	BioLegend	115509	6D5	Rat
PE/Cyanine7 anti-mouse TCR β chain Antibody	BioLegend	109221	H57-597	Rat
Alexa Fluor® 700 anti-mouse CD11c Antibody	BioLegend	117319	N418	Rat
APC/Cyanine7 anti-mouse NK-1.1 Antibody	BioLegend	108723	PK136	Rat
APC/Fire™ 810 anti-mouse Ly-6G/Ly-6C (Gr-1) Antibody	BioLegend	108469	RB6-8C5	Rat
PE/Fire™ 810 anti-mouse I-A/I-E Antibody	BioLegend	107667	M5/114.15.2	Rat
APC anti-mouse CD192 (CCR2) Antibody	BioLegend	150627	SA203G11	Rat
PE Anti-HLA DR + DP + DQ antibody	Abcam	ab23901	WR18	Mouse

Magnetic beads

Description	Manufacturer	Catalog No.
Mouse anti-F4/80 Microbeads	Milteny	5210707948
Mouse anti-CD146 Microbeads	Milteny	5190725032
Mouse anti-CD326 (EpCAM) Microbeads	Milteny	70285065-00

LEGENDplex beads

Description	Manufacturer	Beads ID
IL-23	BioLegend	A4
IL-1α	BioLegend	A5
IFN-γ	BioLegend	A6
TNF-α	BioLegend	A7
MCP-1	BioLegend	A8
IL-12p70	BioLegend	A10
IL-1β	BioLegend	B2
IL-10	BioLegend	B3
IL-6	BioLegend	B4
IL-27	BioLegend	B5
IL-17A	BioLegend	B6
IFN-β	BioLegend	B7
GM-CSF	BioLegend	B9

3.1.10. Primers

All primers for RT-PCR assays were designed using online tools from the National Library of Medicine (NCBI, USA), and produced by Eurofins Genomics GmbH (Germany). The sequences of mouse and human primers are listed below in tables.

Table 10. Primer sequences used for gene expression analyses

Genes	Forward 5'-3'	Reverse 5'-3'
18S	AACTTTCGATGGTAGTCGCCGT	TCCTTGGATGTGGTAGCCGTTT
Acta2	TGACAGAGGCACCACTGAACC	TCCAGAGTCCAGCACAATACCAGT
Aim2	CTGCCGCCATGCTTCCTTA	AGTCCCAGGATCAGCCTAGA
Calm1	TATATATCGCGGCACACAGGC	ATGGTGCCATTGCCATCAGC
Calm2	CCCTTGCAGCATGAGTTCAAA	ACGCAGAGTTACAGCTCCAC
Casr	TGCCTTGTGATCCTCTTTCCAT	TCCACGGAAGTTATACCTGATG
Ccne1	CTCCCACAACATCCAGACCC	AGCAACCTACAACACCCGAG
Ccl2	GTG TTG GCT CAG CCA GAT GC	GACACCTGCTGCTGGTGATCC
Ccl3	ACCATGACACTCTGCAACCAAG	TCTGCCGGTTTCTCTTAGTCAGG
Ccl5	CTGCTGCTTTGCCTACCTCTCC	GGCACACACTTGGCGGTTCC
Ccr2	TCGCTGTAGGAATGAGAAGAAGAGG	CAAGGATTCCTGGAAGGTGGTCAA
Cd163	GTGCTGGATCTCCTGGTTGT	CGTTAGTGACAGCAGAGGCA
Cd36	TGAATGGTTGAGACCCCGTG	CGTGGCCCGGTTCTACTAAT
Cldn1	TGGGGCTGATCGCAATCTTT	CACTAATGTCGCCAGACCTGA
Col1a1	TCTGACTGGAAGAGCGGAGAG	GGCACAGACGGCTGAGTAGG
Cxcl5	TCCTCAGTCATAGCCGCAAC	GCTTTCTTTTTGTCACTGCCC
Cyp2e1	ATAGAAGTTGGAACCTGCCC	CTTTGCCAACTTGGTTAAAGAC
Fgf1	TTATACGGCTCGCAGACAC	TGCTTCTTGGAGGTGTAAGTG
Fgf2	CGACCCACACGTCAAACTAC	GCACACACTCCCTTGATAGAC
Icam1	CATCACCGTGTATTCGTTTC	GTGAGGTCCTTGCCTACTTG
Ifng	GGAGGAACTGGCAAAAGGATGG	TGTTGCTGATGGCCTGATTGTC
Ikbkg	CTTGTTTTGGCTCAGCCTGC	GTCCTCAGCCATCTGCTGTT
Il10	GGCTGAGGCGCTGTCATCG	TCATTCATGGCCTTGTAGACACC
Il1a	CGCTTGAGTCGGCAAAGAAAT	AAGGTGCTGATCTGGGTTGG
Il1b	GAGCTGAAAGCTCTCCACCTC	CTTTCCTTTGAGGCCCAAGGC
Il23	ACCAGCGGGACATATGAATCT	AGACCTTGGCGGATCCTTTG
Il6	GCTACCAAACTGGATATAATCAGGA	CCAGGTAGCTATGGTACTCCAGAA
Irak4	CCCAAACCGTCAAAAGCCTG	GTTCTCGTGCTGACACGTTG
Itpr2	CGAGGGTGATAATGTGAATGCTG	AGGATCCCAAACACCTGTGC
Mki67	ACCATCATTGACCGCTCCTT	TTGACCTTCCCCATCAGGGT
Mrc1	TTCCGCTGGGTGTCAGATTC	TCTCGCTTCCCTCAAAGTGC
Myd88	ATGACCCCCTAGGACAAACG	GAGAATCTGGCTCCGCATCA
Nfkbia	TGTGATCACCAACCAGCCAG	AGACACGTGTGGCCATTGTAG
Nlrc4	GGATTGCTTGGCCAGGAGAG	CAGGTCTTCTTCTGTGACCTGA

Nlrp1	ATAGAGGAGCAGGCAGGTCT	CGTGCTCCTGGAAAGGTTCT
Nlrp2	GGCCTCCTGAATGAGACTCG	TTGTTCATCCGGGGACCTTT
Nlrp3	TGGGTTCTGGTCAGACACGAG	GGGGCTTAGGTCCACACAGAAA
Nos2	GCCCAGCCAGCCCAAC	GCACATCAAAGCGGCCATAG
Olcn	TTGAACTGTGGATTGGCAGC	CAAGATAAGCGAACCTTGGCG
Orm1	AGTGCTGAGGAAACATGGGG	GCTGACCGCACCTATCCTTT
Orm2	TTGGTGCGGCTGTCCTAAA	GCTGACTGCACCTGTCCTTTT
Cdkn1a/P21	AGAATAAAAGGTGCCACAGGC	AATCTGTCAGGCTGGTCTGC
Pdgfrb	CATGTCTGAGACCCGGTACG	AGTCGTAAGGCAACTGCACA
Pecam1	GAAGGTGCATGGCGTATC	TTCTTGCAAGGAACAATTGAC
Spp1	AAGAAGCATCCTTGCTTGGGT	GGTCGTAGTTAGTCCTTGGCT
Tgfb1	GCTCGCTTTGTACAACAGCACC	GCGGTCCACCATTAGCACG
Timd4	AGAGACACAAGAGGCCAGACA	TAGGGGCTGGAGGCTTATTCC
Tnfa	ACCACGCTCTTCTGTCTACTGA	TCCACTTGGTGGTTTGCTACG
Tnfrsf12a	GCCTCGAAGAAGTGCTCCTAAA	CCTTAAGATGAGCCCAGGGGA
Tjp1	GAGCAGGCTTTGGAGGAGAC	CATTGCTGTGCTCTTAGCGG
Tirap	ACCTGCATCCAGAACAGTAAGT	GGAGGGCATTTGAGATCCGT
Vcam1	TGTTTGCAGTCTCTCAAGC	GGCTGTCTATCTGGGTTCTC

Sequences of human primers

Genes	**Forward 5'-3'**	**Reverse 5'-3'**
ACTB	GATTCCTATGTGGGCGACGA	CACAGGACTCCATGCCCAG
AIM2	CCCAGGGATCAGGAGTTGATAAG	GACTTTTGGTGCAGCACGTT
CASR	GGGAGCCACTCACCTTTGTG	AGGCACTGGCATCTGTCTCA
CD163	AAAAAGCCACAACAGGTCGC	GGTATCTTAAAGGCTCACTGGGT
IKBKG	GACTCTGCTGACAGCCCTTG	CCTGGCATTCCTTAGTGGCA
IL10	GGTTGCCAAGCCTTGTCTGAG	GATGACAGCGCCGTAGCC
IL1B	AGCCATGGCAGAAGTACCTG	CCTGGAAGGAGCACTTCATCT
IL6	GGCATCTCAGCCCTGAGAAAG	CACCAGGCAAGTCTCCTCATT
IRAK4	AAGGCATTCCCCGCCTTAAT	TTTGGGAACAGCATCTGGGA
MRC1	TTCCTTTGGACGGATGGACG	GTCAAGGAAGGGTCGGATCG
MYD88	CAGCCAGAGGAGAGGAGGAT	GGTTGGTGTAGTCGCAGACA
NFKBIA	ATGTCAATGCTCAGGAGCCC	GGTCAGTCACTCGAAGCACA
NLRC4	AGGCCTCACTGAAACGGAA	AAACTACTCTTCATTCTGGCTGA
NLRP1	TCAAACTCCTGGACGTGAGC	CAGAGCTCCAGTTCCTTCCG
NLRP2	AACAGAAGCACAAGACAAAGAC	GTGCTTGGGCTAGGATGTGT
NLRP3	CTGGCATCTGGGGAAACCT	CTTAGGCTTCGGTCCACACA
TGFB1	GCCCTGGACACCAACTATTGCT	ACGCTCCAAATGTAGGGGCAGG
TNFA	GCCCATGTTGTAGCAAACCC	GGAGGTTGACCTTGGTCTGG
TNFRSF12A	CCTCGCAGAAGTGCACCTAAA	TCAGGTAGACAGCCTTCCCC
TIRAP	GCGCAGGCCTTACATAGGAA	GGAGCAGCCATCAGGGTATG

3.2. Methods

3.2.1. Primary cell isolation

3.2.1.1.Mouse liver perfusion and digestion

1) Before starting, pre-warm EGTA / enzyme buffers in the 42°C water bath; assemble tubes and catheters in the pump.

   NOTE: The temperature can be adjusted to ensure the solutions are perfused in mouse liver at mouse body temperature.

2) Sacrifice the mice with an inhalation of isoflurane (60 µg/g body weight) for 3 min.

3) Fix mouse the feet on the operating board, with the abdominal side up. Spray the abdomen with 70% ethanol to sterilize the area and wet the fur.

4) Open the abdominal cavity. Gently push the intestines and colon to the right side, to expose the portal vein and inferior vena cava without punching into the organs.

5) Cannulate the portal vein using an I.V. catheter. Perfuse the liver with EGTA buffer (40 mL) at a flow rate of 2 mL/min. Section the vena cava at a distal position to allow for perfusate clearance.

   OPTIONAL: For blood collection, insert a needle into inferior vena cava prior to starting perfusion. Start perfusion and collect blood with a 1.5 mL Eppendorf tube. Pull out the needle after collection.

6) **CAUTION**: It is critical to avoid bubbles during perfusion. Check for the presence of bubbles in the tubing prior to inserting the catheter. When switching perfusion reagents, make sure to stop the pump prior to transferring the tubing from one tube to the other.

   NOTE: The liver should appear homogeneously brighter within seconds after initiating the perfusion and cutting the inferior vena cava. If this is not the case, the perfusion is not optimal, and this will lead to difficulties during cell isolation.

   NOTE: During the perfusion, it is necessary to press inferior vena cava with a vessel clamp for 30-40 sec to check the perfusion quality. The liver lobes start

inflating rapidly.

7) Continue perfusion with the digestion buffer I (50 mL) at a flow rate of 2 mL/min.
8) Stop the perfusion and remove the catheter. Carefully remove the whole liver (dissect and discard the gallbladder).
9) Gently mince the liver tissue with vessel clamps in preparation for further isolation procedures.

   OPTIONAL: Separate liver tissues if multiple cell type isolation is required. For the HSC, KC and LSEC isolation, an extra digestion (in a 37℃ incubator at a mild shaking level for 25 - 35 min) is necessary.

3.2.1.2.Mouse primary hepatocyte isolation

1) Pass the liver cell suspension through a 70-μm strainer to a 50 mL Falcon tube. Fill the tube up with HBSS to 50 mL. Centrifuge the cell suspension at 4°C, 50 × g for 5 min.
2) Aspirate the supernatant and resuspend the hepatocyte pellet in 50 mL HBSS. Centrifuge the cell suspension again at 4°C, 50 × g for 5 min.

   NOTE: Keep the supernatant if necessary.
3) Aspirate the supernatant and resuspend the hepatocyte pellet in 50 mL Percoll-50% solution. Centrifuge the cells at 4°C, 400 × g for 10 min.
4) Aspirate the supernatant and resuspend the hepatocyte pellet with 50 mL HBSS buffer. Centrifuge the hepatocytes at room temperature, 50 × g for 10 min.
5) Resuspend the hepatocyte pellet in medium for counting and seeding.

3.2.1.3.Mouse primary hepatic stellate cell isolation

1) Filter the liver cell suspension through a 70-μm strainer. Fill the tube up with GBSS/B buffer to 50 mL. Centrifuge the cell suspension at 4°C, 580 × g for 10 min.

2) Aspirate the supernatant until 10 mL remains in the tube. Add 100 µL DNase I solution and fill it up to 50 mL with GBSS/B buffer. Centrifuge again at 580 × g for 10 min at 4 °C.
3) Aspirate the supernatant until 10 mL remains in the tube. Add 100 µL of DNase I solution and fill it up to 32 mL with GBSS/B buffer. Add 16 mL Nycodenz solution and mix thoroughly. Split 48 mL cell-Nycodenz suspension equally into four 15-ml Falcon tubes.
4) Gently overlay with cell-Nycodenz suspension with 1.5 mL of GBSS/B buffer using a 3-ml syringe with a 26-gauge needle attached. Centrifuge the suspension at 4 °C, 1,380 × g with no break for 17 min.

   CAUTION: Make sure to overlay the GBSS/B buffer gently above the cell-Nycodenz suspension to create a discontinuous gradient. A clear separation should be observed.
5) Use a 5-ml pipette to collect the cells and transfer them into a new 50-ml Falcon tube. Resuspend the cell pellets in MACS buffer for the magnetic cell sorting.

   OPTIONAL: Repeat the procedure (steps 3-5) with cell pellets to obtain more cells.
6) Fill the Falcon tube up to 50 mL with GBSS/B buffer. Gently resuspend the collected HSCs. Centrifuge at 4 °C, 580 × g for 10 min.
7) Resuspend the cell pellet in medium for counting and seeding.

3.2.1.4.Magnetic cell sorting

1) Centrifuge the cell suspension at 4°C, 400 × g for 10 min.
2) Discard the supernatant and resuspend in 90 µL MACS buffer per 10^7 cells.
3) Add 10 µL /10^7 cells magnetic beads (F4/80 for KCs or CD146 for LSECs, respectively) into the cell suspension. Mix well and incubate on ice for 15 min.
4) Add 900 µL MACS buffer per 10^7 cells and centrifuge at 4°C, 300 × g for 10 min.

5) Discard the supernatant and resuspend cells in 500 µL of MACS buffer. Place the MS column in the magnetic separator and rinse it with 500 µL of MACS buffer. Add the cell suspension into the column. Collect the flow-through containing unlabeled cells for the next magnetic cell sorting.

   OPTIONAL: An LS column can be used if a higher amount of cell sorting is required.

6) Wash the column with 3 x 500 µL of MACS buffer. Move the column out from the magnetic separator. Add 1 mL MACS buffer into the column. Firmly flush out the buffer from the column with the plunger. Collect the labelled retained cells in a 15-mL Falcon tube. Centrifuge the cell suspension at 4°C, 400 × g for 10 min.
7) Resuspend the cell pellet in medium for counting and seeding.

3.2.1.5.Peripheral blood mononuclear cell (or CIC) isolation

NOTE: This section refers to blood collected from either: (1) mouse vena cava during the liver perfusion. If needed, more blood may be collected from the heart using a 1 mL syringe containing 0.5 mL EGTA buffer before or during the liver perfusion; or (2) human median cubital vein.

1) Centrifuge blood samples at 4°C, 400 × g for 10 min.
2) Aspirate the supernatant and resuspend the cell pellets with 10 mL 1× red blood cell lysing buffer.
3) Incubate the cell suspension on ice for 15 min.
4) Centrifuge at 4°C, 400 × g for 10 min.
5) Aspirate the supernatant and resuspend the cell pellet in cell culture medium for counting and seeding.
6) For human monocyte isolation, CICs were seeded in a petri dish. After 4 hours, wash out non-adherent cells but preserve adherent cells to obtain monocyte-like cells.

3.2.1.6. Mouse MoMF isolation

Femurs with muscle and fascia completely removed were collected from sacrificed mice and rinsed in cold DPBS buffer. Remove both ends of the femurs and flush out the bone marrow with cell culture medium (William's E medium + 10% FBS + 1% penicillin/streptomycin). Cell suspensions were seeded in petri dishes after going through a 70-μm cell strainer. Bone marrow cells were treated with 20 ng/mL macrophage colony-stimulating factor (M-CSF) for 7 to 10 days to generate macrophage-like phenotypes.

3.2.2. Mouse cholangiocyte organoid culture

MDR2 KO mouse intrahepatic cholangiocytes were isolated using the MACS approach with mouse EpCAM beads. Cholangiocyte organoids were cultivated by Mr. Tian Lan (a laboratory colleague) following the well-established protocol(87). Organoids were dissociated into single cells. Then, cells were seeded in collagen-coated plates with regular cell culture medium and incubated at 37℃ 5% CO_2.

3.2.3. Cell treatment

3.2.3.1. THP-1 cell activation

Cells were treated with 50 ng/mL PMA for 2 days to achieve immature macrophages (unpolarized). The activation status was assessed by morphological and attaching features.

3.2.3.2. Cell injury induction

Mouse primary cholangiocytes and hepatocytes were treated with 2 μg/mL biliatresone, 1 mM CDCA, 25 mM APAP or 300 μM free fatty acids (FFAs, oleic acid:palmitic acid = 1:1) for 24 hours.

3.2.3.3. Macrophage stimulation

THP-1 derived macrophages, human MoMFs, mouse MOMFs and mouse liver macrophages were respectively treated with 1 μg/mL ORM2 (or 100ng/mL LPS) for 24 hours. 75 μM 2-APB was introduced to mouse primary liver macrophages to suppress intracellular calcium intake.

3.2.4. Gene interference assay

Mouse primary liver macrophages and cholangiocytes (primary and organoid-derived) were seeded in the required petri dishes 12 – 24 hours before gene interference assay in a serum-reduced cell culture medium (William's E medium + 1% FBS + 1% penicillin/streptomycin). The mixture of 10 pmol small-interfering RNA (siRNA) (target or control) and 1 μL Lipofectamine™ RNAiMAX reagent was made for every 100 μL of serum-free William's E medium, and incubated at room temperature for 30 min. Then, the siRNA mixture was introduced to the cells, and replaced with regular cell culture medium after 4 – 6 hours of incubation at 37℃, 5% CO_2. Effective mRNA expression suppression was estimated to be maintained for 7 days. More technical details can be found in the manufacturer's instructions.

3.2.5. Quantitative real-time PCR assay

Total RNA was extracted and isolated using a Rneasy Micro Kit (QIAGEN, Germany). Reverse transcription was conducted with a cDNA synthesis kit (Abclonal, China), and real-time quantification was subsequently performed using a Universal SYBR Green Fast qPCR Mix (Abclonal, China). The relative RNA expression levels were calculated using the -ΔΔCt method. The sequences of primers included in this study are listed in **3.1.9**.

3.2.6. Immunohistochemistry (IHC)

3.2.6.1. IHC – horseradish peroxidase (HRP) approach

<Day 1>

1) Deparaffinize with 2 × 5 min Xylene bath under a biosafety cabinet. Then, decreasing Ethanol concentrations (96% / 80% / 70% / 50%) for 2 min each, and rinsing in deionized (DI) water.
2) Antigen retrieval: Use 10X EDTA (pH 9.0) to make a 1× EDTA solution with DI water. Start the water bather and set it to 98 ℃. Rinse slides in EDTA buffer and incubate them in the water bath for 20 min in a plastic slide holder. Let the slides cool down in the buffer at room temperature for 30 min, cover top.

3) Rinse slides in PBS, 3 × 2 min, circle samples with a PAP pen during washes.

4) Make H_2O_2 solution (3%) with DI water and incubate for 10 min at room temperature.

5) Rinse slides in PBS, 3 × 2 min.

6) Block the slides for 30 min in 2.5% normal horse serum.

7) Perform different dilutions of the primary antibody in PBS + 1% BSA, add 100 uL per sample, then incubate overnight at 4 ℃.

<Day 2>

1) Rinse slides once in PBS-T 0.1%, then in PBS, 3 × 2 min.
2) Apply horse anti-rabbit IgG polymer reagent (in HRP kit) and incubate for 1h at room temperature.
3) Rinse slides in PBS, 3 × 2 min.
4) Apply DAB solution (30 uL DAB in 1ml solution) to each slide, observe under microscope to set an appropriate time (usually 30s to 90s).
5) Rinse slides in PBS, 3 × 2 min.
6) Apply Hematoxylin solution to each slide in glass slide containers, observe under microscope to set an appropriate time (around 2 min).
7) Rinse slides in normal water.
8) Reverse deparaffinization step, Ethanol to Xylene.

9) Mount the slides. Dry the mounted slides in a hood for 30 min.
10) Observe samples under the microscope.

3.2.6.2. IHC – immunofluorescent staining

<Day 1>

1) Deparaffinize with 2 × 5 min Xylene bath under a hood. Then, decreasing Ethanol concentrations (96% / 80% / 70% / 50%) for 2 min each, and rinsing in DI water.
2) Antigen retrieval: Use 10X EDTA (pH 9.0) to make a 1 × EDTA solution with DI water (Or Universal buffer, Citrate buffer). Start the water bath and set it to 98 ℃. Rinse slides in EDTA buffer and incubate them in the water bath for 20 min in a plastic slide holder. Let the slides cool down in the buffer at room temperature for 30 min, cover top.
3) Rinse slides in PBS, 3 × 2 min, circle samples with a PAP pen during washing.
4) Apply Image-iT and incubate for 30 min at room temperature.
5) Rinse slides in PBS, 3 × 2 min.
6) Block the slides in PBS for 1 hour in PBS + 2 % NGS.
7) Apply primary antibody (1:200) in PBS + 1% BSA, and add 100 uL per sample. Then, incubate samples overnight at 4 ℃.

<Day 2>

1) Rinse slides once in PBS-T 0.1%, then in PBS, 3× 2min.
2) Apply appropriate secondary antibody diluted 1:500 in PBS + 1% BSA, incubate for 1h at room temperature. Optional: If amplification is required, incubate samples for 15 min with Amplifier Antibody, in Amplified kit, rinse in PBS, then for 30 min in VectorFluor Reagent, in Amplified kit.
3) Rinse slides in PBS, 3 × 2 min.
4) Incubate in DAPI diluted 1:1000 in PBS for 5 min at room temperature.
5) Rinse slides in DI water, 3 × 2 min.
6) Apply aqueous mounting medium and mount the slides.

7) Observe samples under the microscope.

3.2.6.3. IHC – multiplex immunofluorescent staining

Based on regular fluorescent staining approaches, sequential multiplex immunostaining was performed as described in previous studies from our laboratory(88, 89).

3.2.7. Immunocytochemistry (ICC)

1) Fixation buffer preparation: Dissolve 2 g paraformaldehyde (PFA) in 50 mL 1×-PBS. Put in a water bath (70 – 98 ℃) for 40 min. Store at 4 ℃ for 2 weeks.
2) Cell fixation: Wash cells with PBS. Pre-warm 2% PFA at “37 ℃ and overlay them on each well (or re-suspend cell pellet). Incubate at room temperature for 15 min under a hood. Rinse cells with PBS before staining.
3) IHC staining: Block in blocking buffer (PBS + 5% normal goat serum + 0.3% Triton-X) for 50 min at room temperature. Without washing, apply primary antibodies diluted (1:200) in antibody buffer (PBS + 1% BSA + 0.3% Triton-X). Incubate with primary antibodies at room temperature for 4h or overnight. Rinse 3 times with PBS. Apply secondary antibodies diluted (around 1:1000) in antibody buffer (PBS + 1% BSA + 0.3% Triton-X). Incubate with secondary antibodies for 30 min at room temperature. Rinse 3 times in PBS. Apply DAPI solution in PBS, incubate at room temperature for 10 min. Rinse slides 3 times in PBS.
4) For cellular senescence detection: Cells are fixed in 2% PFA for 10 min, and then processed using a Senescence detection kit, following the manufacturers’ instructions. Stained cells can be observed under a fluorescent microscope.

3.2.8. Live cell staining

Viable adherent cells in petri dishes or chamber slides were stained with diverse live cell dyes or kits for different purposes: (1) Cells were stained with Hoechst 33342 to

indicate the nucleus. (2) Cells were stained with BODIPY dye to illustrate intracellular lipid droplets. (3) Cells were stained with a CellMask plasma membrane stain kit to depict the cell membrane. (4) Cells were stained with an Apoptosis/ Necrosis Assay Kit to assess cell apoptosis, cell death and viability. Stained live cells can be immediately observed and traced under a fluorescent microscope.

3.2.9. Transcriptome analysis

Total RNA was extracted and purified using a Rneasy Micro Kit (QIAGEN, Germany). The quality control, library build-up and whole transcriptome detection was performed by the Genomics platform, Max Delbrück Center (MDC) / Berlin Institute of Health (BIH).

3.2.10. Bioinformatic analysis

To extract meaningful biological insights from the vast amount of raw sequencing data, we used a suite of R packages tailored for different stages of the analysis pipeline. The initial quality control and preprocessing steps were performed using the 'BiocParallel' and 'ShortRead' packages, which allow for efficient parallel processing and effective handling of raw sequence reads. Subsequent alignment and quantification of transcript abundance was performed using the 'edgeR' packages, facilitating differential expression analysis and identification of significantly modulated genes(90). Functional enrichment analysis was performed using the Gene Ontology (GO) and Kyoto Encyclopedia of Genes and Genomes (KEGG) databases(91, 92). Cell type enrichment analysis was performed using the 'Xcell' package(93). Published datasets were obtained from the Gene Expression Omnibus (GEO) database (https://www.ncbi.nlm.nih.gov/gds).

3.2.11. Image analysis

Images derived from IHC and ICC were analyzed using Image J (NIH, USA). To

analyze multiplex immunofluorescent staining, the working pipeline of image analysis was established and tailored in our laboratory. The technical details are described in our previous study(89).

3.2.12. Co-culture experiments

3.2.12.1. Co-culture using conditioned medium

Conditioned medium was collected from the cell supernatant by removing debris using centrifugation (1000 × g, 10 min). Then, conditioned medium was applied on target cells in normal cultivation conditions. For each culture, the numbers of conditioned medium-generating and -treated cells were comparable.

3.2.12.2. Co-culture using compartmented chambers

Diverse types of cells under different conditions and interventions were separately seeded in compartmented chambers (μ-Slide 2-Well Co-Culture chamber, Ibidi) Then, cell compartments were connected by adding extra medium to raise the water levels. While the interventions are being finished, cells can be fixed for IHC detection, or harvested for mRNA detection.

3.2.12.3. BoC experiments

1) Sterilize the surface and inner cavities of the biochip by pipetting in 70% ethanol and incubating for 40 min.
2) Wash the cavities 3 times with DPBS buffer.
3) Pipette 500 mL collagen coating buffer in each cavity and incubate for 15 min.
4) Wash the cavities 3 times with DPBS buffer. Fill each cavity with 500 μL medium. Block connections between the cavities with plugs.
5) Cell seeding and intervention strategies:
    a) On Day 1, seed 300,000 organoid-derived cholangiocytes in the upper cavity.

b) On Day 2, silence *Orm2* expression of cholangiocytes in the BoC (following the methods in Section 3.2.4).

c) On Day 3, seed 300,000 LSECs and 100,000 liver macrophages in the lower cavity. Incubate overnight at 37°C, 5% CO_2.

d) On Day 4, flip back the chip. Seed 200,000 HSCs in the upper cavity. Incubate at 37°C, 5% CO_2 for 48 hours (until Day 6).

6) Bio-chip perfusion strategies (on Day 6):

a) Connect the tubing to each lower cavity. Add 1 mL medium containing 100,000 CICs into each reservoir.

b) Start perfusion through the pumping channels at 50 μL / min.

c) Transfer chip-pump assemblies into the incubator. Incubate at 37°C, 5% CO_2 for 30 min (from 30 min to 48 hours depending on the experimental needs). **CAUTION**: Bubbles should be avoided during cell seeding into the biochip, medium changing and CIC perfusion.

7) Sampling strategies (**Figure. 4**):

a) Apply live cell dye on cells and observe under microscope.

b) Harvest the perfusion medium and centrifuge at 4°C, 400 × g for 10 min. Collect CICs in the cell pellets. Keep the supernatant for further analyses.

c) Cut off membranes to harvest resident cells for RNA extraction, or for IHC detection after fixation with 4% PFA.

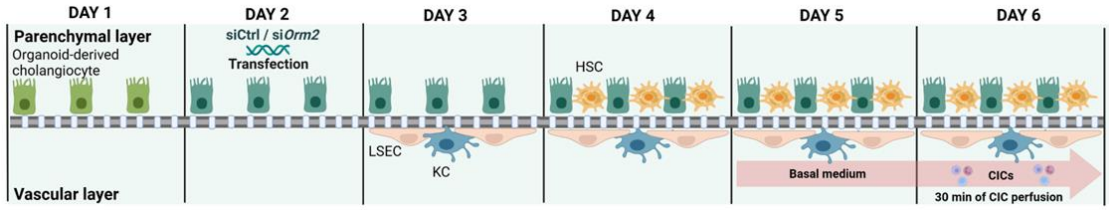

Figure 4. Biliary niche-on-a-chip modeling strategy.

3.2.13. Flow cytometry

Mouse CICs were isolated from CFP mice. After lysing red blood cells, the CICs were

perfused in the BoC for 30 minutes. The perfusate was then collected, and the cells were centrifuged at 400 × g for 5 minutes. The cells were incubated with a fixable viability dye (Zombie NIR™ Fixable Viability Kit; Biolegend, USA) at a 1:5000 dilution for 10 minutes at 4°C. Subsequently, they were incubated with fluorochrome-conjugated antibodies in blocking buffer (PBS + 2% BSA + 2% normal mouse/rat/rabbit/human serum) for 20 minutes at 4°C. Cells were fixed with PBS containing 1% formalin for 10 minutes at 4°C. Finally, the cells were suspended in 200 µL of PBS and 10 µL of counting beads (10^6 beads/mL) were added to each sample. Multispectral flow cytometry was performed using the Cytek® Aurora.

3.2.14. Schematic figures

The schematic figures that are displayed in this dissertation were made with BioRender.

3.2.15. Statistical analysis

GraphPad Prism 9.0 software (GraphPad Software, USA) and R studio (version: 2023.03.1 Build 446; plugins ‘ggplot2’) were used to generate plots(94). The heatmaps displayed in most figures represent relative values as compared to the appropriate control. Student’s t-tests and one-way ANOVA were performed as appropriate and as detailed in figure legends. Data are presented as the mean ± S.D. $p < 0.05$ was considered to be significantly different.

4. Results

4.1. ORM2 upregulation as a hallmark of intrahepatic cholangiocyte injury

To explore the cellular crosstalk mediators released by damaged intrahepatic BECs/cholangiocytes, bulk RNA-seq datasets generated from a targeted BEC injury mouse model were used. The technical details have been previously described. In brief, intrahepatic cholangiocytes were microdissected from livers of ih*CD59*$^{\text{BEC-TG}}$ mice administered with intermedilysin, and bulk RNA sequencing was performed from this purified fraction(59). Another bulk RNA-seq dataset was obtained from cholangiocytes isolated from mouse models (dnTGFBRII and control) to recapitulate chronically injured cholangiocytes(95). *Orm2* and *Adam11* were significantly screened as key overlapping upregulated genes (DEGs) with statistical significance (**Figure. 5A**). Furthermore, bulk RNA-seq datasets were gathered from alternative liver injury models to assess the expression of *Orm2* and *Adam11*. Notably, the *Orm2* gene was consistently upregulated in various injured mouse livers and not *Adam11*. Details of the datasets can be accessed using GSE IDs in the GEO database (**Figure. 5B**). In addition, the single-cell RNA (scRNA)-seq dataset (based on a mouse liver steatosis model)(96) indicated that *Orm2* expression is impaired in Hepatocytes but increased in BECs (injury *vs.* healthy) (**Figure. 5C**). There is no expression difference of *Adam11* in hepatocytes and BECs (injury *vs.* healthy) (**Figure. 5D**). Lastly, human liver samples obtained from healthy, MASLD (fibrosis stage 1 & 4) and PSC donors were for IHC detection. Significantly, DR was more prominent in advanced disease stages. ORM2 was revealed to be highly expressed by reactive BECs (**Figure. 5E**). The results suggest that ORM2 upregulation may be a crucial factor released by intrahepatic BECs upon liver injury.

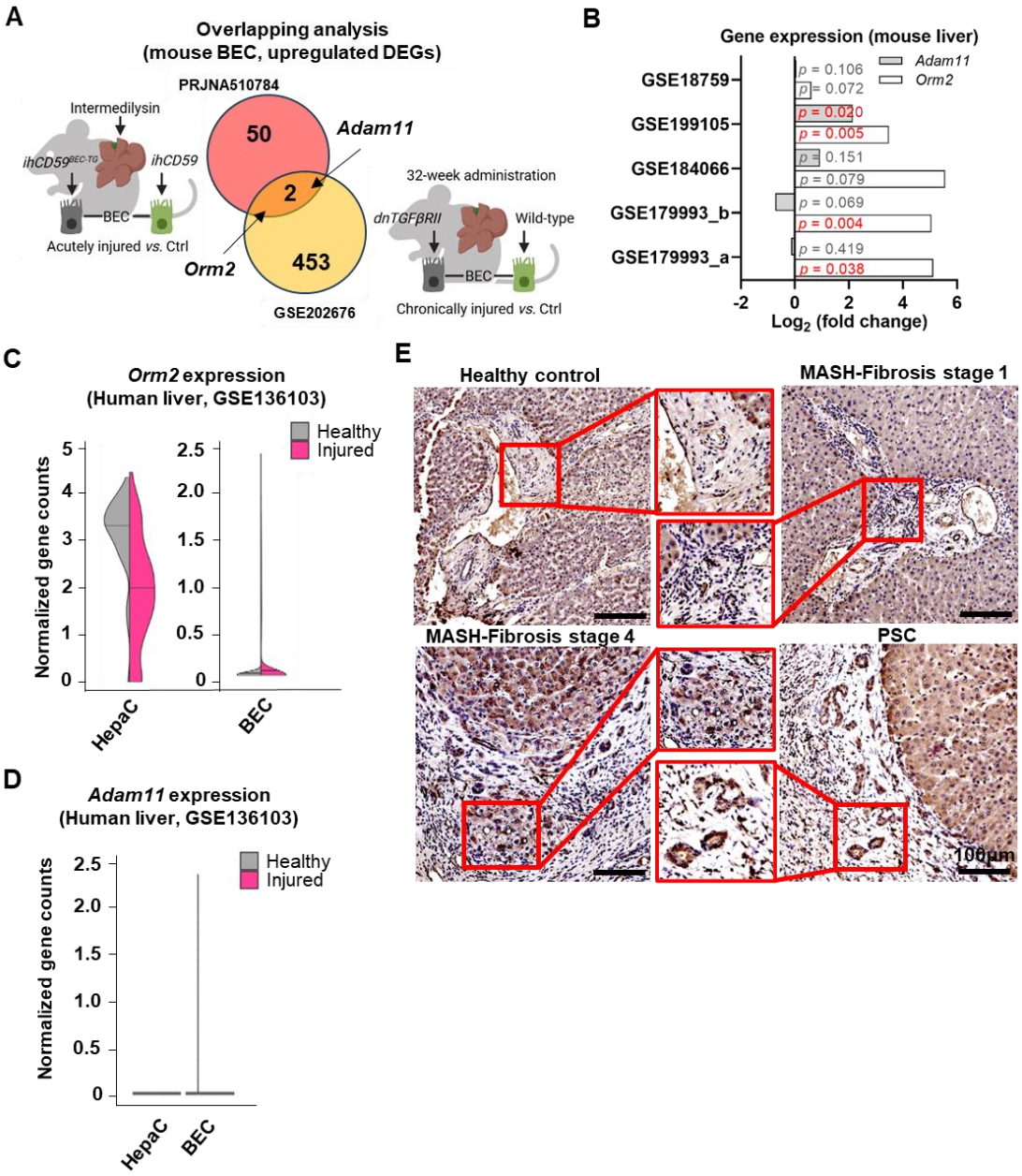

Figure 5. ORM2 is upregulated in intrahepatic ductular cells upon liver injury. (A) Overlapping upregulated DEGs in mouse cholangiocytes from two datasets (PRJNA510784 and GSE202676). (B) Expression of *Orm2* and *Adam11* in healthy and injured mouse livers. Expression of (C) *Orm2* and (D) *Adam11* in human Hepatocytes and BECs (injury vs. healthy). (E) ORM2 production detected by IHC on human liver samples obtained from healthy, MASH (fibrosis stage 1 & 4) and PSC donors. Student's t-tests were used. * represents $p < 0.05$.

4.2. ORM2 is differentially expressed in hepatocytes and cholangiocytes upon injury

Biliatresone was introduced in mouse primary BEC cultures to induce cell injury.

Concentrations of biliatresone were titrated, and 2 μg/mL was determined to induce 50% of BEC death (**Figure. 6A, B**). Furthermore, *Orm2* expression was measured in mouse primary Hepatocytes and BECs upon introducing different chemicals. In BECs, biliatresone exclusively enhanced *Orm2* gene expression (**Figure. 6C**) and protein production (**Figure. 6D**). In Hepatocytes, APAP and biliatresone significantly impaired *Orm2* gene expression (**Figure. 6E**) and protein production (**Figure. 6F**). Results of *in vitro* experiments indicate that ORM2 production is highly pronounced in BECs but impaired in Hepatocytes after acute injury.

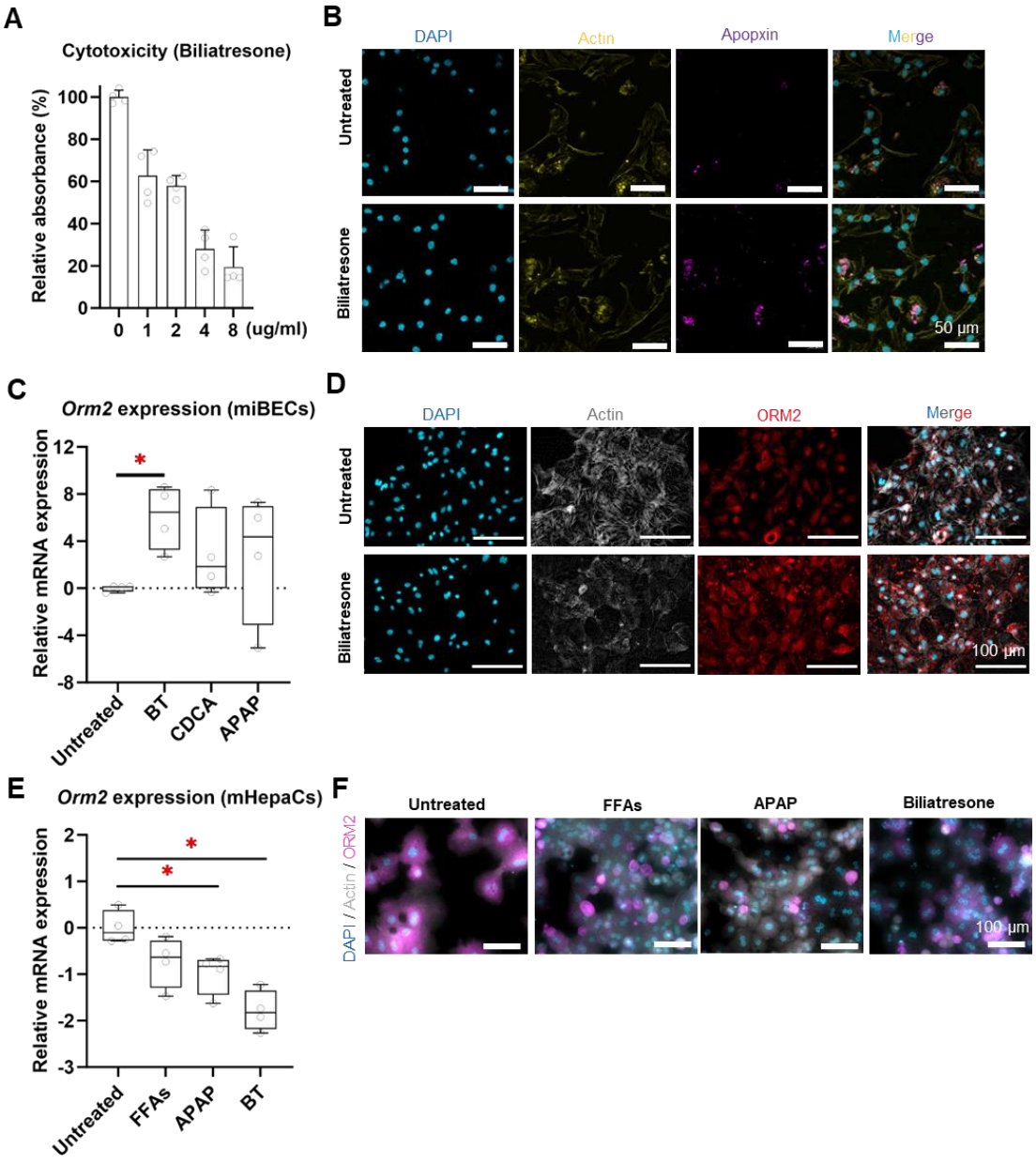

Figure 6. ORM2 production is increased in cholangiocytes but decreased in hepatocytes upon acute *in vitro* injury. (A) Relative cell numbers upon gradient concentrations of biliatresone. (B) Cellular Apopxin levels measured on BECs via the ICC approach. (C) *Orm2* expression of BECs upon BT, CDCA and APAP treatments. (D) ORM2 protein depicted on BECs upon biliatresone treatment via the ICC approach. (E) *Orm2* expression of Hepatocytes upon FFAs, APAP and BT treatments. (F) ORM2 protein depicted on Hepatocytes upon biliatresone treatment via the ICC approach. FFAs: free fatty acids. APAP: acetaminophen; BT: biliatresone. One-way ANOVA was performed. * represents $p < 0.05$.

4.3. ORM2 mobilizes monocytic accumulation in the biliary niche in liver

4.3.1. Administration of ORM2 enhances the gene expression of monocyte signatures in mouse liver

Cell enrichment analysis was conducted using gene signature-based algorithms (Xcell). The bulk RNA-seq dataset was obtained from the livers of obese mouse models, which were respectively administered with ORM2 or vehicle control (PBS) for 10 days (1.0 mg/kg)(97). Results show that the frequencies of monocytes and $CD4^+$ T cells were drastically increased upon ORM2 administration in the absence of additional liver injury induction (*vs*. Ctrl) (**Figure. 7A and 7B**), while no significant changes were revealed in other cell types (**Figure. 7C – 7N**).

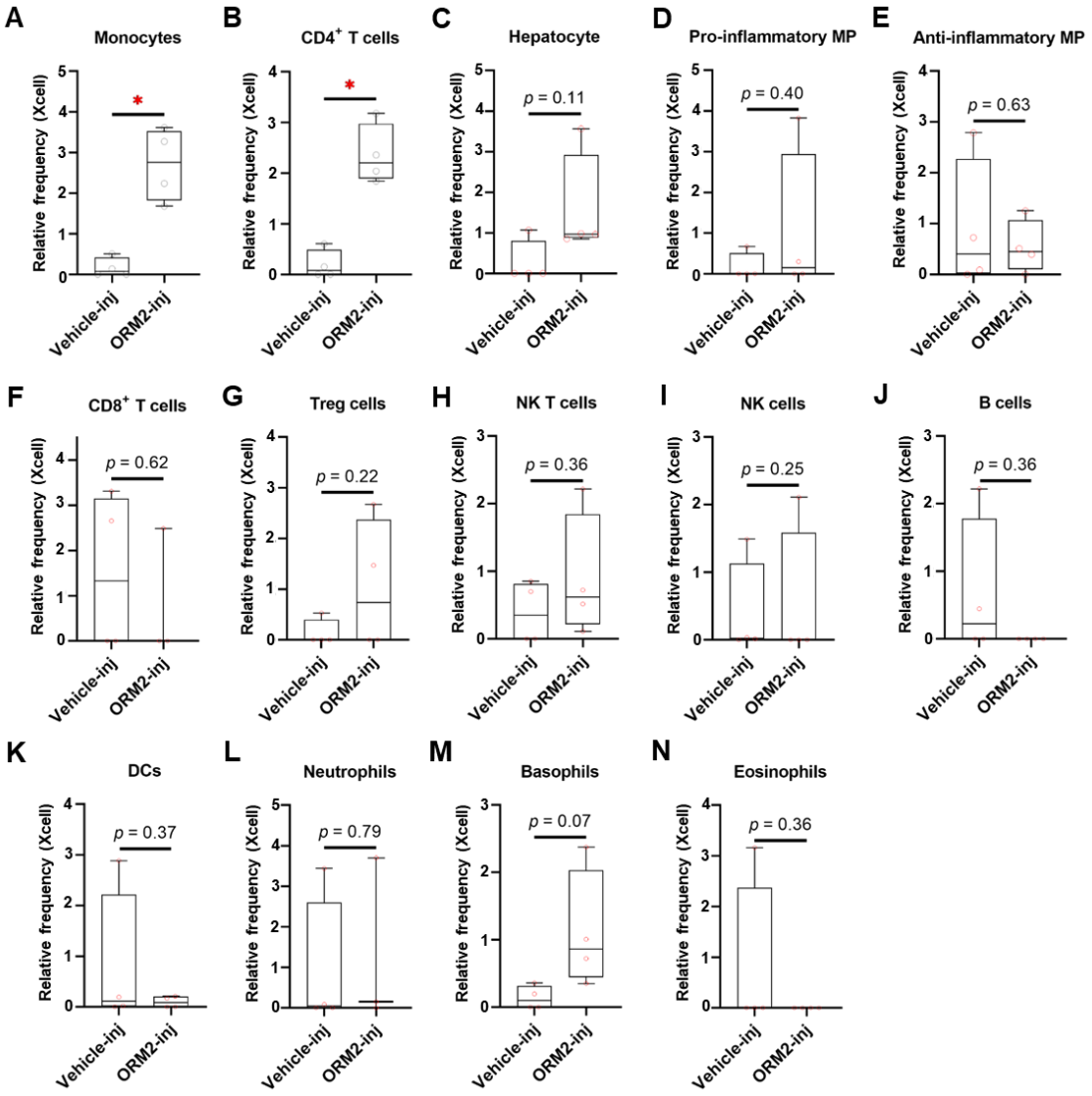

Figure 7. Administration of ORM2 enhances the gene expression of monocyte signatures in mouse liver. Cell frequencies of (A) monocytes, (B) $CD4^+$ T cells, (C) hepatocytes, (D) pro-inflammatory macrophages (MP), (E) anti-inflammatory macrophages, (F) neutrophils, (G) $CD8^+$ T cells, (H) Treg cells, (I) NK T cells, (J) NK cells, (K) B cells, (L) DCs, (M) basophils and (N) eosinophils. Student's t-tests were used. * represents $p < 0.05$.

4.3.2. Upregulation of ORM2 is associated with monocytic accumulation towards ductular reaction

Multiplex immunohistochemistry and image analysis approaches were employed to depict spatial correlation among cholangiocytes, monocytes/macrophages and ORM2. It was distinctly observed that, notably, monocytes/macrophages presented located close to ductular cells, which also highly expressed ORM2 protein (**Figure. 8A**). In-depth quantitative analysis and correlation illustrated that the intensity of the ORM2

signal was positively correlated with the intensity of the ductular cell (CK19^{+} and CK7^{+}) signal, as well as monocyte (IBA^{+}) numbers in neighbors (**Figure. 8B**). Taken together, ORM2 that derives from ductular cells is significantly associated with monocytes in MASH livers.

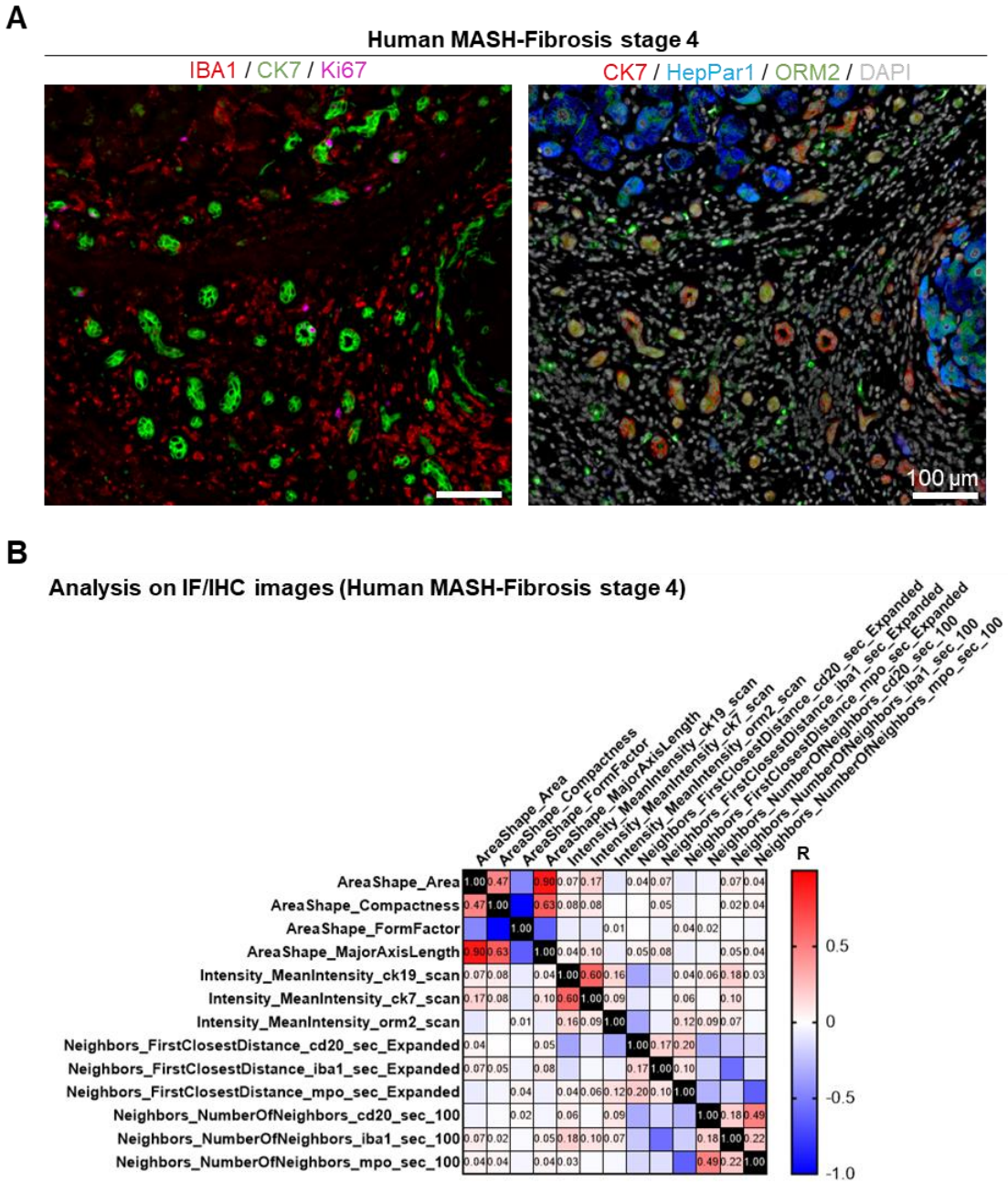

Figure 8. Upregulation of ORM2 is associated with monocytic accumulation towards ductular cells. (A) Multiplex immunohistochemistry demonstrates close correlations among cholangiocytes (CK7^{+}), monocytes/macrophages (IBA^{+}), and ORM2. The HepPar1 marker indicates hepatocytes. The Ki67 marker indicates proliferating cells. Images depict the same field of view from a singular tissue section. (B) Quantitative and correlation analysis on multiplex immunohistochemistry images are depicted in a matrix plot. The R values of

correlation coefficient are indicated with statistical significance ($p < 0.05$).

4.3.3. *Orm2* gene interference on cholangiocytes

Orm2 expression was measured in three mouse cholangiocyte linages (primary WT BECs, WT Od-BECs and MDR2$^{-/-}$ Od-BECs), which showed that MDR2-/- OD-BECs expressed higher levels of *Orm2* than other BECs (**Figure. 9A**). siRNA (targeting *Orm2*) transfection successfully suppressed the gene expression and protein levels of ORM2 in Od-BECs (**Figure. 9B and 9C**). However, si*Orm2* + biliatresone drastically caused cell damage compared to other groups (**Figure. 9C**). Therefore, *Mdr2*$^{-/-}$ Od-BECs was used for further investigations of BECs in this study.

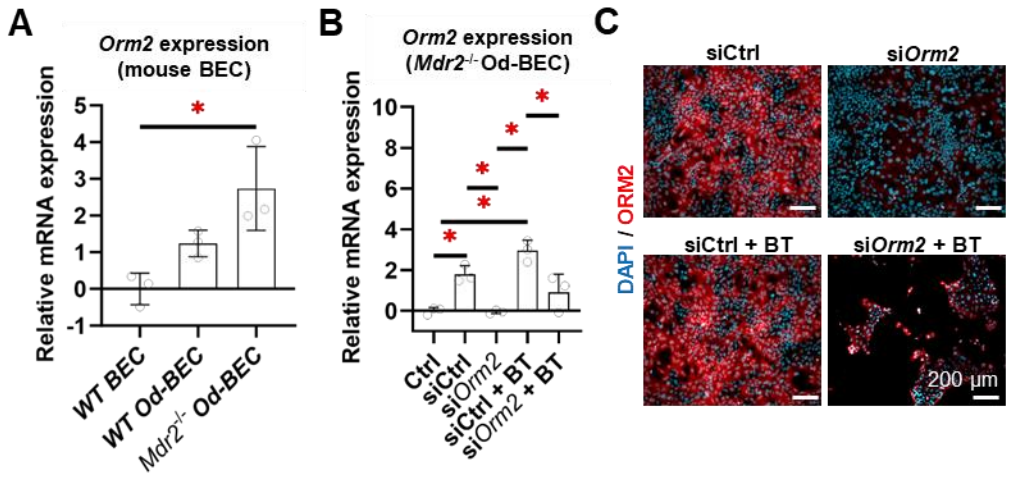

Figure 9. siRNA transfection suppresses Orm2 gene expression in cholangiocytes. (A) Gene expression of *Orm2* on primary WT BECs, WT Od-BECs and *Mdr2*$^{-/-}$ Od-BECs. (B) Gene expression and (C) fluorescent observation of ORM2 on mouse cholangiocytes upon siCtrl and si*Orm2* transfection ± biliatresone treatment. WT: wild-type; Od: organoid-derived; BT: biliatresone. A one-way ANOVA test was used. * represents $p < 0.05$.

4.3.4. Biliary niche-on-a-chip (BoC) system recapitulates monocyte attraction by cholangiocyte-derived ORM2

To investigate the ORM2 effects on immune modulation in the biliary niche, Od-BECs, HSCs (from Act CFP mice), LSECs and liver macrophages were seeded in the BoC system, with siCtrl and si*Orm2* transfected into BECs. Fresh CICs from reporter mice (Act CFP) were introduced to the circulation of the BoC (**Figure. 10A**). In addition,

CICs remaining in the perfusate were collected for flow cytometry measurements (**Figure. 10B**), whereby total immune cells ($CD45^+$), B cells, $CD4^+$ T cells, $CD8^+$ T cells, monocytes, neutrophils, DCs $CCR2^+$ cells and $Cr1^+CD11b^+$ cells were distinguished. In line with this, fresh CICs from reporter mice (Act DsRed) were perfused in the BoC. CICs (β-Actin+) that emigrated to membranes were recorded (**Figure 10C**), showing that CIC accumulation was significantly decreased with Orm2-interfering BECs (vs. BEC-siCtrl) (**Figure. 10D**). The numbers of monocytes that emigrated to membranes were significantly reduced with *Orm2*-interfering BECs (*vs.* Ctrl-BECs) (**Figure. 10E**). Taken together, these results indicate that BEC-derived ORM2 can exacerbate monocyte accumulation in the biliary niche.

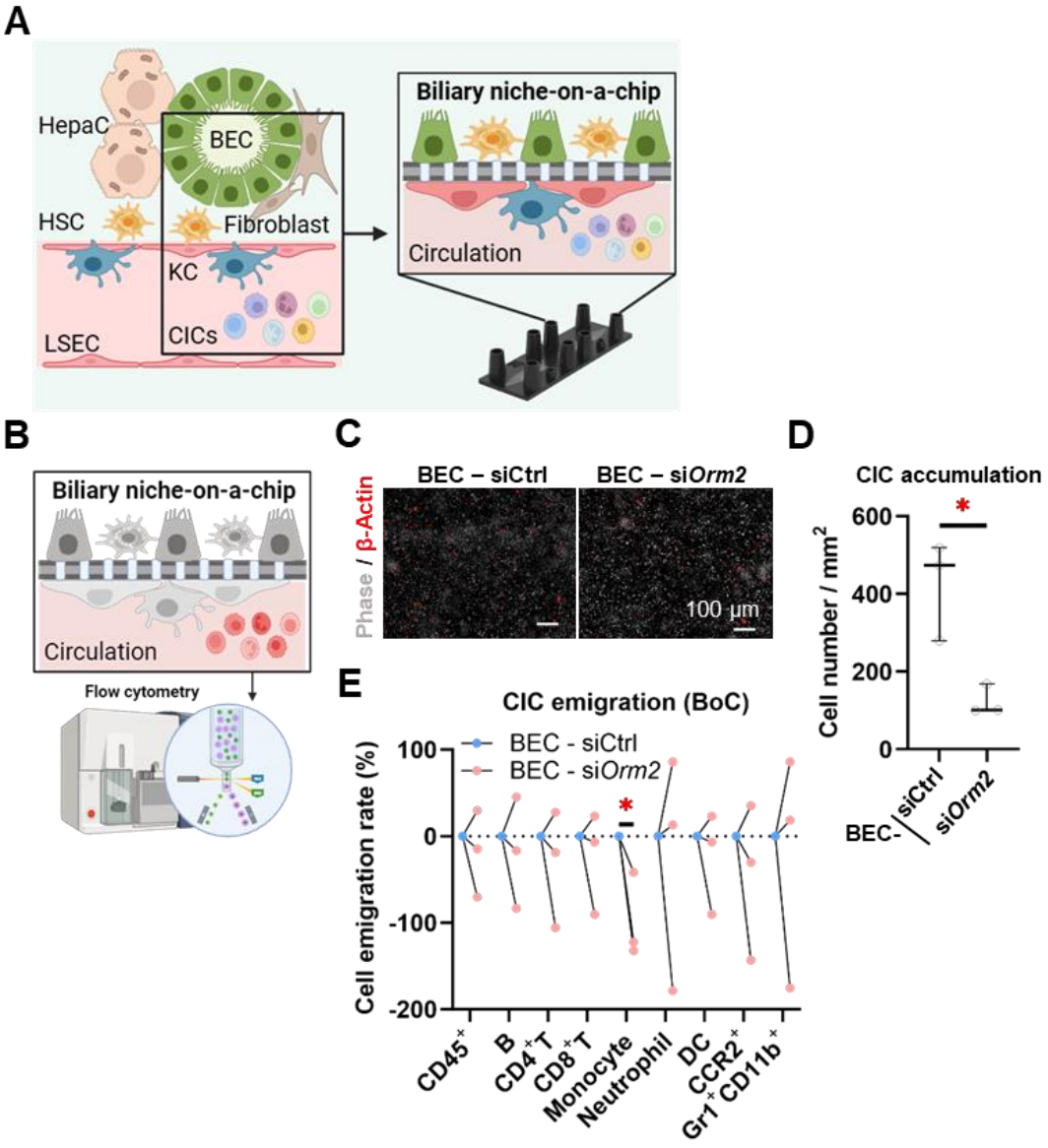

Figure 10. Cholangiocyte-derived ORM2 exacerbates monocyte accumulation in the BoC. Schematic diagrams of the (A) BoC system and (B) CIC measurement via microscope or flow cytometry. CICs were isolated from reporter mice (Act DsRed or Act CFP). (C) Fluorescent observation and (D) quantitative analysis of CIC (β-Actin$^+$) that emigrated to membrane. (E) Emigration of total immune cells (CD45$^+$), B cells, CD4$^+$ T cells, CD8$^+$ T cells, monocytes, neutrophils, DCs CCR2$^+$ cells and Gr1$^+$CD11b$^+$ cells from the perfusate to the LoC indirectly assessed by flow cytometry on the remaining perfusate cells. Student's t-tests were used. * represents $p < 0.05$.

4.3.5. Biliary niche-on-a-chip (BoC) system recapitulates influences of cholangiocyte-derived ORM2

To investigate the ORM2 effects in the biliary niche, Od-BECs, HSCs (from Act DsRed mice), LSECs and liver macrophages were seeded in the BoC system, with siCtrl and si*Orm2* transfected into BECs. Firstly, BECs and HSCs were observed on the upper side of the membrane (**Figure. 11A**). BEC proliferation (Ki67$^+$F-Actin$^+$β-Actin$^-$) was not significantly changed, while COL1A1 levels were declined with *Orm2*-interfering BECs (*vs.* BEC-siCtrl) (**Figure. 11B, 11C and 11D**). Simultaneously, HSC (β-Actin$^+$) was observed from the membrane (**Figure. 11E and 11F**), showing that the HSC area was significantly decreased with *Orm2*-interfering BECs (*vs.* BEC-siCtrl) (**Figure. 11G**). In addition, a group of genes (*Ifng*, *Tjp1*, *Spp1*, *Mki67*, *Cldn1*, *Acta2*, *Cxcl5*, *Col1a1*, *Il23*, *Tgfb1*, *Vcam1*, *Il10*, *Icam1*, *Pecam1*, *Ocln*, *Tnfa*, *Il6*, *Il1a*, *Ccl5*, *Orm2*, *Ccl2*, *Pdgfrb* and *Il1b*) was measured on cells adhering to the membranes, which revealed that expression of *Il1b*, *Pdgfrb*, *Ccl2*, *Orm2* and *Ccl5* was suppressed with *Orm2*- interfering BECs (*vs.* BEC-siCtrl) (**Figure. 11H**). Taken together, the results indicate that BEC-derived ORM2 can exacerbate fibrogenesis while attenuating cell proliferation in the biliary niche.

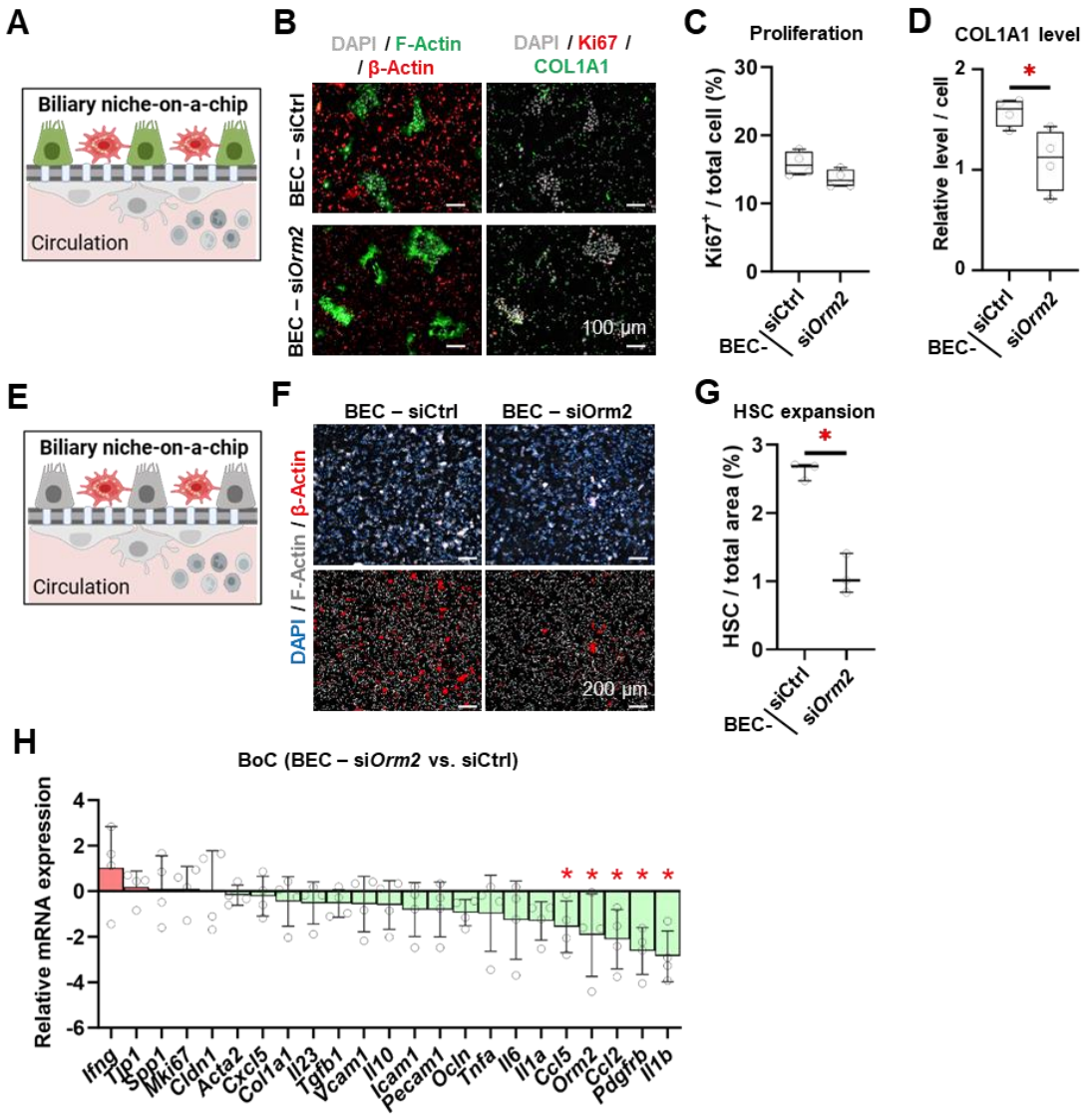

Figure 11. Cholangiocyte-derived ORM2 exacerbates fibrogenesis but attenuates cell proliferation in the BoC. (A) Scheme of HSC and BEC observation in BoC. (B) Fluorescent observation, as well as quantitative analysis of (C) Ki67^{+} cells and (D) COL1A1 levels. (E) Scheme of HSC observation in BoC. (F) Fluorescent observation and (G) quantitative analysis of β-Actin areas. (H) Expression of *Ifng*, *Tjp1*, *Spp1*, *Mki67*, *Cldn1*, *Acta2*, *Cxcl5*, *Col1a1*, *Il23*, *Tgfb1*, *Vcam1*, *Il10*, *Icam1*, *Pecam1*, *Ocln*, *Tnfa*, *Il6*, *Il1a*, *Ccl5*, *Orm2*, *Ccl2*, *Pdgfrb* and *Il1b* measured on cells from membranes. Student's t-tests were used. * represents $p < 0.05$.

4.3.6. Micro-coculture chamber system recapitulates influences of cholangiocyte-derived ORM2

To investigate the ORM2 effects on multi-cellular crosstalk, Od-BECs, HSCs and liver macrophages were seeded in a micro-coculture chamber, while Od-BECs were transfected with siCtrl and si*Orm2* (**Figure. 12A**). The switch of cellular crosstalk was

administrated by changing volumes of culture medium (**Figure. 12B**). Within this multicellular system, higher potentials of proliferation ($Ki67^{+}$) were revealed with *Orm2*-interfering BECs (*vs.* BEC-siCtrl) (**Figure. 12C and 12D**). Furthermore, *Orm2*-interfered BECs reduced single HSC cytoplasmic areas (*vs.* BEC-siCtrl), revealing a reduced activation towards a myofibroblast phenotype (**Figure. 12E and 12F**). The results indicate that BEC-derived ORM2 can suppress the growth of BECs but promote fibrogenesis of HSCs.

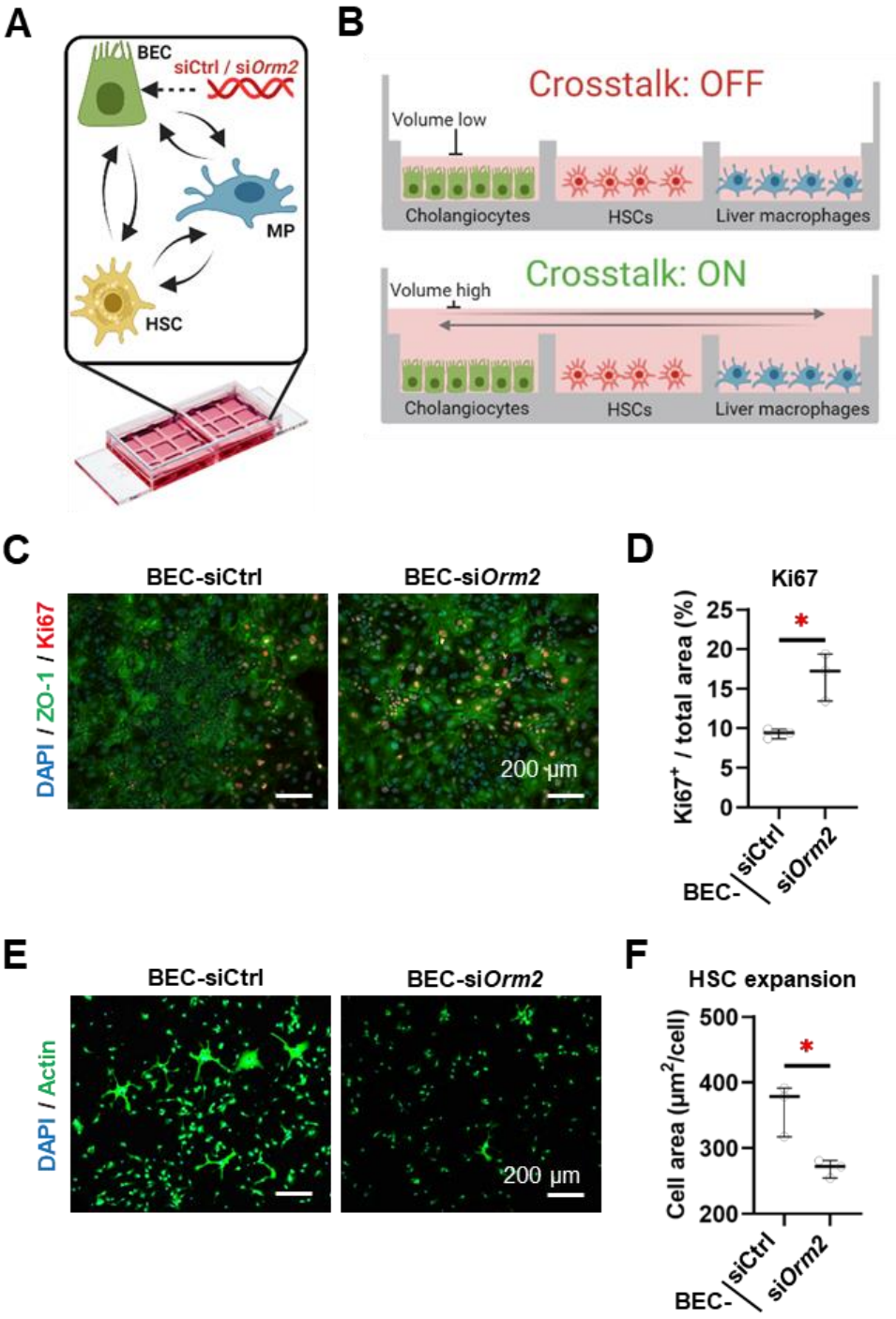

Figure 12. Cholangiocyte-derived ORM2 suppresses the growth of cholangiocytes but promotes fibrogenesis of HSCs in presence of liver macrophages. (A) Schematic diagram of micro-coculture chamber system. (B) Fluorescent observation and (C) quantitative analysis of Ki67 protein in organoid-derived BECs upon BEC-siCtrl and BEC-si*Orm2* transfection. (E) Fluorescent observation and (F) quantitative analysis of cell expansion in HSCs upon BEC-siCtrl and BEC-si*Orm2* transfection. Student's t-tests were used. * represents $p < 0.05$.

4.4. ORM2 induces liver macrophage reprogramming

4.4.1. ORM2 induces transcriptome alterations of liver macrophages

To understand the influences of ORM2 on macrophages, macrophages from diverse established sources (human THP-1 cell line, human MoMFs, mouse liver F4/80$^+$ cells and mouse MOMFs) were collected and treated with human or mouse recombinant ORM2 protein for 24 hours. A list of macrophage-associated target genes (*MRC1*, *CD163*, *IL6*, *IL10*, *TGFB1*, *TNFA*, *IL1B*, *TNFRSF12A*, *NLRP1*, *NLRP2*, *NLRP3*, *NLRC4*, *AIM2*, *CASR*, *MYD88*, *IRAK4*, *IKBKG*, *NFKIBA*, and their mouse orthologs) were measured respectively. Interestingly, different macrophages presented variable expression levels of these genes, and thereby similar changes can be revealed between human THP-1 cells and mouse liver macrophages, as well as between human and mouse MOMFs (**Figure. 13A**). Mouse liver macrophages were selected in the following studies. Cell proliferation of liver macrophages upon untreated, gradient concentrations of ORM2 and 100 ng/mL LPS were assessed, and no significant differences were elucidated (**Figure. 13B**). Furthermore, mouse liver macrophages with/without 1 μg/mL ORM2 treatment were sampled and processed for whole transcriptome analysis. DEGs were illustrated in a volcano plot, showing 452 significantly upregulated and 115 significantly downregulated genes (ORM2-treated *vs.* untreated) (**Figure. 13C**). The top 20 upregulated and downregulated genes were listed in all samples (**Figure. 13D**). Function enrichment analysis indicates that ORM2-treated macrophages are actively involved in cell communications, immune responses, secretion, and lipid response, potentially via activation of several key signaling pathways (e.g., PI3K/Akt, Jak-STAT, cAMP, cGMP-PKG pathways) (**Figure. 13E**). In addition, a bulk RNA-seq dataset from LPS-treated mouse liver macrophages was retrieved, from which it was determined that ORM2 exerts distinctly different influences on liver macrophages in comparison to LPS (**Figure. 13F**). The results indicate that ORM2 strongly alters the transcriptome profiles of liver macrophages.

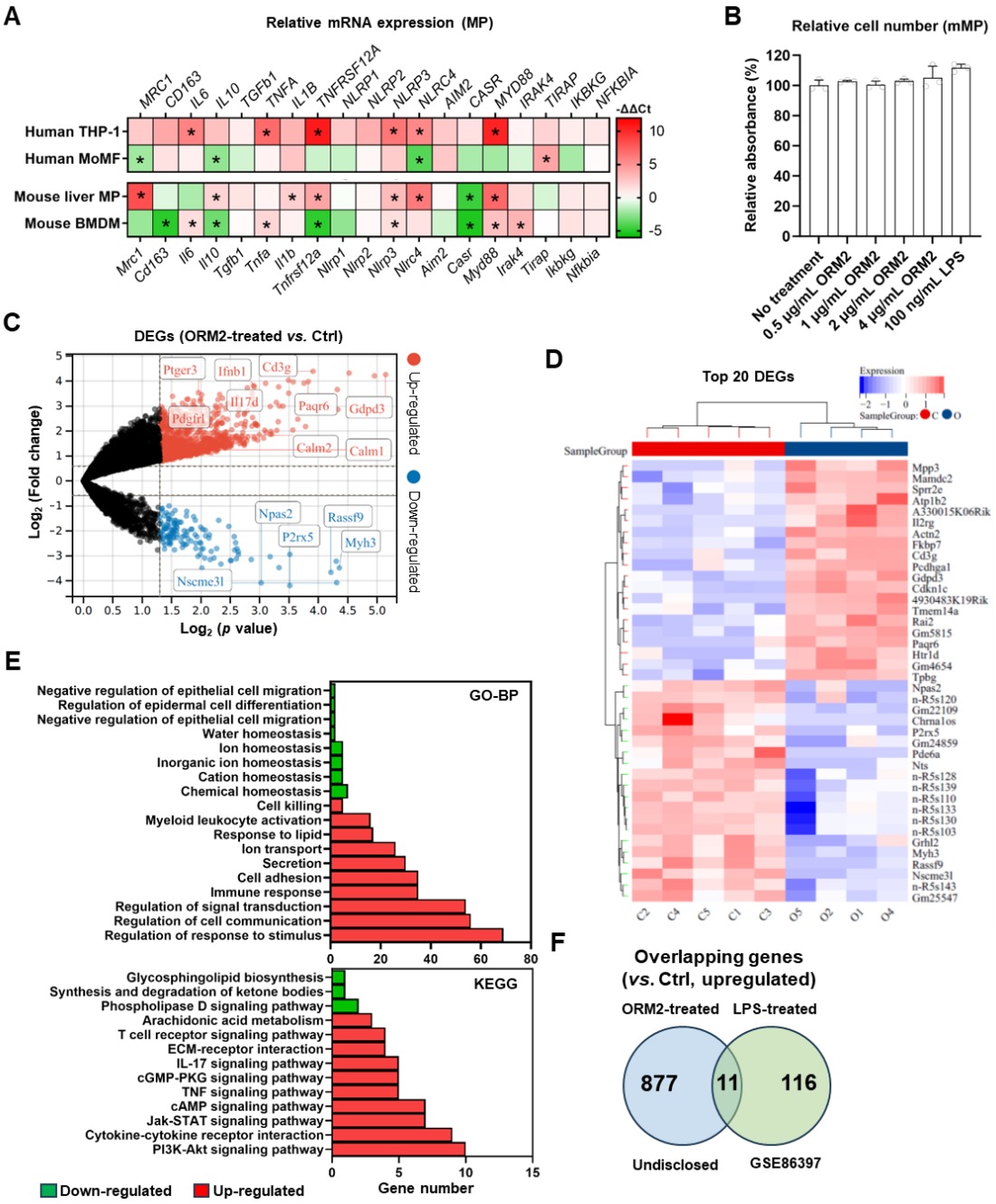

Figure 13. ORM2 induces potent transcriptome alterations in liver macrophages. (A) mRNA expression of target genes measured on human THP-1 cell line, human MoMFs, mouse liver F4/80^{+} cells and mouse MOMFs. (B) Relative cell numbers of mouse liver macrophages upon untreated, gradient concentrations (0.5, 1, 2 and 4 μg/mL) of ORM2 and 100 ng/mL LPS. (C) Volcano plot depicting DEGs (ORM2-treated *vs.* Ctrl). (D) Heatmap depicting top 20 significantly up-/downregulated DEGs (ORM2-treated *vs.* Ctrl). (E) GO-biological process (BP) and KEGG function enrichment on significant upregulated genes (ORM2-treated *vs.* Ctrl). (F) Significantly overlapping DEGs between ORM2- and LPS-treated mouse liver macrophages (each *vs.* Ctrl). The dataset of LPS-treated mouse liver macrophages was obtained from the public database. Student's t-tests were used. * represents $p < 0.05$.

4.4.2. ORM2 increases liver macrophage phagocytic functions

With regard to several key pathways (e.g., JAK-STAT) that were significantly induced by ORM2, the highly relevant macrophage feature of phagocytosis was evaluated on liver macrophages. Fluorescent YG beads captured by macrophages ($Actin^{+}$) were recorded after 30 min incubation (**Figure. 14A**), showing that ORM2 and LPS treatments significantly increased phagocytosis of liver macrophages (**Figure. 14B**). In addition, TIM4, a phagocytosis-related marker, was assessed on liver macrophages using ICC (**Figure. 14C**), showing that ORM2 and LPS treatments significantly increased TIM4 protein levels on liver macrophages (**Figure. 14D**). The results indicate that ORM2 can enhance the phagocytosis capacity of liver macrophages to a similar level as LPS.

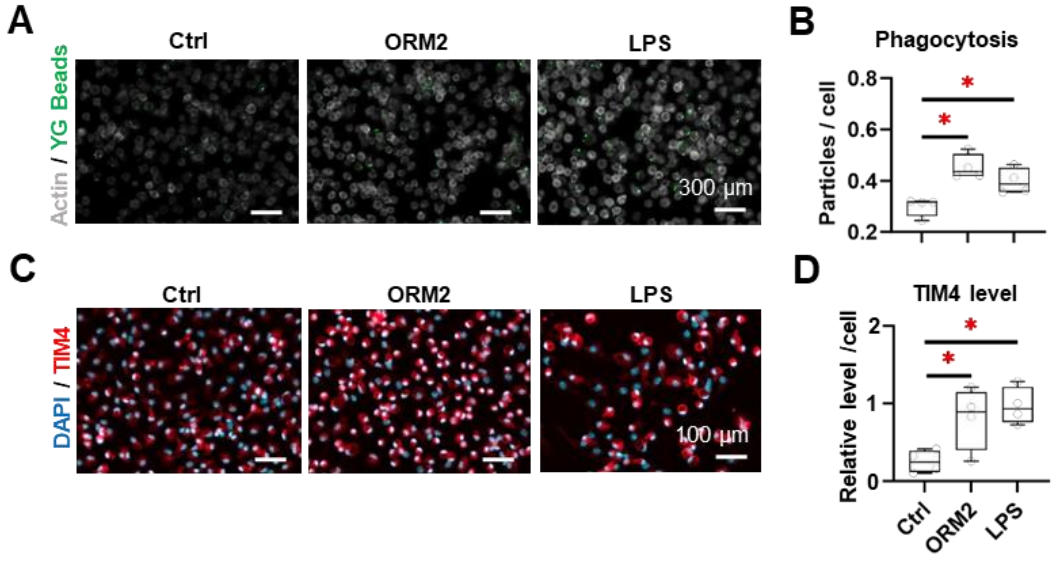

Figure 14. ORM2 favors macrophage phagocytosis. (A) Fluorescent observation and (B) quantitative analysis of phagocytosed YG beads upon ORM2 and LPS treatments. (C) Fluorescent observation and (D) quantitative analysis of TIM4 protein levels in mouse liver macrophages upon ORM2 and LPS treatments. A one-way ANOVA test was used. * represents $p < 0.05$.

4.4.3. ORM2 enhances lipid intake in liver macrophages

Lipid metabolism is regarded as one of key biological functions in liver macrophages. Accordingly, FFAs were introduced on ORM2-treated/untreated mouse liver macrophages. Then, the cellular lipid accumulation was exhibited using BODIPY dye

(**Figure. 15A**), showing that ORM2 increased lipid intake of liver macrophages (**Figure. 15B**). In addition, the CD36 protein levels of liver macrophages were increased by ORM2 and LPS treatments (**Figure. 15C and 15D**). The results indicate that ORM2 may enhance the lipid handling capacity of liver macrophages.

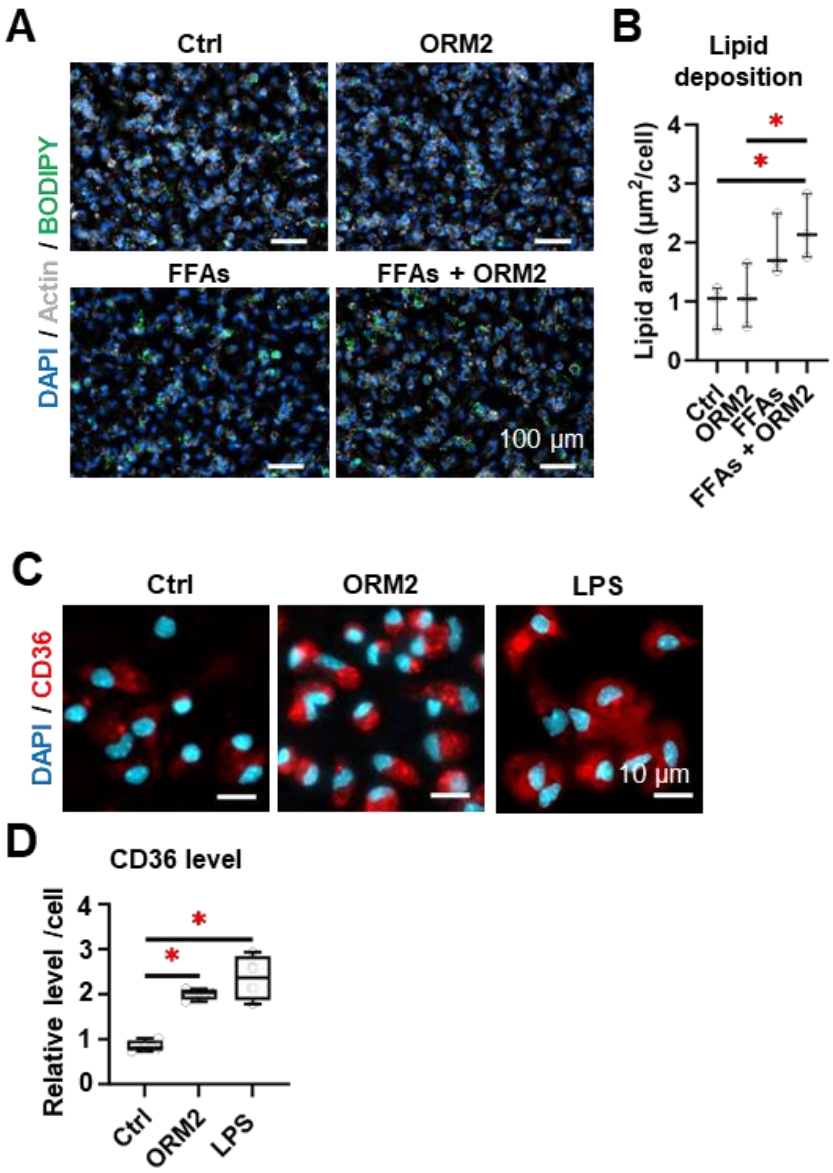

Figure 15. ORM2 influences macrophage lipid metabolism. (A) Fluorescent observation and (B) quantitative analysis of cellular lipid accumulation in mouse liver macrophages upon FFAs ± ORM2 treatments. (C) Fluorescent observation and (D) quantitative analysis of CD36 protein levels in mouse liver macrophages upon LPS and ORM2 treatments. A one-way ANOVA test was used. * represents $p < 0.05$.

4.4.4. ORM2 induces cellular stress processes in liver macrophages

Cell stress was also evaluated on macrophages treated with ORM2 and LPS. SA-β-

GAL, a key marker for cell-cycle arrest, was detected on liver macrophages (**Figure. 16A**), showing that ORM2 and LPS treatments induced cell-cycle arrest and potential senescence (**Figure. 16B**). In parallel, Apopxin, reflecting apoptosis occurrence, was detected on liver macrophages (**Figure. 16C**), showing that ORM2 and LPS treatments induced cellular apoptosis (**Figure. 16D**). The results indicate that ORM2 can exacerbate macrophage stress.

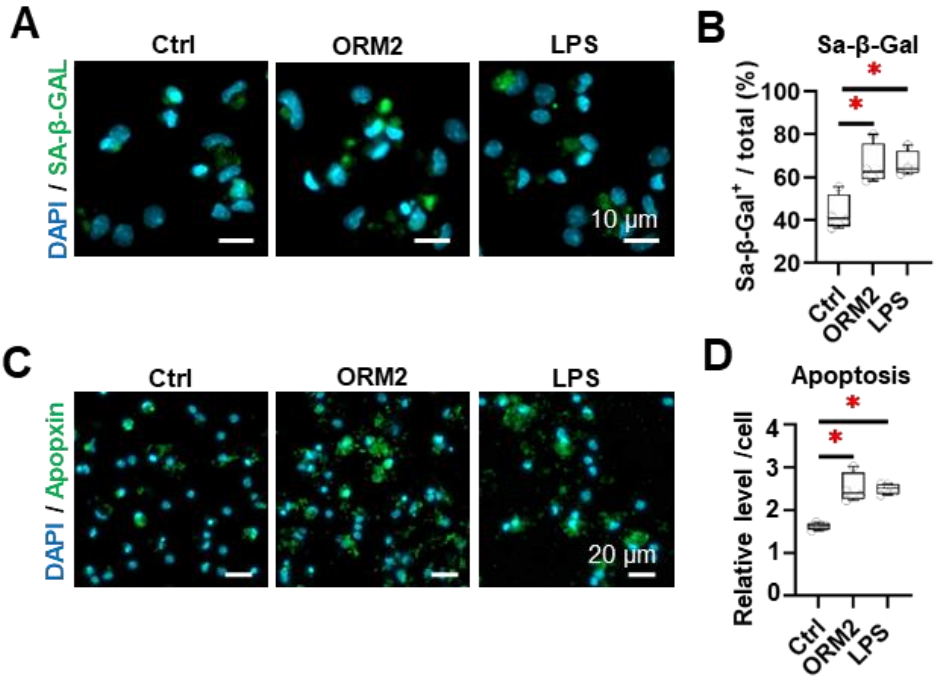

Figure 16. ORM2 induces macrophage stress processes. (A) Fluorescent observation and (B) quantitative analysis of SA-β-GAL levels in mouse liver macrophages upon ORM2 and LPS treatments. (C) Fluorescent observation and (D) quantitative analysis of Apopxin levels in mouse liver macrophages upon LPS and ORM2 treatments. A one-way ANOVA test was used. * represents $p < 0.05$.

4.5. ORM2-activated macrophages influence their microenvironment in the biliary niche

4.5.1. ORM2 enhances inflammatory cytokine secretion by liver macrophages

Based on the whole transcriptome profile of mouse liver macrophages, expression differences of secretome were depicted in a volcano plot (**Figure. 17A**). A group of

inflammatory cytokines (including CCL-2, IL-1α, IL-1β, IL-6, IL-10, IL-23 and TNF-α) were measured from the cell supernatant, and thereby a significant elevation by ORM2 treatment was determined (**Figure. 17B**). The results indicate that ORM2 significantly enhances the secretome of macrophages.

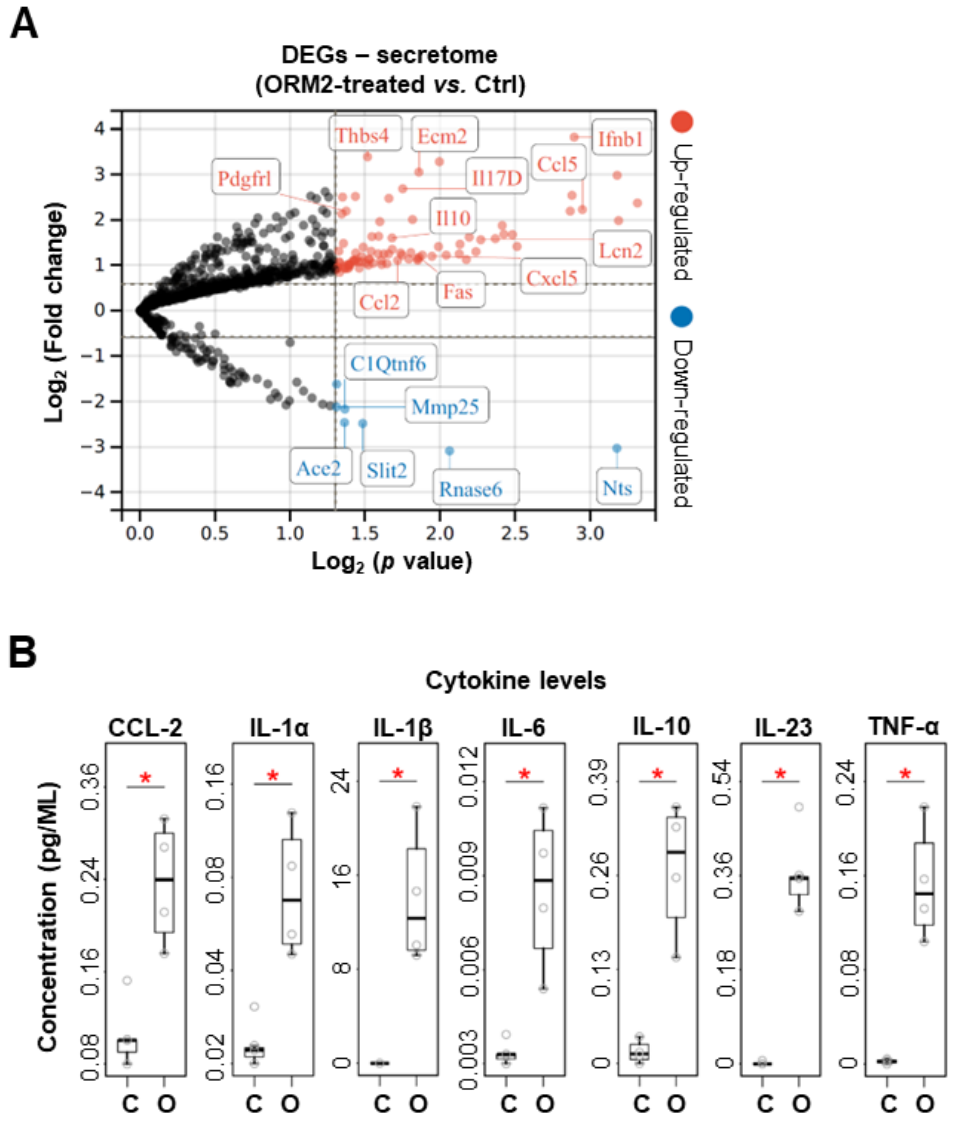

Figure 17. ORM2 induces significant secretome alterations of macrophages. (A) Volcano plot depicting expression differences of macrophage secretome upon ORM2 treatment. (B) Cytokines (CCL-2, IL-1α, IL-1β, IL-6, IL-10, IL-23 and TNF-α) measured from macrophage supernatant upon ORM2 treatment. C: Ctrl; O: ORM2-treated. Student's t-tests were used. * represents $p < 0.05$.

4.5.2. ORM2-activated macrophages influence BECs

To investigate the influences of ORM2-activated macrophages on BECs, proliferative/

organoid-derived (Od) BECs were treated with ORM2-activated macrophage-derived conditioned medium for 24 hours. Cellular proliferation ($Ki67^{+}$) and tight junction ($ZO\text{-}1^{+}$) in *Mdr2*$^{-/-}$ Od-BECs were demonstrated with ORM2, untreated macrophage-derived supernatant and ORM2-treated macrophage-derived supernatant treatments (**Figure. 18A**). ORM2 protein levels were demonstrated in primary BECs with ORM2, untreated macrophage-derived supernatant and ORM2-treated macrophage-derived supernatant treatments (**Figure. 18B**). Quantitative analysis of ORM2 protein levels implied a significant increase by ORM2-treated macrophage-derived supernatant (**Figure. 18C**). In addition, a proliferation tracking assay implied that ORM2-treated macrophage-derived supernatant sustainably impaired BEC growth or viability in 5 days (**Figure. 18D**). The results indicate that ORM2-activated macrophages can impair BEC proliferation but promote ORM2 production.

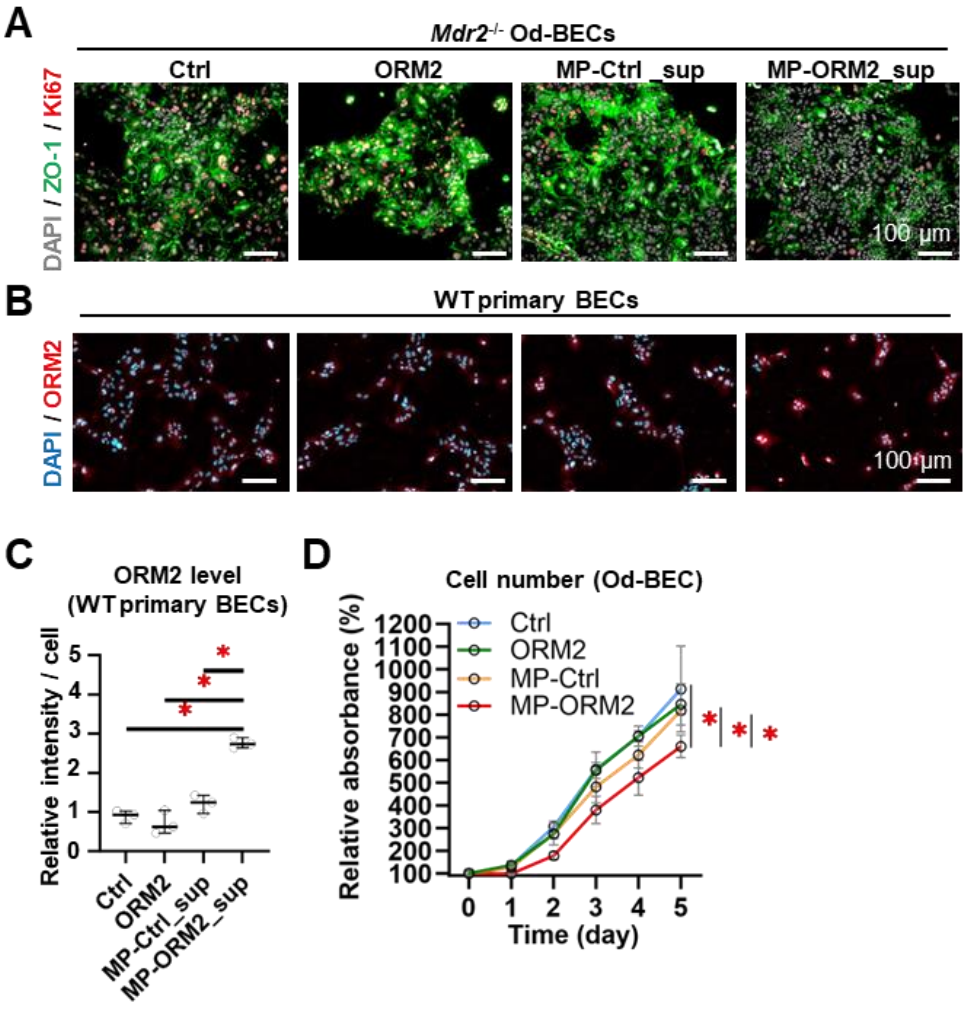

Figure 18. ORM2-activated macrophages exacerbate BEC stress and ORM2 production.

Organoid-derived BECs were cultured in the presence of ORM2-treated liver macrophage conditioned medium. (A) Fluorescent observation of Ki67 and ZO-1 in mouse *Mdr2*$^{-/-}$ Od-BECs as well as (B) fluorescent observation of ORM2 and (C) relative immunostaining intensities in mouse primary BECs upon ORM2, untreated macrophage-derived supernatant and ORM2-treated macrophage-derived supernatant exposure. (D) Dynamic cellular proliferation tracked on mouse Od-BECs within 5 days upon ORM2, untreated macrophage-derived supernatant and ORM2-treated macrophage-derived supernatant exposure. Od-BEC: organoid-derived biliary epithelial cells. MP-Ctrl: conditioned medium from untreated mouse liver macrophages. MP-ORM2: conditioned medium from ORM2-treated mouse liver macrophages. A one-way ANOVA test was used. * represents $p < 0.05$.

4.5.3. ORM2-activated macrophages promote fibrogenesis driven by HSCs

To investigate the influences of ORM2-activated macrophages on HSCs, mouse primary HSCs were treated with ORM2-activated macrophage-derived conditioned medium for 24 hours. Cell size (Actin) and collagen production (COL1A1) were assessed on mouse liver macrophages (**Figure. 19A**), showing that: (1) both untreated macrophage-derived supernatant and ORM2-treated macrophage-derived supernatant promoted HSC expansion, whereas ORM2-treated macrophage-derived supernatant exerted significantly stronger effects (**Figure. 19B**); (2) in COL1A1 protein levels, no significant differences appeared among these four types of interventions (**Figure. 19C**). Taken together, the results indicate that ORM2-activated macrophages can promote HSC-driven fibrogenesis.

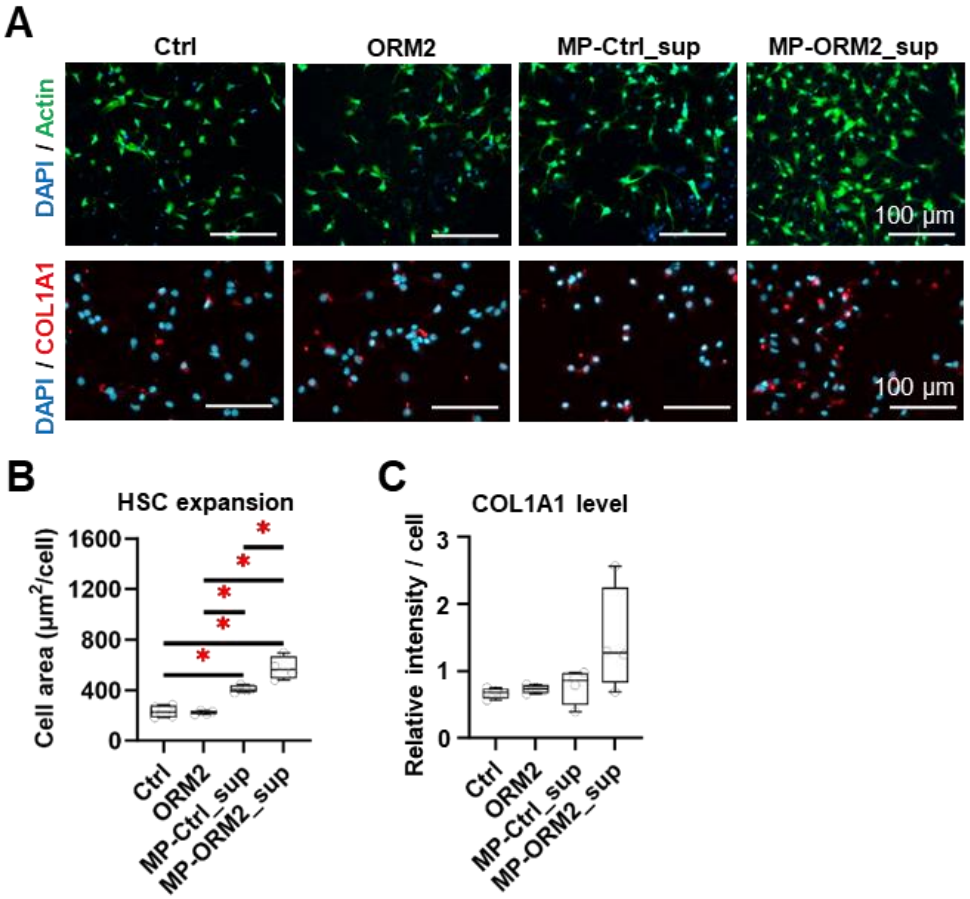

Figure 19. ORM2-activated macrophages promote fibrogenesis mediated by HSCs. (A) Fluorescent observation and quantitative analysis of (B) Actin area and (C) COL1A1 protein levels of mouse HSCs with ORM2, untreated macrophage-derived supernatant and ORM2-treated macrophage-derived supernatant treatments. MP-Ctrl: conditioned medium from untreated mouse liver macrophages. MP-ORM2: conditioned medium from ORM2-treated mouse liver macrophages. A one-way ANOVA test was used. * represents $p < 0.05$.

4.5.4. ORM2-activated macrophages exacerbate cell stress and ORM2 production in Hepatocytes.

To investigate the influences of ORM2-activated macrophages on hepatocytes, mouse primary hepatocytes were treated with ORM2-activated macrophage-derived conditioned medium for 24 hours. ORM2 protein levels were assessed on mouse liver macrophages (**Figure. 20A**), showing that ORM2 directly enhanced ORM2 production by hepatocytes and ORM2-treated macrophage-derived supernatant further amplified this response. Contrastingly, untreated macrophage-derived supernatant suppressed ORM2 production (**Figure. 20B**). Additionally, ORM2-treated macrophage-derived

supernatant significantly reduced hepatocyte numbers (**Figure. 20C**). The results indicate that ORM2-activated macrophages can impair hepatocyte survival but increase their ORM2 production.

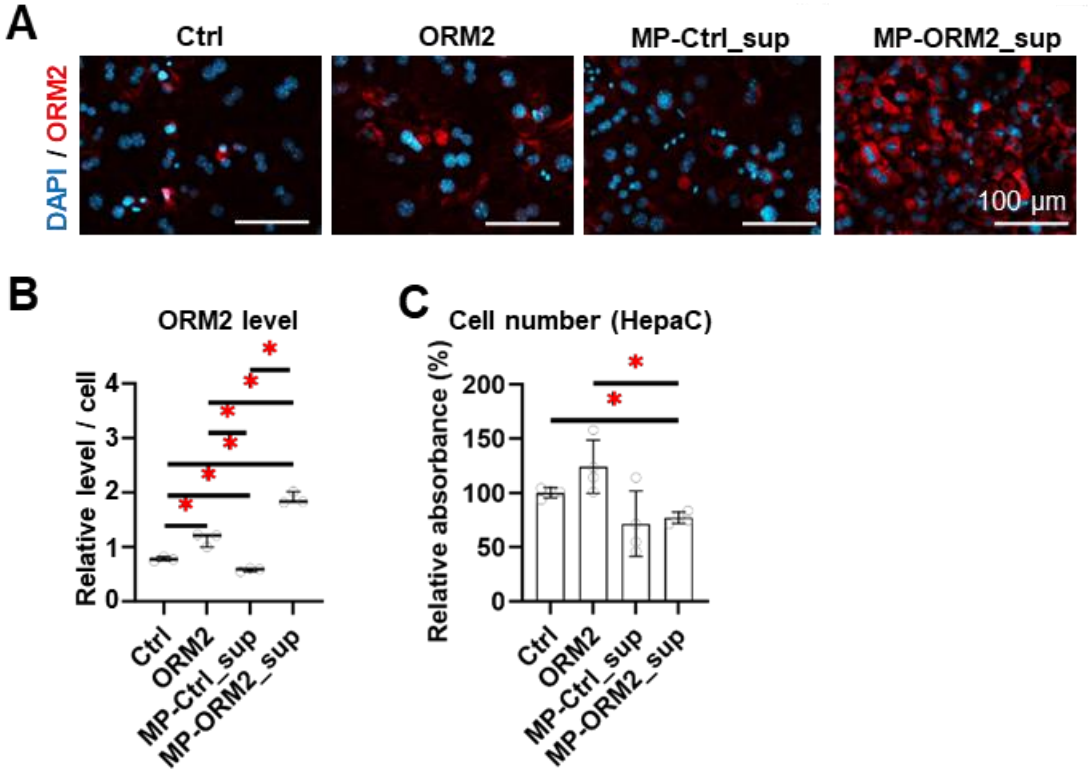

Figure 20. ORM2-activated macrophages exacerbate cell stress and ORM2 production in Hepatocytes. (A) Fluorescent observation and (B) quantitative analysis of ORM2 protein levels of mouse Hepatocytes with ORM2, untreated macrophage-derived supernatant and ORM2-treated macrophage-derived supernatant treatments. (C) Relative cell numbers of Hepatocytes measured with ORM2, untreated macrophage-derived supernatant and ORM2-treated macrophage-derived supernatant treatments. MP-Ctrl: conditioned medium from untreated mouse liver macrophages. MP-ORM2: conditioned medium from ORM2-treated mouse liver macrophages. A one-way ANOVA test was used. * represents $p < 0.05$.

4.5.5. ORM2-activated macrophages induce transcriptome alterations of BECs, HSCs and hepatocytes.

The gene expression of related cell markers (for Od-BEC: *Mki76*, *Ccne1*, *P21*, *Tjp1*, *Cldn1*, *Ocln* and *Orm2*; for HSC: *Acta2*, *Col1a1*, *Tgfb1* and *Pdgfrb*; for Hepatocyte: *Ccne1*, *P21*, *Alb*, *Cyp2e1*, *Orm2* and *Mki67*.) was respectively measured and is depicted (**Figure. 21**). The results indicate from the transcriptome levels that ORM2-activated

macrophages: 1) suppressed *Mki67* expression but enhanced *Orm2* expression of Od-BECs; 2) promote expression of fibrogenesis markers (*Col1a1*, *Tgfb1* and *Pdgfrb*) of HSCs; 3) promote expression of *Orm2*.

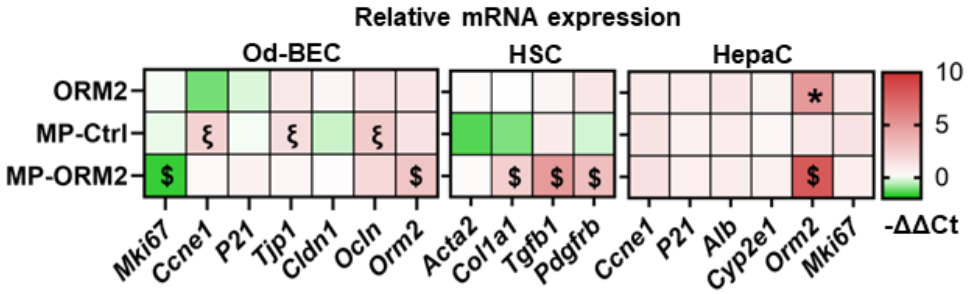

Figure 21. ORM2-activated macrophages alter gene expression of key markers on BECs, HSCs and Hepatocytes. Gene expression of related cell markers (for Od-BEC: *Mki76*, *Ccne1*, *P21*, *Tjp1*, *Cldn1*, *Ocln* and *Orm2*; for HSC: *Acta2*, *Col1a1*, *Tgfb1* and *Pdgfrb*; for Hepatocyte: *Ccne1*, *P21*, *Alb*, *Cyp2e1*, *Orm2* and *Mki67*). MP-Ctrl: conditioned medium from untreated mouse liver macrophages. MP-ORM2: conditioned medium from ORM2-treated mouse liver macrophages. A one-way ANOVA test was used. * represents $p < 0.05$. (ORM2-treated vs. Ctrl). ξ represents $p < 0.05$ (MP-Ctrl treated vs. Ctrl). $ represents $p < 0.05$ (MP-ORM2 treated vs. MP-Ctrl treated).

4.6. ORM2 reprograms liver macrophages through ITPR2-dependent calcium pathway

4.6.1. ORM2 enhances calcium pathway in liver macrophages

According to evidence from previous studies, ORM2 can activate the cellular calcium pathway through binding ITPR2(97). Intracellular calcium level detection illustrated that the calcium intake of liver macrophages can be elevated by ORM2 and LPS but suppressed by 2APB, an inhibitor of calcium transportation (**Figure. 22A**). Gene expression of *Calm1* and *Calm2* was significantly enhanced by ORM2 treatment (**Figure. 22B**). CALM1/2/3 protein levels were increased by ORM2 (**Figure. 22C and 22D**). Taken together, ORM2 can enhance the calcium pathway in liver macrophages.

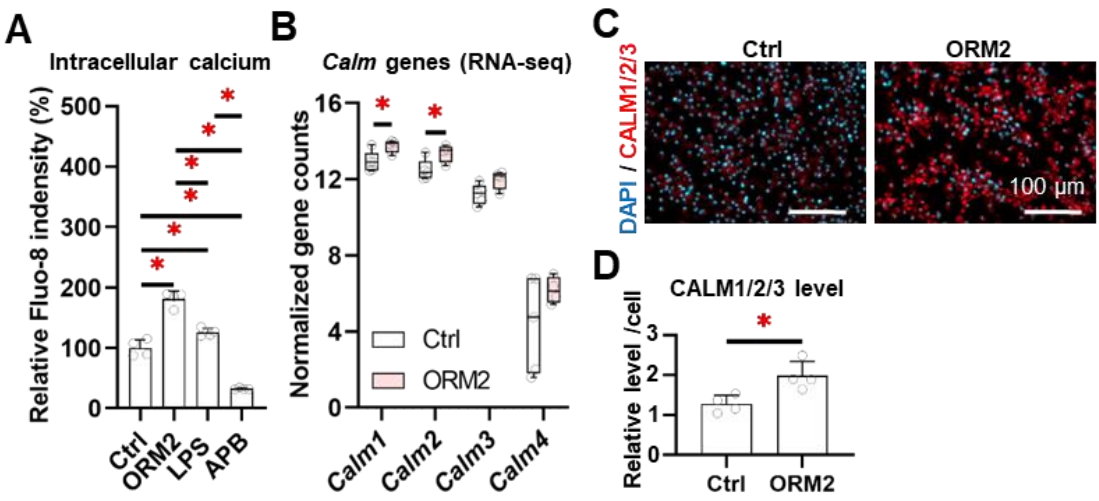

Figure 22. ORM2 enhances calcium pathway in liver macrophages. (A) Intracellular calcium levels measured on mouse liver macrophages upon ORM2, LPS and 2APB treatments. (B) Expression of *Calm1*, *Calm2*, *Calm3* and *Calm4* measured on mouse liver macrophages. (C) Fluorescent observation and (D) quantitative analysis of CALM1/2/3 protein levels of mouse liver macrophages upon ORM2 treatments. The Student's t-test and one-way ANOVA test were used. * represents $p < 0.05$.

4.6.2. ORM2 activates calcium pathway through ITPR2

The siRNA transfection was introduced to suppress *Itpr2* gene expression of mouse liver macrophages. Successful *Itpr2* gene interference was conducted to effectively suppress ITPR2 production (**Figure. 23A and 23B**). Notably, gene expression and protein levels of CALM1/2 remarkably declined upon *Itpr2* gene interference, blocking ORM2 influences (**Figure. 23C, 23D and 23E**). In addition, intracellular calcium levels remarkably declined upon *Itpr2* gene interference, blocking ORM2 influences (**Figure. 23F)**. The results indicate that ORM2 activates the calcium pathway through ITPR2.

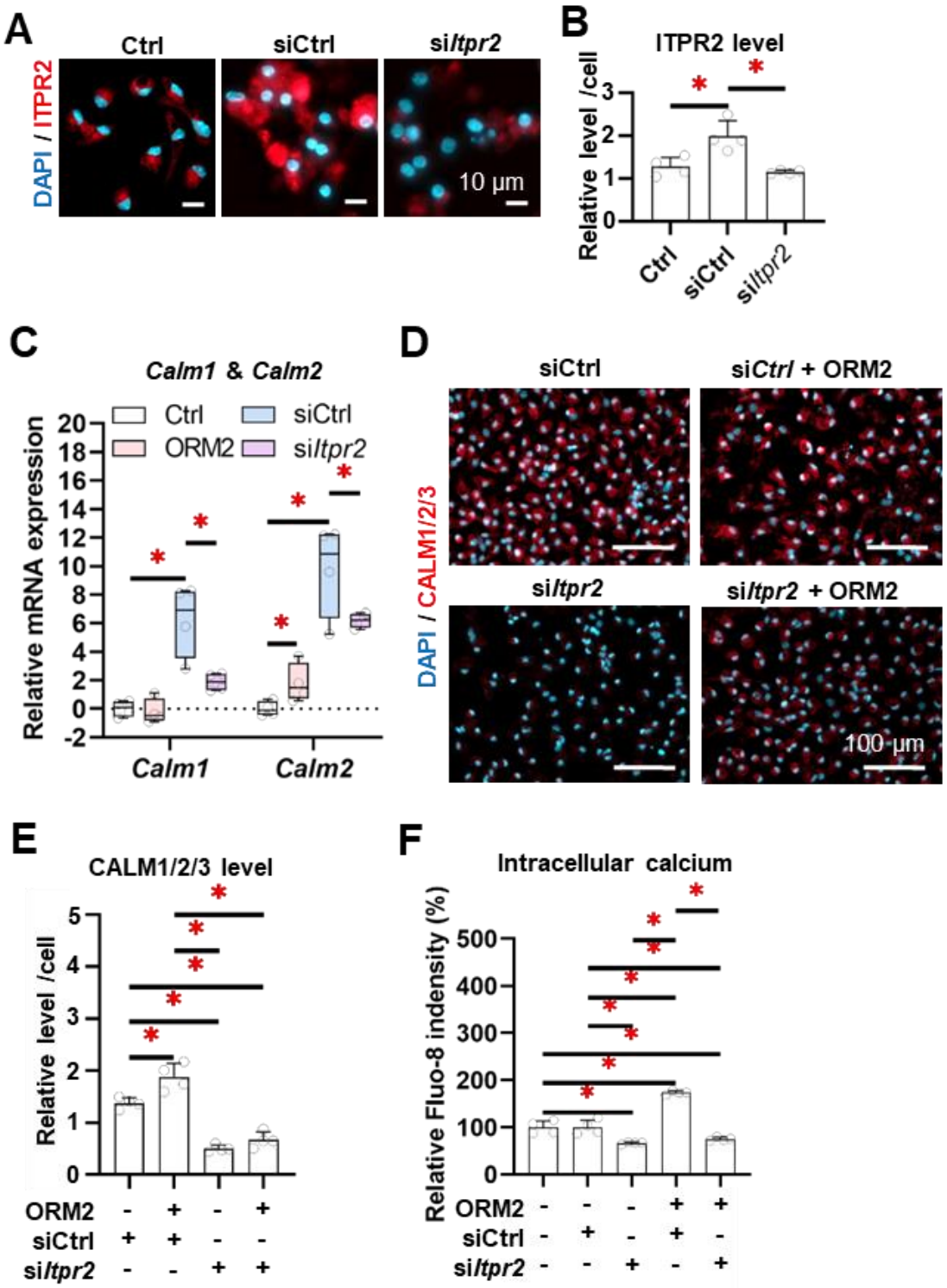

Figure 23. ITPR2 mediates the calcium-dependent functional effects of ORM2 on liver macrophages. (A) Fluorescent observation and (B) quantitative analysis of ITPR2 protein levels of mouse liver macrophages upon siRNA transfection. (C) Gene expression of *Calm1* and *Calm2*, as well as (D) (E) protein levels of CALM1/2/3 detected on mouse liver macrophages. (F) Intracellular calcium levels measured on mouse liver macrophages upon *Itpr2* gene interference. A one-way ANOVA test was used. * represents $p < 0.05$.

4.6.3. ORM2 regulates macrophage phagocytosis through ITPR2

Upon *Itpr2*/Ctrl interference ± ORM2 treatment, phagocytosis was evaluated on mouse liver macrophages. ORM2 significantly enhanced macrophage phagocytosis under both siCtrl and si*Itpr2* transfection, while si*Itpr2* + ORM2 attenuated macrophage phagocytosis compared to siCtrl + ORM2 (**Figure. 24A and 24B**). Simultaneously, ORM2 significantly enhanced TIM4 protein levels under both siCtrl and si*Itpr2* transfection, while si*Itpr2* + ORM2 did not lead to significant differences of TIM4 levels compared to siCtrl + ORM2 (**Figure. 24C and 24D**). The results indicate that ITPR2 downregulation may suppress the effects of ORM2 on phagocytosis enhancement.

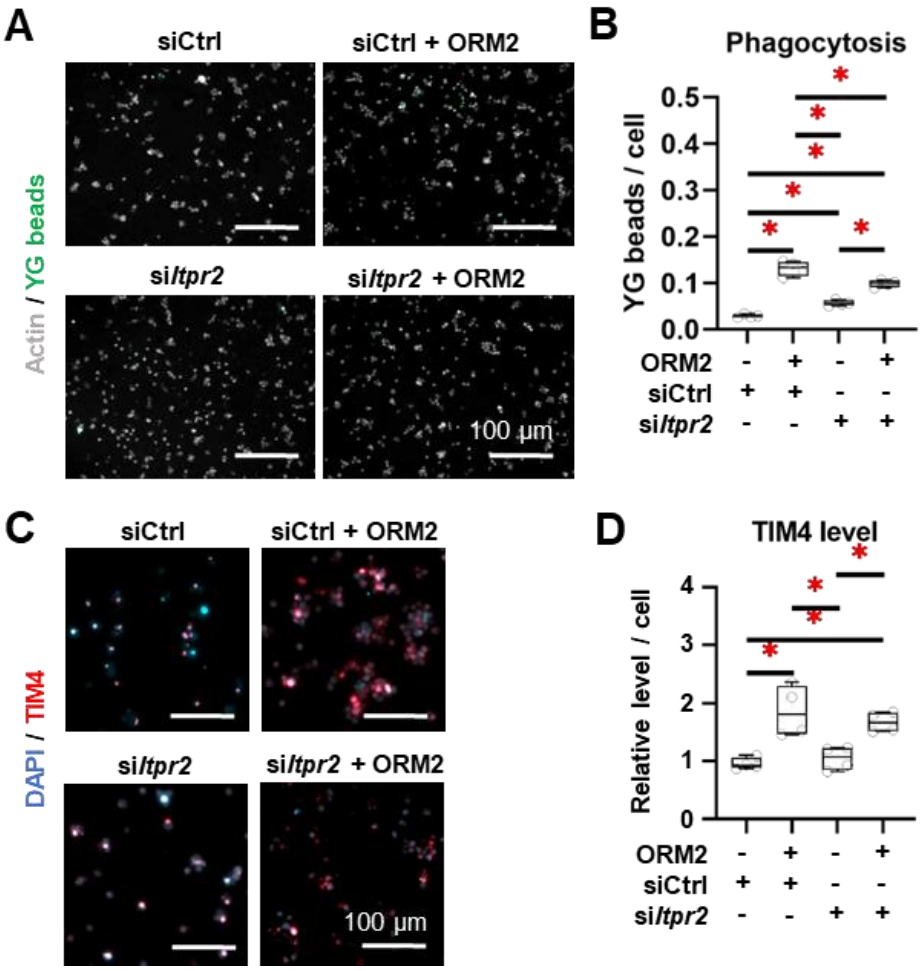

Figure 24. ORM2 regulates macrophage phagocytosis through ITPR2. (A) Fluorescent observation and (B) quantitative analysis of YG beads captured by mouse liver macrophages upon *Itpr2*/Ctrl interference ± ORM2 treatment. (C) Fluorescent observation and (D) quantitative analysis of TIM4 protein in mouse liver macrophages upon *Itpr2*/Ctrl interference ± ORM2 treatment. A one-way ANOVA test was used. * represents $p < 0.05$.

4.6.4. ORM2 enhances macrophage lipid metabolism through ITPR2

Upon the *Itpr2*/Ctrl interference ± ORM2 treatment, the lipid metabolism was evaluated on mouse liver macrophages (cells were treated together with FFAs at the baseline level). ORM2 significantly enhanced macrophage lipid accumulation under siCtrl but not si*Itpr2* transfection (**Figure. 25A and 25B**). Simultaneously, ORM2 significantly enhanced CD36 protein levels under both siCtrl and si*Itpr2* transfection, while si*Itpr2* + ORM2 significantly suppressed CD36 protein levels compared to siCtrl + ORM2 (**Figure. 25C and 25D**). The results indicate that ORM2 enhances macrophage lipid metabolism through ITPR2.

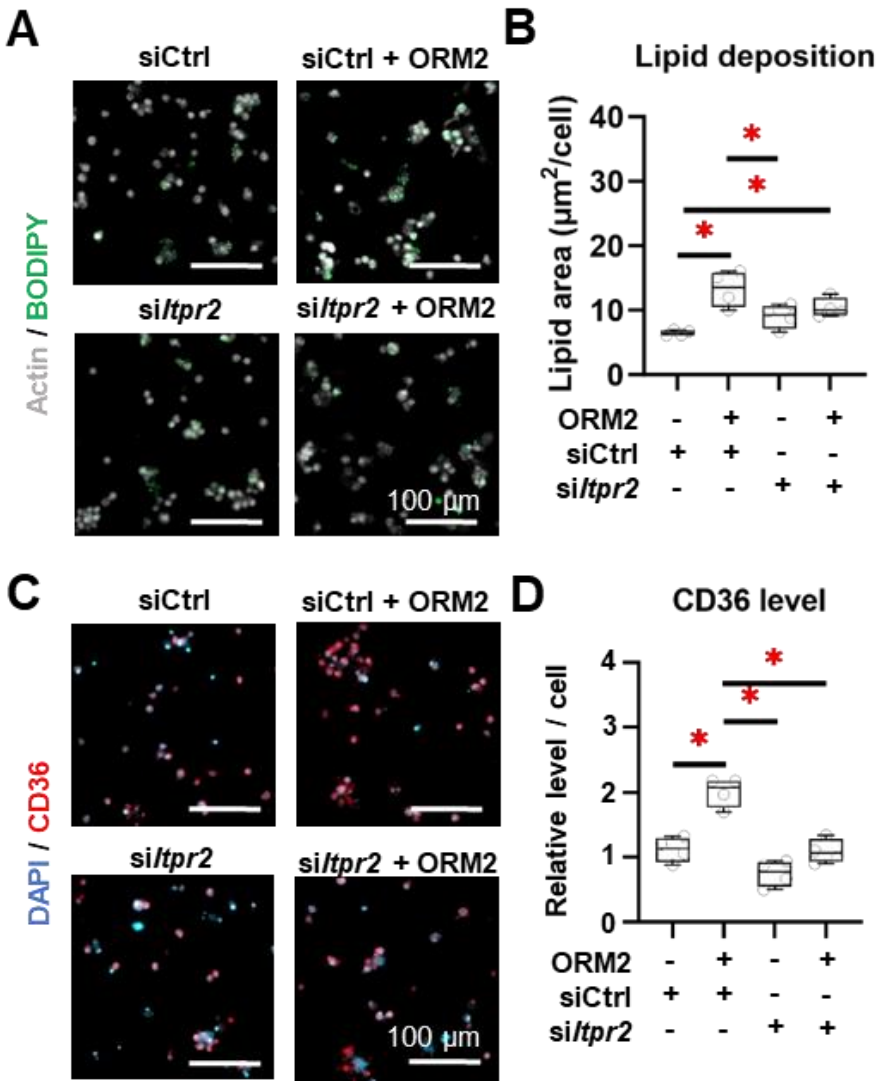

Figure 25. ORM2 enhances macrophage lipid metabolism through ITPR2. Liver macrophages were treated with FFAs at the baseline level. (A) Fluorescent observation and (B)

quantitative analysis of lipid accumulation in mouse liver macrophages upon *Itpr2*/Ctrl interference ± ORM2 treatment. (C) Fluorescent observation and (D) quantitative analysis of CD36 protein in mouse liver macrophages upon *Itpr2*/Ctrl interference ± ORM2 treatment. A one-way ANOVA test was used. * represents $p < 0.05$.

4.6.5. ORM2 induces macrophage cellular stress through ITPR2

Upon *Itpr2*/Ctrl interference ± ORM2 treatment, cellular stress was evaluated on mouse liver macrophages. Notably, si*Itpr2* downregulation strikingly elevated cell-cycle arrest levels, which was likely due to the high relevance of ITPR2 and cellular senescence(98). ORM2 significantly exacerbated macrophage cell-cycle arrest (Sa-β-Gal^{+}) under siCtrl but not si*Itpr2* transfection (**Figure. 26A and 26B**), while no differences were found between si*Itpr2* + ORM2 and siCtrl + ORM2. Simultaneously, ORM2 significantly exacerbated apoptosis (Apopxin^{+}) under siCtrl but not si*Itpr2* transfection, while si*Itpr2* + ORM2 significantly attenuated Apopxin levels compared to siCtrl + ORM2 (**Figure. 26C and 26D**). The results indicate that ORM2 induces macrophage stress, potentially both as senescence and apoptosis, through ITPR2.

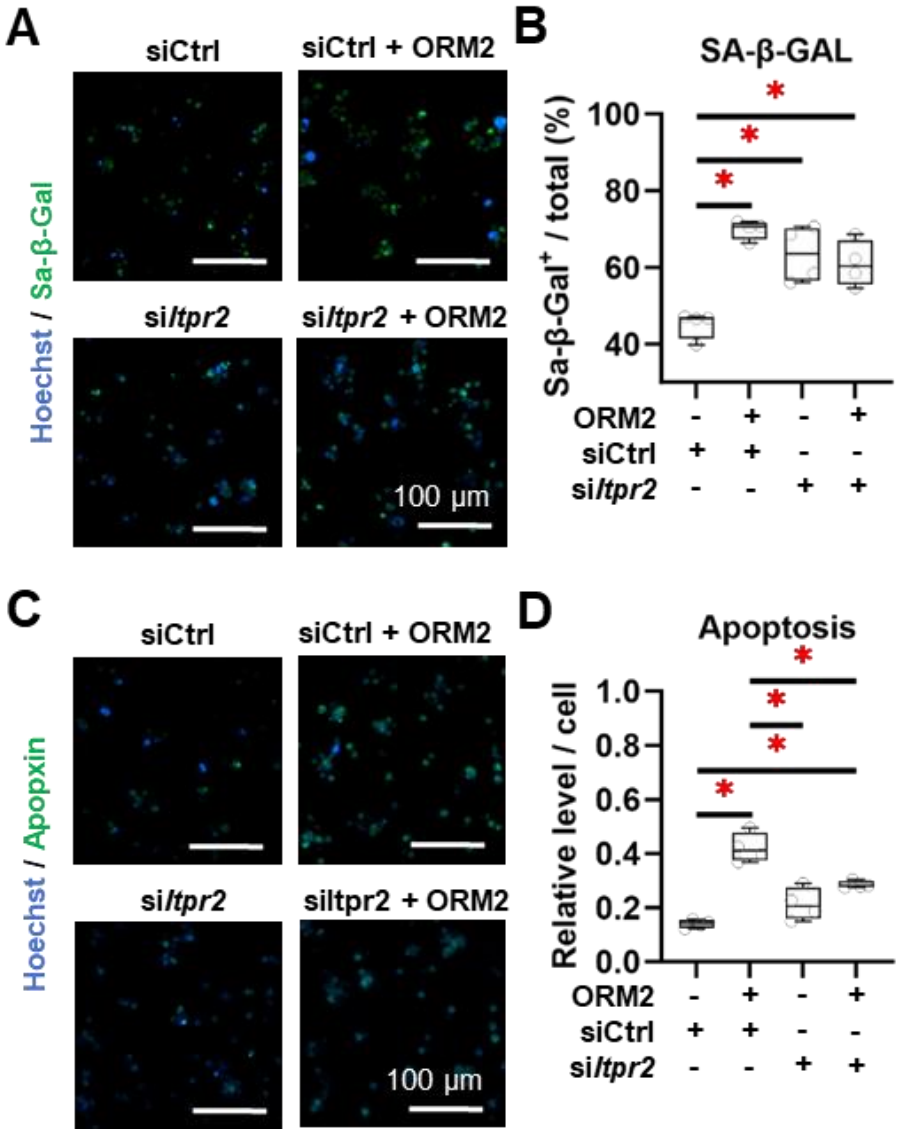

Figure 26. ORM2 induces macrophage cell stress through ITPR2. (A) Fluorescent observation and (B) quantitative analysis of YG beads captured by mouse liver macrophages upon *Itpr2*/Ctrl interference ± ORM2 treatment. (C) Fluorescent observation and (D) quantitative analysis of TIM4 protein in mouse liver macrophages upon *Itpr2*/Ctrl interference ± ORM2 treatment. A one-way ANOVA test was used. * represents $p < 0.05$.

5. Discussion

The scientific study presented in this dissertation elucidates a mechanism that illustrates multicellular crosstalk, involved in the onset and progression of DR upon liver injury. Based on current knowledge and preliminary experiments performed at the early stages of the thesis project, it was hypothesized that the cholangiocyte/BEC – liver macrophage interactions may significantly drive liver disease progression by shaping the microenvironment in the biliary niche, notably through BEC-derived ORM2. Firstly, the *Orm2* gene was screened out by retrieving and re-analyzing cholangiocyte-based transcriptome datasets from bile duct injury mouse models, and later validated using human single-cell transcriptome datasets. Furthermore, the BEC overexpression of the ORM2 protein was validated on MASH and PSC patients' liver samples. *In vitro* investigations on mouse primary liver cells demonstrated that ORM2 was upregulated in injured cholangiocytes but downregulated in injured hepatocytes. To further support our hypothesis, multiplex immunohistochemistry was performed on human MASH samples, which showed that the infiltrated monocyte/macrophage population were accumulating close to reactive ductular cells, in which ORM2 immunostaining was more pronounced. Furthermore, the consequences of an ORM2 treatment on macrophages of diverse mouse and human origins were evaluated. Intriguingly, ORM2 induced macrophage reprogramming by regulating variable signaling pathways (e.g., PI3K-Akt, JAK-STAT and cGMP-PKG). Accordingly, the results of *in vitro* experiments indicated that while ORM2 enhanced the phagocytic and lipid metabolism capacities of macrophages, it also triggered cell stress-related gene expression. These effects were attributed to the activation of the calcium pathway mediated by ITPR2. Of note, ORM2 induced dramatic upregulation of secretome in liver macrophages, encouraging an investigation of the extracellular modulation of ORM2-activated macrophages. Conditioned medium generated from ORM2-activated macrophages significantly suppressed the survival of cholangiocytes and hepatocytes, but it promoted ORM2 production, as well as exacerbating fibrogenic activation of HSCs.

Additionally, an *in vitro* micro-coculture chamber and the BoC models were implemented, elucidating that cholangiocyte-derived ORM2 influenced the biliary niche (including fibrogenesis, cell survival and immune cell accumulation) in the presence of liver macrophages. Taken together, this thesis project indicates that cholangiocyte-derived ORM2 can activate the macrophage calcium-dependent pathway, in turn promoting fibrogenesis but suppressing cell proliferation.

ORM2, belonging to the acute phase proteins (APP) family, has been determined to be enriched in the liver and to immediately react to microenvironment disturbance. Notably, APPs (e.g., ORMs, C-reactive protein) exert functions via mediating early innate immune responses, thereby initiating crucial defense mechanisms against exogenous pathogens and triggering adaptive immune responses(99, 100). Furthermore, APPs can induce the release of potent inflammatory cytokines, typically IL-1β, IL-6, and TNFα, further enhancing cytokine cascades in tissues. Thus, APPs are taken as indicators to evaluate inflammatory responses in the overall organism. Additionally, APPs participate in regulating tissue repair and liver metabolism, not only to maintain homeostasis but also to induce tissue response to various stimuli(99, 100).

ORM2 represents a relatively poorly studied APP. According to a limited number of studies, ORM2 exerts similar functions as other APPs (e.g., ORM1), for example by regulating innate immune responses as well as cellular ion transportation(101, 102). Besides this, emerging studies have indicated a significant regulatory role of ORMs on sphingolipid metabolism(103, 104). However, ORM2 is known to be particularly enriched in liver, which emphasizes its unique functions in mediating hepatic biological processes(105). Several studies have pointed out that ORM2 can enhance hepatocellular lipid metabolism to improve liver steatosis and regulate inflammation via regulating the calcium pathway, while in another context, ORM2 was determined to mediate overall lipid metabolism and obesity progression(97, 106, 107). So far, only a few studies have mentioned the pathways that ORM2 influences. ITPR2, a key receptor of the calcium pathway, was demonstrated as a direct binder to ORM2 in the most recent study, which supports the concept of an ORM2/ITPR2/calcium

pathway(97). According to the Human Protein Atlas database(108), hepatocytes represent the main resources for ORM2 in liver under healthy conditions. Nonetheless, results from this dissertation extend this theory to it mediating cholangiocyte-macrophage crosstalk and the hepatic microenvironment for the first time. Novelly, we found that upon liver injury, ORM2 expression (both gene and protein) was highly accumulated in ductular cells but less expressed in hepatocytes, which encountered the healthy situation. This study may inspire more work on studying the effects of ORM2 as well as other APPs on diverse types of immune cells.

Cholangiocytes, formerly regarded as bystanders, have gradually been becoming essential for a thorough understanding of liver biology and pathology. Emerging studies have elucidated the remarkable secretory capacities of cholangiocytes, not only at healthy status, but more importantly upon injuries(109). Stressed cholangiocytes may progress to apoptosis and cell arrest or obtain proliferation abilities, which are associated with diverse secretory profiles actively shaping their microenvironment(29). Alongside this, monocyte/macrophage populations are attracting growing attention with regard to cholangiopathies. Traditional views must be revised to acknowledge that monocytes/macrophages play fundamental roles in not only hepatocyte- but also cholangiocyte- associated immune modulation, which in combination influence liver regeneration and disease progression(48, 55). In this study, we report on a novel cholangiokine – ORM2, which was revealed to rapidly function upon injury and influence the microenvironment of the biliary niche by reprogramming liver macrophages. Although the clinical relevance of ORM2 in liver diseases remains to be demonstrated, the data presented in this thesis calls for more investigations on cholangiocyte-targeting approaches.

Calcium pathways regulate fundamental biological processes in cells, including metabolism, secretion and cell growth(110, 111). In particular, calcium pathways and the regulation of cellular calcium transportation are known to be crucial in macrophage activation. Ca^{2+} influx was determined to be essential for LPS stimulation on macrophages after binding toll-like receptor (TLR)-4, in accordance with mouse

models(112). In a rat osteoarthritis model, pro-inflammatory polarization of macrophages was regulated via calcium signaling, whereas it was alleviated by transient receptor potential vanilloid 1 (TRPV1)(113). Simultaneously, chenodeoxycholic acid (CDCA), a mitochondrial calcium elevator, was revealed to inhibit anti-inflammatory polarization of macrophages according to investigations on acute myeloid leukemia (AML) patients and mouse models(114). Intriguingly, this study emphasized the concept of calcium-mediated macrophage polarization through ORM2-ITPR2 axis.

Notably, macrophage metabolic reprogramming represents a growing area of interest. In the present study, we also investigated ORM2 effects on liver macrophage metabolic activity. Here, we provide evidence that ORM2 may play a role as one of the metabolic reprogramming inducers in liver macrophages via upregulating calcium pathways, which strikingly exerts stronger effects than LPS. In line with this, it has been outlined in emerging studies that macrophage phenotypes, typically pro-inflammatory and anti-inflammatory, are significantly facilitated due to metabolic reprograming, which can be induced by diverse interventions and cytokines(115-117). Macrophage metabolism, and especially lipid metabolism, serves as an essential cellular process involving the synthesis of triacylglycerol, glycerophospholipids, cardiolipins and sphingolipids for membrane synthesis, and eicosanoids, which support membrane biosynthesis and energy storage(118, 119). Accumulating evidence has elucidated that in macrophage biology, lipid synthesis is correlated with pro-inflammatory phenotypes, whereas fatty acid oxidation is correlated with anti-inflammatory phenotypes, which indicates that the functions of macrophages may be targeted and manipulated through metabolic reprograming approaches(117, 120).

Overall, a key finding of this project is that ORM2-reprogramed liver macrophages not only display remarkable transcriptome alterations but also distinct functional characteristics pointing towards increased effectiveness in counteracting harmful exo- or endogenous insults (including phagocytosis, lipid handling and secretion). However, within the biliary niche, ORM2-reprogramed liver macrophages suppressed

cholangiocyte proliferation and exacerbated fibrogenesis, which may be seen as a disease perpetuating process. Through investigations on the gene and cytokine levels, IL-1α, IL-1β, IL-6, IL-23 and TNF-α were revealed to be upregulated by ORM2 stimulation in liver macrophages. These cytokines are commonly considered as pro-inflammatory factors, causing stress either directly to liver cells or indirectly via immune cells(121-123). Moreover, ORM2-reprogramed liver macrophages seem to participate in inflammation exacerbation. Upon ORM2 treatment, adhesion molecules were enriched in liver macrophages, while CCL-2 and CCL-5 were upregulated, which can orchestrate the accumulation of immune cells, especially myeloid cells. In the ORM2-administered mouse liver models, monocyte infiltration was estimated to increase in presence of the ORM2 supplement. In contrast, the *in vitro* BoC experiments in this study demonstrated that the monocyte accumulation was significantly cut down in the absence of BEC-derived ORM2. In this aspect, liver macrophages act as a mediator for ORM2 to initiate inflammatory cascades in the biliary niche upon liver injury.

Nevertheless, it would be simplistic to label ORM2 as a pro-inflammatory inducer for liver macrophages, because some anti-inflammatory cytokines (e.g., IL-10) can be also enhanced. On the other hand, proliferating cholangiocytes, the principal component of DR, are significantly associated with liver disease progression, although the mechanistic consequences remain unclear. In this aspect, ORM2 may regulate macrophages to suppress BEC proliferation, thereby protecting against excessive liver repair mechanism activation. Therefore, ORM2 may be characterized as a modulator for macrophage biology, potentially counteracting disease progression.

Interestingly, this study also illustrated that ORM2 can promote ORM2 production on hepatocytes and BECs. This phenomenon strongly implies that ORM2 released from activated BECs can trigger a positive feedback loop including hepatocytes and BEC for excessive ORM2 production, thereby potentiating ORM2-related influences in the biliary niche. Taken together, this study explored and discussed a novel mechanism of

diverse impacts of ORM2 in regulating cholangiocyte-macrophage crosstalk upon liver injury (**Figure. 27**).

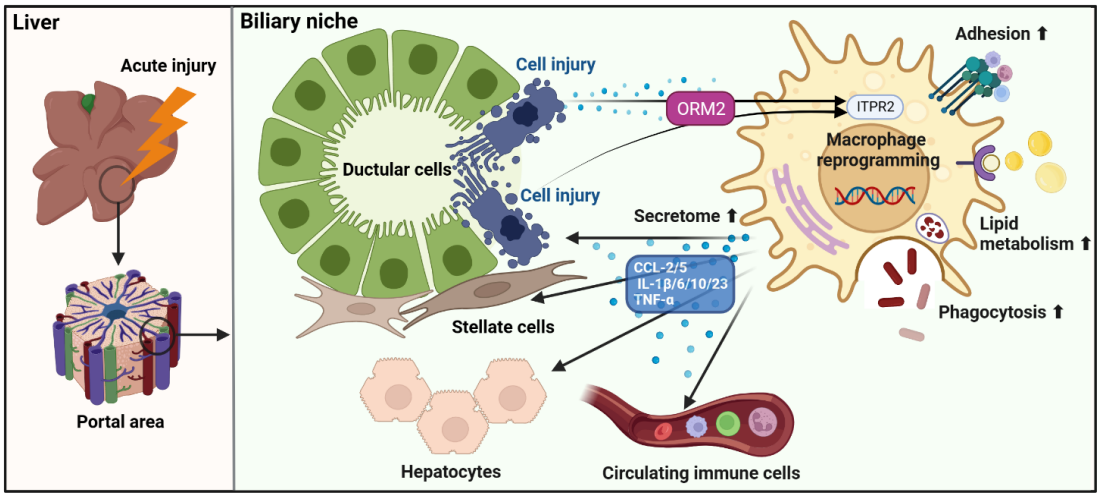

Figure 27. Graphical abstract. Upon biliary injury, cholangiocyte-derived ORM2 induces liver macrophage reprogramming via an ITPR2-dependent calcium pathway, thereby increasing the fibrogenesis of HSCs and monocyte accumulation, as well as exacerbating the cell damage and ORM2 production of BECs and Hepatocytes.

However, some limitations of this study need to be pointed out. Firstly, hepatocytes represent the main source of ORM2 in the liver, despite their extraordinary decline upon injury. Injured cholangiocytes notably release ORM2 to regulate their direct microenvironment in the biliary niche. Nonetheless, the influences from hepatocyte-derived ORM2 remain unclear, which was difficult to investigate in this study, regretfully. Secondly, the functionality of ORM2 in protein-protein interactions still lacks solid evidence. It is convincing, according to the most recent study, that ORM2 significantly binds to ITPR2 to regulate downstream pathways(97). Subsequently, this study, together with the ongoing work in the laboratory, determined that the implication for biochip models is that they can promisingly improve liver research in the aspects of dynamic immune response, cellular interactions, and mechanisms, all of which strengthens the novelty of this study. Importantly, the lack of reliable human primary cell resources (necessarily including hepatocytes, cholangiocytes, HSCs, liver macrophages, LSECs and blood cells) prompted us to utilize a mouse primary cell-

based system. Notably, several studies aimed to use differentiated human induced pluripotent stem cells (iPSCs) for *in vitro* human liver studies, which exert certain advantages over cell lines, but the interspecies relevance remains questionable(76, 124). For future perspectives, a thorough understanding of multicellular interactions upon liver injury is crucial, not only to break down the pathomechanisms of disease progression but also to develop therapeutic strategies. In the last decade, single-cell and spatial multiomics technologies have emerged to decipher liver cell heterogeneity, including liver macrophages and cholangiocytes(125). This unbiased exploration allows for a reconsideration of a previously tricky question: how do cholangiocytes, a tiny group of liver cells, participate in liver homeostasis and diseases? To address this question, well-characterized cholangiocytes are required, as these usually remain indistinct from hepatocyte-like cells, particularly upon injury(126). Thus, on top of usual cholangiocyte markers, more complex models are worth exploring for a precise characterization with the help of artificial intelligence(127). However, obtaining sufficient cholangiocytes from singular samples can be challenging due to cell acquisition methods often requiring the combination of multiple samples. This makes it challenging for single-cell analysis approaches to accurately reveal individual differences and measure cellular interactions(128, 129). Therefore, spatial approaches should be considered to intuitively demonstrate multicellular crosstalk within cholangiocyte-enriched areas, such as the biliary niche or portal areas. Furthermore, a comprehensive and precise characterization of cholangiocyte-associated pathological processes, also known as DR, could be achieved by comparing biliary niches from various locations or disease conditions. Simultaneously, the heterogeneity of liver macrophages within the biliary niche could be captured better. Last but not least, targeting liver macrophages has been regarded as a promising approach to protect against liver diseases, particularly steatotic liver diseases(130). It is worth looking forward to more studies on targeting macrophages to prevent DR progression.

In summary, this dissertation elaborates a study determining that upon biliary injury, cholangiocyte-derived ORM2 can regulate the microenvironment in the biliary niche

via liver macrophages. Moreover, ORM2 can reprogram liver macrophages by regulating various cellular features (e.g., phagocytosis, lipid metabolism, cell stress and cytokine secretion), notably through the enhancement of the calcium pathway. This study reveals a novel mechanistic pathway, not only to elucidate the cellular interactions during the DR process, but also to shed light on the development of therapeutic targets.

6. References

1. Kubes P, Jenne C. Immune Responses in the Liver. Annu Rev Immunol. 2018;36:247-77.
2. Trefts E, Gannon M, Wasserman DH. The liver. Curr Biol. 2017;27(21):R1147-R51.
3. Shin D, Monga SP. Cellular and molecular basis of liver development. Compr Physiol. 2013;3(2):799-815.
4. Pachter HL, Feliciano DV. Complex hepatic injuries. Surg Clin North Am. 1996;76(4):763-82.
5. Rinella ME, Lazarus JV, Ratziu V, Francque SM, Sanyal AJ, Kanwal F, Romero D, Abdelmalek MF, Anstee QM, Arab JP, Arrese M, Bataller R, Beuers U, Boursier J, Bugianesi E, Byrne CD, Castro Narro GE, Chowdhury A, Cortez-Pinto H, Cryer DR, Cusi K, El-Kassas M, Klein S, Eskridge W, Fan J, Gawrieh S, Guy CD, Harrison SA, Kim SU, Koot BG, Korenjak M, Kowdley KV, Lacaille F, Loomba R, Mitchell-Thain R, Morgan TR, Powell EE, Roden M, Romero-Gomez M, Silva M, Singh SP, Sookoian SC, Spearman CW, Tiniakos D, Valenti L, Vos MB, Wong VW, Xanthakos S, Yilmaz Y, Younossi Z, Hobbs A, Villota-Rivas M, Newsome PN, group NNc. A multisociety Delphi consensus statement on new fatty liver disease nomenclature. J Hepatol. 2023;79(6):1542-56.
6. Muratori L, Lohse AW, Lenzi M. Diagnosis and management of autoimmune hepatitis. BMJ. 2023;380:e070201.
7. Castaneda D, Gonzalez AJ, Alomari M, Tandon K, Zervos XB. From hepatitis A to E: A critical review of viral hepatitis. World J Gastroenterol. 2021;27(16):1691-715.
8. Seitz HK, Bataller R, Cortez-Pinto H, Gao B, Gual A, Lackner C, Mathurin P, Mueller S, Szabo G, Tsukamoto H. Alcoholic liver disease. Nat Rev Dis Primers. 2018;4(1):16.
9. Byrne CD, Targher G. NAFLD: a multisystem disease. J Hepatol. 2015;62(1 Suppl):S47-64.
10. Shu W, Yang M, Yang J, Lin S, Wei X, Xu X. Cellular crosstalk during liver regeneration: unity in diversity. Cell Commun Signal. 2022;20(1):117.
11. Richardson JD. Changes in the management of injuries to the liver and spleen. J Am Coll Surg. 2005;200(5):648-69.
12. Gines P, Krag A, Abraldes JG, Sola E, Fabrellas N, Kamath PS. Liver cirrhosis. Lancet. 2021;398(10308):1359-76.
13. Albillos A, Martin-Mateos R, Van der Merwe S, Wiest R, Jalan R, Alvarez-Mon M. Cirrhosis-associated immune dysfunction. Nat Rev Gastroenterol Hepatol. 2022;19(2):112-34.
14. Ezhilarasan D, Najimi M. Intercellular communication among liver cells in the perisinusoidal space of the injured liver: Pathophysiology and therapeutic directions. J Cell Physiol. 2023;238(1):70-81.
15. Koyama Y, Brenner DA. Liver inflammation and fibrosis. J Clin Invest. 2017;127(1):55-64.
16. Peiseler M, Schwabe R, Hampe J, Kubes P, Heikenwalder M, Tacke F. Immune mechanisms linking metabolic injury to inflammation and fibrosis in fatty liver disease - novel insights into cellular communication circuits. J Hepatol. 2022;77(4):1136-60.

17. Shetty S, Lalor PF, Adams DH. Lymphocyte recruitment to the liver: molecular insights into the pathogenesis of liver injury and hepatitis. Toxicology. 2008;254(3):136-46.
18. Lian M, Selmi C, Gershwin ME, Ma X. Myeloid Cells and Chronic Liver Disease: a Comprehensive Review. Clin Rev Allergy Immunol. 2018;54(2):307-17.
19. Viebahn CS, Benseler V, Holz LE, Elsegood CL, Vo M, Bertolino P, Ganss R, Yeoh GC. Invading macrophages play a major role in the liver progenitor cell response to chronic liver injury. J Hepatol. 2010;53(3):500-7.
20. Bird TG, Lu WY, Boulter L, Gordon-Keylock S, Ridgway RA, Williams MJ, Taube J, Thomas JA, Wojtacha D, Gambardella A, Sansom OJ, Iredale JP, Forbes SJ. Bone marrow injection stimulates hepatic ductular reactions in the absence of injury via macrophage-mediated TWEAK signaling. Proc Natl Acad Sci U S A. 2013;110(16):6542-7.
21. Heymann F, Mossanen JC, Peiseler M, Niemietz PM, Araujo David B, Krenkel O, Liepelt A, Batista Carneiro M, Kohlhepp MS, Kubes P, Tacke F. Hepatic C-X-C chemokine receptor type 6-expressing innate lymphocytes limit detrimental myeloid hyperactivation in acute liver injury. Hepatol Commun. 2023;7(4).
22. Boyer JL, Soroka CJ. Bile formation and secretion: An update. J Hepatol. 2021;75(1):190-201.
23. Tabibian JH, Masyuk AI, Masyuk TV, O'Hara SP, LaRusso NF. Physiology of cholangiocytes. Compr Physiol. 2013;3(1):541-65.
24. Elferink RO. Cholestasis. Gut. 2003;52 Suppl 2(Suppl 2):ii42-8.
25. Banales JM, Huebert RC, Karlsen T, Strazzabosco M, LaRusso NF, Gores GJ. Cholangiocyte pathobiology. Nat Rev Gastroenterol Hepatol. 2019;16(5):269-81.
26. Mancinelli R, Franchitto A, Gaudio E, Onori P, Glaser S, Francis H, Venter J, Demorrow S, Carpino G, Kopriva S, White M, Fava G, Alvaro D, Alpini G. After damage of large bile ducts by gamma-aminobutyric acid, small ducts replenish the biliary tree by amplification of calcium-dependent signaling and de novo acquisition of large cholangiocyte phenotypes. Am J Pathol. 2010;176(4):1790-800.
27. Marzioni M, Glaser SS, Francis H, Phinizy JL, LeSage G, Alpini G. Functional heterogeneity of cholangiocytes. Semin Liver Dis. 2002;22(3):227-40.
28. Alpini G, Roberts S, Kuntz SM, Ueno Y, Gubba S, Podila PV, LeSage G, LaRusso NF. Morphological, molecular, and functional heterogeneity of cholangiocytes from normal rat liver. Gastroenterology. 1996;110(5):1636-43.
29. Cai X, Tacke F, Guillot A, Liu H. Cholangiokines: undervalued modulators in the hepatic microenvironment. Front Immunol. 2023;14:1192840.
30. Sato K, Meng F, Giang T, Glaser S, Alpini G. Mechanisms of cholangiocyte responses to injury. Biochim Biophys Acta Mol Basis Dis. 2018;1864(4 Pt B):1262-9.
31. Monga SP, Nejak-Bowen K. Ductular Reaction and Liver Regeneration: Fulfilling the Prophecy of Prometheus! Cell Mol Gastroenterol Hepatol. 2023;15(3):806-8.
32. Manco R, Clerbaux LA, Verhulst S, Bou Nader M, Sempoux C, Ambroise J, Bearzatto B, Gala JL, Horsmans Y, van Grunsven L, Desdouets C, Leclercq I. Reactive cholangiocytes differentiate into proliferative hepatocytes with efficient DNA repair in mice with chronic liver injury. J Hepatol. 2019;70(6):1180-91.
33. Raven A, Lu WY, Man TY, Ferreira-Gonzalez S, O'Duibhir E, Dwyer BJ, Thomson JP, Meehan RR, Bogorad R, Koteliansky V, Kotelevtsev Y, Ffrench-Constant C, Boulter L,

Forbes SJ. Cholangiocytes act as facultative liver stem cells during impaired hepatocyte regeneration. Nature. 2017;547(7663):350-4.
34. Williams MJ, Clouston AD, Forbes SJ. Links between hepatic fibrosis, ductular reaction, and progenitor cell expansion. Gastroenterology. 2014;146(2):349-56.
35. Sato K, Marzioni M, Meng F, Francis H, Glaser S, Alpini G. Ductular Reaction in Liver Diseases: Pathological Mechanisms and Translational Significances. Hepatology. 2019;69(1):420-30.
36. He YH, Pan JX, Xu LM, Gu T, Chen YW. Ductular reaction in non-alcoholic fatty liver disease: When Macbeth is perverted. World J Hepatol. 2023;15(6):725-40.
37. Chen Y, Gao WK, Shu YY, Ye J. Mechanisms of ductular reaction in non-alcoholic steatohepatitis. World J Gastroenterol. 2022;28(19):2088-99.
38. Pinzani M, Luong TV. Pathogenesis of biliary fibrosis. Biochim Biophys Acta Mol Basis Dis. 2018;1864(4 Pt B):1279-83.
39. Carey EJ, Ali AH, Lindor KD. Primary biliary cirrhosis. Lancet. 2015;386(10003):1565-75.
40. Giordano DM, Pinto C, Maroni L, Benedetti A, Marzioni M. Inflammation and the Gut-Liver Axis in the Pathophysiology of Cholangiopathies. Int J Mol Sci. 2018;19(10).
41. Strazzabosco M, Fiorotto R, Cadamuro M, Spirli C, Mariotti V, Kaffe E, Scirpo R, Fabris L. Pathophysiologic implications of innate immunity and autoinflammation in the biliary epithelium. Biochim Biophys Acta Mol Basis Dis. 2018;1864(4 Pt B):1374-9.
42. Lopez BG, Tsai MS, Baratta JL, Longmuir KJ, Robertson RT. Characterization of Kupffer cells in livers of developing mice. Comp Hepatol. 2011;10(1):2.
43. Krenkel O, Tacke F. Liver macrophages in tissue homeostasis and disease. Nat Rev Immunol. 2017;17(5):306-21.
44. Crofton KM, Reiter LW. Pyrethroid insecticides and the gamma-aminobutyric acidA receptor complex: motor activity and the acoustic startle response in the rat. J Pharmacol Exp Ther. 1987;243(3):946-54.
45. Guilliams M, Scott CL. Liver macrophages in health and disease. Immunity. 2022;55(9):1515-29.
46. Dou L, Shi X, He X, Gao Y. Macrophage Phenotype and Function in Liver Disorder. Front Immunol. 2019;10:3112.
47. Dixon LJ, Barnes M, Tang H, Pritchard MT, Nagy LE. Kupffer cells in the liver. Compr Physiol. 2013;3(2):785-97.
48. Wen Y, Lambrecht J, Ju C, Tacke F. Hepatic macrophages in liver homeostasis and diseases-diversity, plasticity and therapeutic opportunities. Cell Mol Immunol. 2021;18(1):45-56.
49. Slevin E, Baiocchi L, Wu N, Ekser B, Sato K, Lin E, Ceci L, Chen L, Lorenzo SR, Xu W, Kyritsi K, Meadows V, Zhou T, Kundu D, Han Y, Kennedy L, Glaser S, Francis H, Alpini G, Meng F. Kupffer Cells: Inflammation Pathways and Cell-Cell Interactions in Alcohol-Associated Liver Disease. Am J Pathol. 2020;190(11):2185-93.
50. Chen J, Deng X, Liu Y, Tan Q, Huang G, Che Q, Guo J, Su Z. Kupffer Cells in Non-alcoholic Fatty Liver Disease: Friend or Foe? Int J Biol Sci. 2020;16(13):2367-78.
51. Hammerich L, Tacke F. Hepatic inflammatory responses in liver fibrosis. Nat Rev Gastroenterol Hepatol. 2023;20(10):633-46.

52. You Q, Holt M, Yin H, Li G, Hu CJ, Ju C. Role of hepatic resident and infiltrating macrophages in liver repair after acute injury. Biochem Pharmacol. 2013;86(6):836-43.
53. Ramachandran P, Pellicoro A, Vernon MA, Boulter L, Aucott RL, Ali A, Hartland SN, Snowdon VK, Cappon A, Gordon-Walker TT, Williams MJ, Dunbar DR, Manning JR, van Rooijen N, Fallowfield JA, Forbes SJ, Iredale JP. Differential Ly-6C expression identifies the recruited macrophage phenotype, which orchestrates the regression of murine liver fibrosis. Proc Natl Acad Sci U S A. 2012;109(46):E3186-95.
54. Kohlhepp MS, Liu H, Tacke F, Guillot A. The contradictory roles of macrophages in non-alcoholic fatty liver disease and primary liver cancer-Challenges and opportunities. Front Mol Biosci. 2023;10:1129831.
55. Bruneau A, Guillot A, Tacke F. Macrophages in cholangiopathies. Curr Opin Gastroenterol. 2022;38(2):114-20.
56. Syal G, Fausther M, Dranoff JA. Advances in cholangiocyte immunobiology. Am J Physiol Gastrointest Liver Physiol. 2012;303(10):G1077-86.
57. Pinto C, Giordano DM, Maroni L, Marzioni M. Role of inflammation and proinflammatory cytokines in cholangiocyte pathophysiology. Biochim Biophys Acta Mol Basis Dis. 2018;1864(4 Pt B):1270-8.
58. Locatelli L, Cadamuro M, Spirli C, Fiorotto R, Lecchi S, Morell CM, Popov Y, Scirpo R, De Matteis M, Amenduni M, Pietrobattista A, Torre G, Schuppan D, Fabris L, Strazzabosco M. Macrophage recruitment by fibrocystin-defective biliary epithelial cells promotes portal fibrosis in congenital hepatic fibrosis. Hepatology. 2016;63(3):965-82.
59. Guillot A, Guerri L, Feng D, Kim SJ, Ahmed YA, Paloczi J, He Y, Schuebel K, Dai S, Liu F, Pacher P, Kisseleva T, Qin X, Goldman D, Tacke F, Gao B. Bile acid-activated macrophages promote biliary epithelial cell proliferation through integrin alphavbeta6 upregulation following liver injury. J Clin Invest. 2021;131(9).
60. Peng ZW, Ikenaga N, Liu SB, Sverdlov DY, Vaid KA, Dixit R, Weinreb PH, Violette S, Sheppard D, Schuppan D, Popov Y. Integrin alphavbeta6 critically regulates hepatic progenitor cell function and promotes ductular reaction, fibrosis, and tumorigenesis. Hepatology. 2016;63(1):217-32.
61. Tacke F, Zimmermann HW. Macrophage heterogeneity in liver injury and fibrosis. J Hepatol. 2014;60(5):1090-6.
62. Kazankov K, Jorgensen SMD, Thomsen KL, Moller HJ, Vilstrup H, George J, Schuppan D, Gronbaek H. The role of macrophages in nonalcoholic fatty liver disease and nonalcoholic steatohepatitis. Nat Rev Gastroenterol Hepatol. 2019;16(3):145-59.
63. Scherbaum WA, Schrell U, Gluck M, Fahlbusch R, Pfeiffer EF. Autoantibodies to pituitary corticotropin-producing cells: possible marker for unfavourable outcome after pituitary microsurgery for Cushing's disease. Lancet. 1987;1(8547):1394-8.
64. Barrow F, Khan S, Fredrickson G, Wang H, Dietsche K, Parthiban P, Robert S, Kaiser T, Winer S, Herman A, Adeyi O, Mouzaki M, Khoruts A, Hogquist KA, Staley C, Winer DA, Revelo XS. Microbiota-Driven Activation of Intrahepatic B Cells Aggravates NASH Through Innate and Adaptive Signaling. Hepatology. 2021;74(2):704-22.
65. Thapa M, Chinnadurai R, Velazquez VM, Tedesco D, Elrod E, Han JH, Sharma P, Ibegbu C, Gewirtz A, Anania F, Pulendran B, Suthar MS, Grakoui A. Liver fibrosis occurs through dysregulation of MyD88-dependent innate B-cell activity. Hepatology.

2015;61(6):2067-79.
66. Niemietz P, Peiseler M, Kohlhepp M, Horn P, Matchett K, Wang Y, Haas L, Zhang T, Bruneau A, Guillot A, Berger H, Liepelt A, Warzecha K, Demske C, Mockel D, Lammers T, Henderson N, Heymann F, Tacke F. C-C chemokine receptor type 7 (CCR7) regulates hepatic CD8+ T cell homeostasis and response to acute liver injury. Hepatology. 2024.
67. Harada K, Shimoda S, Sato Y, Isse K, Ikeda H, Nakanuma Y. Periductal interleukin-17 production in association with biliary innate immunity contributes to the pathogenesis of cholangiopathy in primary biliary cirrhosis. Clin Exp Immunol. 2009;157(2):261-70.
68. Jiang X, Otterdal K, Chung BK, Maucourant C, Ronneberg JD, Zimmer CL, Ogaard J, Boichuk Y, Holm S, Geanon D, Schneditz G, Bergquist A, Bjorkstrom NK, Melum E. Cholangiocytes Modulate Cluster of Differentiation 100 Expression in the Liver and Facilitate Pathogenic T-Helper 17 Cell Differentiation. Gastroenterology. 2023.
69. Guillot A, Winkler M, Silva Afonso M, Aggarwal A, Lopez D, Berger H, Kohlhepp MS, Liu H, Ozdirik B, Eschrich J, Ma J, Peiseler M, Heymann F, Pendem S, Mahadevan S, Gao B, Diehl L, Gupta R, Tacke F. Mapping the hepatic immune landscape identifies monocytic macrophages as key drivers of steatohepatitis and cholangiopathy progression. Hepatology. 2023;78(1):150-66.
70. Dwyer BJ, Jarman EJ, Gogoi-Tiwari J, Ferreira-Gonzalez S, Boulter L, Guest RV, Kendall TJ, Kurian D, Kilpatrick AM, Robson AJ, O'Duibhir E, Man TY, Campana L, Starkey Lewis PJ, Wigmore SJ, Olynyk JK, Ramm GA, Tirnitz-Parker JEE, Forbes SJ. TWEAK/Fn14 signalling promotes cholangiocarcinoma niche formation and progression. J Hepatol. 2021;74(4):860-72.
71. Fickert P, Wagner M. Preface - Animal models in liver disease. Biochim Biophys Acta Mol Basis Dis. 2019;1865(5):867-8.
72. Kaur S, Kidambi S, Ortega-Ribera M, Thuy LTT, Nieto N, Cogger VC, Xie WF, Tacke F, Gracia-Sancho J. In Vitro Models for the Study of Liver Biology and Diseases: Advances and Limitations. Cell Mol Gastroenterol Hepatol. 2023;15(3):559-71.
73. Xiang Y, Miller K, Guan J, Kiratitanaporn W, Tang M, Chen S. 3D bioprinting of complex tissues in vitro: state-of-the-art and future perspectives. Arch Toxicol. 2022;96(3):691-710.
74. Brooks A, Liang X, Zhang Y, Zhao CX, Roberts MS, Wang H, Zhang L, Crawford DHG. Liver organoid as a 3D in vitro model for drug validation and toxicity assessment. Pharmacol Res. 2021;169:105608.
75. Weaver RJ, Blomme EA, Chadwick AE, Copple IM, Gerets HHJ, Goldring CE, Guillouzo A, Hewitt PG, Ingelman-Sundberg M, Jensen KG, Juhila S, Klingmuller U, Labbe G, Liguori MJ, Lovatt CA, Morgan P, Naisbitt DJ, Pieters RHH, Snoeys J, van de Water B, Williams DP, Park BK. Managing the challenge of drug-induced liver injury: a roadmap for the development and deployment of preclinical predictive models. Nat Rev Drug Discov. 2020;19(2):131-48.
76. Rezvani M, Vallier L, Guillot A. Modeling Nonalcoholic Fatty Liver Disease in the Dish Using Human-Specific Platforms: Strategies and Limitations. Cell Mol Gastroenterol Hepatol. 2023;15(5):1135-45.
77. Shroff T, Aina K, Maass C, Cipriano M, Lambrecht J, Tacke F, Mosig A, Loskill P. Studying metabolism with multi-organ chips: new tools for disease modelling,

pharmacokinetics and pharmacodynamics. Open Biol. 2022;12(3):210333.
78. Deguchi S, Takayama K. State-of-the-art liver disease research using liver-on-a-chip. Inflamm Regen. 2022;42(1):62.
79. Ingber DE. Human organs-on-chips for disease modelling, drug development and personalized medicine. Nat Rev Genet. 2022;23(8):467-91.
80. Groger M, Dinger J, Kiehntopf M, Peters FT, Rauen U, Mosig AS. Preservation of Cell Structure, Metabolism, and Biotransformation Activity of Liver-On-Chip Organ Models by Hypothermic Storage. Adv Healthc Mater. 2018;7(2).
81. Mosig AS. Organ-on-chip models: new opportunities for biomedical research. Future Sci OA. 2017;3(2):FSO130.
82. Puschhof J, Pleguezuelos-Manzano C, Clevers H. Organoids and organs-on-chips: Insights into human gut-microbe interactions. Cell Host Microbe. 2021;29(6):867-78.
83. Wikswo JP, Curtis EL, Eagleton ZE, Evans BC, Kole A, Hofmeister LH, Matloff WJ. Scaling and systems biology for integrating multiple organs-on-a-chip. Lab Chip. 2013;13(18):3496-511.
84. Liu H, Kohlhepp M, Yin G, Hundertmark J, Heymann F, Aina K, Mosig A, Tacke F, Guillot A. OS-114-YI - Dissecting NAFLD pathomechanisms using primary mouse liver and blood cells in a microfluidic perfusable compartmentalized liver-on-a-chip model. Journal of Hepatology. 2023;78:S87.
85. Scotte M, Daveau M, Hiron M, Delers F, Lemeland JF, Teniere P, Lebreton JP. Interleukin-6 (IL-6) and acute-phase proteins in rats with biliary sepsis. Eur Cytokine Netw. 1991;2(3):177-82.
86. Tysoe OC, Justin AW, Brevini T, Chen SE, Mahbubani KT, Frank AK, Zedira H, Melum E, Saeb-Parsy K, Markaki AE, Vallier L, Sampaziotis F. Isolation and propagation of primary human cholangiocyte organoids for the generation of bioengineered biliary tissue. Nat Protoc. 2019;14(6):1884-925.
87. Broutier L, Andersson-Rolf A, Hindley CJ, Boj SF, Clevers H, Koo BK, Huch M. Culture and establishment of self-renewing human and mouse adult liver and pancreas 3D organoids and their genetic manipulation. Nat Protoc. 2016;11(9):1724-43.
88. Guillot A, Kohlhepp MS, Tacke F. Multiplex Immunostaining to Spatially Resolve the Cellular Landscape in Human and Mouse Livers. Methods Mol Biol. 2023;2669:245-55.
89. Guillot A, Kohlhepp MS, Bruneau A, Heymann F, Tacke F. Deciphering the Immune Microenvironment on A Single Archival Formalin-Fixed Paraffin-Embedded Tissue Section by An Immediately Implementable Multiplex Fluorescence Immunostaining Protocol. Cancers (Basel). 2020;12(9).
90. Robinson MD, McCarthy DJ, Smyth GK. edgeR: a Bioconductor package for differential expression analysis of digital gene expression data. Bioinformatics. 2010;26(1):139-40.
91. Gene Ontology C. Gene Ontology Consortium: going forward. Nucleic Acids Res. 2015;43(Database issue):D1049-56.
92. Kanehisa M, Goto S. KEGG: kyoto encyclopedia of genes and genomes. Nucleic Acids Res. 2000;28(1):27-30.
93. Aran D, Hu Z, Butte AJ. xCell: digitally portraying the tissue cellular heterogeneity landscape. Genome Biol. 2017;18(1):220.

94. Wilkinson L. Visualizing Big Data Outliers through Distributed Aggregation. IEEE Trans Vis Comput Graph. 2018;24(1):256-66.
95. Kennedy L, Carpino G, Owen T, Ceci L, Kundu D, Meadows V, Kyritsi K, Franchitto A, Onori P, Isidan A, Zhang W, Ekser B, Alvaro D, Gaudio E, Gershwin ME, Francis H, Glaser S, Alpini G. Secretin alleviates biliary and liver injury during late-stage primary biliary cholangitis via restoration of secretory processes. J Hepatol. 2023;78(1):99-113.
96. Ramachandran P, Dobie R, Wilson-Kanamori JR, Dora EF, Henderson BEP, Luu NT, Portman JR, Matchett KP, Brice M, Marwick JA, Taylor RS, Efremova M, Vento-Tormo R, Carragher NO, Kendall TJ, Fallowfield JA, Harrison EM, Mole DJ, Wigmore SJ, Newsome PN, Weston CJ, Iredale JP, Tacke F, Pollard JW, Ponting CP, Marioni JC, Teichmann SA, Henderson NC. Resolving the fibrotic niche of human liver cirrhosis at single-cell level. Nature. 2019;575(7783):512-8.
97. Zhou B, Luo Y, Ji N, Hu C, Lu Y. Orosomucoid 2 maintains hepatic lipid homeostasis through suppression of de novo lipogenesis. Nat Metab. 2022;4(9):1185-201.
98. Ziegler DV, Vindrieux D, Goehrig D, Jaber S, Collin G, Griveau A, Wiel C, Bendridi N, Djebali S, Farfariello V, Prevarskaya N, Payen L, Marvel J, Aubert S, Flaman JM, Rieusset J, Martin N, Bernard D. Calcium channel ITPR2 and mitochondria-ER contacts promote cellular senescence and aging. Nat Commun. 2021;12(1):720.
99. Gabay C, Kushner I. Acute-phase proteins and other systemic responses to inflammation. N Engl J Med. 1999;340(6):448-54.
100. Ehlting C, Wolf SD, Bode JG. Acute-phase protein synthesis: a key feature of innate immune functions of the liver. Biol Chem. 2021;402(9):1129-45.
101. Jo M, Kim JH, Song GJ, Seo M, Hwang EM, Suk K. Astrocytic Orosomucoid-2 Modulates Microglial Activation and Neuroinflammation. J Neurosci. 2017;37(11):2878-94.
102. Luo Z, Lei H, Sun Y, Liu X, Su DF. Orosomucoid, an acute response protein with multiple modulating activities. J Physiol Biochem. 2015;71(2):329-40.
103. Liu P, Xie T, Wu X, Han G, Gupta SD, Zhang Z, Yue J, Dong F, Gable K, Niranjanakumari S, Li W, Wang L, Liu W, Yao R, Cahoon EB, Dunn TM, Gong X. Mechanism of sphingolipid homeostasis revealed by structural analysis of Arabidopsis SPT-ORM1 complex. Sci Adv. 2023;9(13):eadg0728.
104. Sasset L, Chowdhury KH, Manzo OL, Rubinelli L, Konrad C, Maschek JA, Manfredi G, Holland WL, Di Lorenzo A. Sphingosine-1-phosphate controls endothelial sphingolipid homeostasis via ORMDL. EMBO Rep. 2023;24(1):e54689.
105. Elpek GO. Orosomucoid in liver diseases. World J Gastroenterol. 2021;27(45):7739-47.
106. Li L, Chen J, Sun H, Niu Q, Zhao Y, Yang X, Sun Q. Orm2 Deficiency Aggravates High-Fat Diet-Induced Obesity through Gut Microbial Dysbiosis and Intestinal Inflammation. Mol Nutr Food Res. 2024;68(1):e2300236.
107. Cai L, Oyeniran C, Biswas DD, Allegood J, Milstien S, Kordula T, Maceyka M, Spiegel S. ORMDL proteins regulate ceramide levels during sterile inflammation. J Lipid Res. 2016;57(8):1412-22.
108. Colwill K, Renewable Protein Binder Working G, Graslund S. A roadmap to generate renewable protein binders to the human proteome. Nat Methods. 2011;8(7):551-8.

109. Bogert PT, LaRusso NF. Cholangiocyte biology. Curr Opin Gastroenterol. 2007;23(3):299-305.
110. Rossi A, Pizzo P, Filadi R. Calcium, mitochondria and cell metabolism: A functional triangle in bioenergetics. Biochim Biophys Acta Mol Cell Res. 2019;1866(7):1068-78.
111. Berridge MJ. The Inositol Trisphosphate/Calcium Signaling Pathway in Health and Disease. Physiol Rev. 2016;96(4):1261-96.
112. Schappe MS, Szteyn K, Stremska ME, Mendu SK, Downs TK, Seegren PV, Mahoney MA, Dixit S, Krupa JK, Stipes EJ, Rogers JS, Adamson SE, Leitinger N, Desai BN. Chanzyme TRPM7 Mediates the Ca(2+) Influx Essential for Lipopolysaccharide-Induced Toll-Like Receptor 4 Endocytosis and Macrophage Activation. Immunity. 2018;48(1):59-74 e5.
113. Lv Z, Xu X, Sun Z, Yang YX, Guo H, Li J, Sun K, Wu R, Xu J, Jiang Q, Ikegawa S, Shi D. TRPV1 alleviates osteoarthritis by inhibiting M1 macrophage polarization via Ca(2+)/CaMKII/Nrf2 signaling pathway. Cell Death Dis. 2021;12(6):504.
114. Liu J, Wei Y, Jia W, Can C, Wang R, Yang X, Gu C, Liu F, Ji C, Ma D. Chenodeoxycholic acid suppresses AML progression through promoting lipid peroxidation via ROS/p38 MAPK/DGAT1 pathway and inhibiting M2 macrophage polarization. Redox Biol. 2022;56:102452.
115. Bussi C, Heunis T, Pellegrino E, Bernard EM, Bah N, Dos Santos MS, Santucci P, Aylan B, Rodgers A, Fearns A, Mitschke J, Moore C, MacRae JI, Greco M, Reinheckel T, Trost M, Gutierrez MG. Lysosomal damage drives mitochondrial proteome remodelling and reprograms macrophage immunometabolism. Nat Commun. 2022;13(1):7338.
116. Liu PS, Wang H, Li X, Chao T, Teav T, Christen S, Di Conza G, Cheng WC, Chou CH, Vavakova M, Muret C, Debackere K, Mazzone M, Huang HD, Fendt SM, Ivanisevic J, Ho PC. alpha-ketoglutarate orchestrates macrophage activation through metabolic and epigenetic reprogramming. Nat Immunol. 2017;18(9):985-94.
117. El Kasmi KC, Stenmark KR. Contribution of metabolic reprogramming to macrophage plasticity and function. Semin Immunol. 2015;27(4):267-75.
118. Yan J, Horng T. Lipid Metabolism in Regulation of Macrophage Functions. Trends Cell Biol. 2020;30(12):979-89.
119. Rohrig F, Schulze A. The multifaceted roles of fatty acid synthesis in cancer. Nat Rev Cancer. 2016;16(11):732-49.
120. Liu Y, Xu R, Gu H, Zhang E, Qu J, Cao W, Huang X, Yan H, He J, Cai Z. Metabolic reprogramming in macrophage responses. Biomark Res. 2021;9(1):1.
121. Ochoa-Sanchez R, Rose CF. Pathogenesis of Hepatic Encephalopathy in Chronic Liver Disease. J Clin Exp Hepatol. 2018;8(3):262-71.
122. Schmidt-Arras D, Rose-John S. IL-6 pathway in the liver: From physiopathology to therapy. J Hepatol. 2016;64(6):1403-15.
123. Brenner C, Galluzzi L, Kepp O, Kroemer G. Decoding cell death signals in liver inflammation. J Hepatol. 2013;59(3):583-94.
124. Sun XC, Kong DF, Zhao J, Faber KN, Xia Q, He K. Liver organoids: established tools for disease modeling and drug development. Hepatol Commun. 2023;7(4).
125. Xie B, Gao D, Zhou B, Chen S, Wang L. New discoveries in the field of metabolism by applying single-cell and spatial omics. J Pharm Anal. 2023;13(7):711-25.
126. Saviano A, Henderson NC, Baumert TF. Single-cell genomics and spatial

transcriptomics: Discovery of novel cell states and cellular interactions in liver physiology and disease biology. J Hepatol. 2020;73(5):1219-30.
127. Erfanian N, Heydari AA, Feriz AM, Ianez P, Derakhshani A, Ghasemigol M, Farahpour M, Razavi SM, Nasseri S, Safarpour H, Sahebkar A. Deep learning applications in single-cell genomics and transcriptomics data analysis. Biomed Pharmacother. 2023;165:115077.
128. Huang R, Zhang X, Gracia-Sancho J, Xie WF. Liver regeneration: Cellular origin and molecular mechanisms. Liver Int. 2022;42(7):1486-95.
129. Sun G, Li Z, Rong D, Zhang H, Shi X, Yang W, Zheng W, Sun G, Wu F, Cao H, Tang W, Sun Y. Single-cell RNA sequencing in cancer: Applications, advances, and emerging challenges. Mol Ther Oncolytics. 2021;21:183-206.
130. Tacke F. Targeting hepatic macrophages to treat liver diseases. J Hepatol. 2017;66(6):1300-12.

7. Statutory Declaration

“I, Hanyang Liu, by personally signing this document in lieu of an oath, hereby affirm that I prepared the submitted dissertation on the topic [Crosstalk between cholangiocytes and liver macrophages upon liver injury (Wechselwirkungen zwischen Cholangiozyten und Lebermakrophagen bei Leberschädigung)], independently and without the support of third parties, and that I used no other sources and aids than those stated.

All parts which are based on the publications or presentations of other authors, either in letter or in spirit, are specified as such in accordance with the citing guidelines. The sections on methodology (in particular regarding practical work, laboratory regulations, statistical processing) and results (in particular regarding figures, charts and tables) are exclusively my responsibility.

Furthermore, I declare that I have correctly marked all of the data, the analyses, and the conclusions generated from data obtained in collaboration with other persons, and that I have correctly marked my own contribution and the contributions of other persons (cf. declaration of contribution). I have correctly marked all texts or parts of texts that were generated in collaboration with other people.

My contributions to any publications to this dissertation correspond to those stated in the below joint declaration made together with the supervisors. All publications created within the scope of the dissertation comply with the guidelines of the ICMJE (International Committee of Medical Journal Editors; www.icmje.org) on authorship. In addition, I declare that I shall comply with the regulations of Charité – Universitätsmedizin Berlin on ensuring good scientific practice.

I declare that I have not yet submitted this dissertation in identical or similar form to another Faculty.

The significance of this statutory declaration and the consequences of a false statutory declaration under criminal law (Sections 156, 161 of the German Criminal Code) are known to me.”

Date	Signature

8. Curriculum Vitae

My curriculum vitae does not appear in the electronic version of my paper for reasons of data protection

9. List of publications

1. Cai X, Tacke F, Guillot A, **Liu H**[#]. Cholangiokines: undervalued modulators in the hepatic microenvironment. Front Immunol. 2023 May 16;14:1192840.
2. Kohlhepp MS, **Liu H**[*], Tacke F, Guillot A. The contradictory roles of macrophages in non-alcoholic fatty liver disease and primary liver cancer-Challenges and opportunities. Front Mol Biosci. 2023 Feb 10;10:1129831.
3. Guillot A, Winkler M, Silva Afonso M, Aggarwal A, Lopez D, Berger H, Kohlhepp MS, **Liu H**, Özdirik B, Eschrich J, Ma J, Peiseler M, Heymann F, Pendem S, Mahadevan S, Gao B, Diehl L, Gupta R, Tacke F. Mapping the hepatic immune landscape identifies monocytic macrophages as key drivers of steatohepatitis and cholangiopathy progression. Hepatology. 2023 Jul 1;78(1):150-166.
4. Chen S, Tang L, Guillot A, **Liu H**[#]. Bariatric Surgery Associates with Nonalcoholic Steatohepatitis/Hepatocellular Carcinoma Amelioration via SPP1 Suppression. Metabolites. 2022 Dec 21;13(1):11.
5. Cai X, Guillot A, **Liu H**[#]. Cellular Senescence in Hepatocellular Carcinoma: The Passenger or the Driver? Cells. 2022 Dec 29;12(1):132.
6. Chen S, Jiang Y, Qi X, Song P, Tang L, **Liu H**[#]. Bioinformatics analysis to obtain critical genes regulated in subcutaneous adipose tissue after bariatric surgery. Adipocyte. 2022 Dec;11(1):550-561.
7. Rehman AU, Olsson PO, Akhtar A, Padhiar AA, **Liu H**, Dai Y, Gong Y, Zhou Y, Khan N, Yang H, Tang L. Systematic molecular analysis of the human secretome and membrane proteome in gastrointestinal adenocarcinomas. J Cell Mol Med. 2022 Jun;26(12):3329-3342.
8. Chen S, Cai X, Liu Y, Shen Y, Guillot A, Tacke F, Tang L, **Liu H**[#]. The macrophage-associated microRNA-4715-3p / Gasdermin D axis potentially indicates fibrosis progression in nonalcoholic fatty liver disease: evidence from

transcriptome and biological data. Bioengineered. 2022 May;13(5):11740-11751.

9. Puengel T[*], **Liu H**[*], Guillot A, Heymann F, Tacke F, Peiseler M. Nuclear Receptors Linking Metabolism, Inflammation, and Fibrosis in Nonalcoholic Fatty Liver Disease. Int J Mol Sci. 2022 Feb 28;23(5):2668.
10. Chen S, Wei Y, **Liu H**, Gong Y, Zhou Y, Yang H, Tang L. Analysis of Collagen type X alpha 1 (COL10A1) expression and prognostic significance in gastric cancer based on bioinformatics. Bioengineered. 2021 Dec;12(1):127-137.
11. Chen S, Gong Y, Shen Y, Liu Y, Fu Y, Dai Y, Rehman AU, Tang L, **Liu H**[#]. INHBA is a novel mediator regulating cellular senescence and immune evasion in colorectal cancer. J Cancer. 2021 Aug 13;12(19):5938-5949.
12. Dai Y, Li F, Jiao Y, Wang G, Zhan T, Xia Y, **Liu H**, Yang H, Zhang J, Tang L. Mortalin/glucose-regulated protein 75 promotes the cisplatin-resistance of gastric cancer via regulating anti-oxidation/apoptosis and metabolic reprogramming. Cell Death Discov. 2021 Jun 11;7(1):140.
13. Gong Y, Chen S, Fu Y, Liu Y, Wang Y, Yang H, **Liu H**[#], Tang L[#]. MUC4 is a novel mediator in *H. pylori* infection-related pancreatic cancer. Oncol Lett. 2021 Feb;21(2):123.
14. Yang H, Zhu J, Wang G, **Liu H**, Zhou Y, Qian J. STK35 Is Ubiquitinated by NEDD4L and Promotes Glycolysis and Inhibits Apoptosis Through Regulating the AKT Signaling Pathway, Influencing Chemoresistance of Colorectal Cancer. Front Cell Dev Biol. 2020 Oct 8;8:582695.
15. Qian J, Jiao Y, Wang G, **Liu H**, Cao X, Yang H. Mechanism of TGF-β1 inhibiting Kupffer cell immune responses in cholestatic cirrhosis. Exp Ther Med. 2020 Aug;20(2):1541-1549.
16. Cai Z, Wei Y, Chen S, Gong Y, Fu Y, Dai X, Zhou Y, Yang H, Tang L, **Liu H**[#]. Screening and identification of key biomarkers in alimentary tract cancers: A bioinformatic analysis. Cancer Biomark. 2020;29(2):221-233.
17. Yang H, **Liu H**, Jiao Y, Qian J. Roux-en-Y Gastrointestinal Bypass Promotes

Activation of TGR5 and Peptide YY. Endocr Metab Immune Disord Drug Targets. 2020;20(8):1262-1267.

18. Fu Y, Yao N, Ding D, Zhang X, **Liu H**, Ma L, Shi W, Zhu C, Tang L. TMEM158 promotes pancreatic cancer aggressiveness by activation of TGFβ1 and PI3K/AKT signaling pathway. J Cell Physiol. 2020 Mar;235(3):2761-2775.
19. Jiao Y, Yang H, Qian J, Gong Y, **Liu H**, Wu S, Cao L, Tang L. miR-3664-5P suppresses the proliferation and metastasis of gastric cancer by attenuating the NF-κB signaling pathway through targeting MTDH. Int J Oncol. 2019 Mar;54(3):845-858.
20. **Liu H**, Song J, Zhou Y, Cao L, Gong Y, Wei Y, Yang H, Tang L. Methylxanthine derivatives promote autophagy in gastric cancer cells targeting PTEN. Anticancer Drugs. 2019 Apr;30(4):347-355.
21. Zhou Y, **Liu H**, Song J, Cao L, Tang L, Qi C. Sinomenine alleviates dextran sulfate sodium-induced colitis via the Nrf2/NQO-1 signaling pathway. Mol Med Rep. 2018 Oct;18(4):3691-3698.
22. Song J, Zhou Y, Gong Y, **Liu H**, Tang L. Rottlerin promotes autophagy and apoptosis in gastric cancer cell lines. Mol Med Rep. 2018 Sep;18(3):2905-2913.
23. **Liu H**, Zhou Y, Tang L. Caffeine induces sustained apoptosis of human gastric cancer cells by activating the caspase-9/caspase-3 signalling pathway. Mol Med Rep. 2017 Sep;16(3):2445-2454.

(*: co-first author. #: corresponding author)

10. Acknowledgements

Time and luck have incredibly brought me to this stage. I am deeply indebted to Prof. Dr. med. Frank Tacke and Dr. rer. nat. Adrien Guillot, for their unwavering support, insightful feedback, and professional guidance. Their dedication and mentorship have shaped the direction and quality of this research. Thank you for providing me the chance to finish my doctoral study and research project in the Department of Hepatology and Gastroenterology at Charité - Universitätsmedizin Berlin. Sincerely, I could never have gone through this journey successfully without Dr. rer. nat. Adrien Guillot, who not only constantly provides me tuition to carry out my research work but also encourages me to seize opportunities for self-improvement. Additionally, I am so grateful that the financial support provided by the Chinese Scholarship Council (CSC), which has made my life and study in Germany smooth and stable.

Particularly, I want to thank colleagues from the department (Dr. rer. nat. Marlene Sophia Kohlhepp, Dr. rer. nat. Yeni Ait Ahmed, Dr. rer. nat. Felix Heymann, Dr. Jana Hundertmark, Ms. Guo Yin, Mr. Tian Lan, Mr. Queency Okechukwu, Mrs. Natalja Amiridze, Mr. Lukas Jonathan Geisler, Mrs. Jana Knorr, Mrs. Yuting Wang, Ms. Juan Wang, Ms. Tianjiao Zhang, Mrs. Barbara Malik and Mrs. Ines Eichhorn), AG Rezvani (Dr. med. Milad Rezvani, Dr. Natalia Martagón Calderón, Mr. Julian Weihs and Ms. Susanna Quach) and Dr. Xiurong Cai from AG Schmitt for their practical support and constructive advice.

Last but not least, I would regret not mentioning my family. Their support and sacrifices always inspired and motivated me during this 3-year doctoral study in Germany. Of course, all the friendships I have got here significantly make my mind rich and life colorful.

11. Statistician's certificate

CHARITÉ

CharitéCentrum für Human- und Gesundheitswissenschaften

Charité | Campus Charité Mitte | 10117 Berlin

Institut für Biometrie und klinische Epidemiologie (iBikE)

Direktor: Prof. Dr. Frank Konietschke

Postanschrift:
Charitéplatz 1 | 10117 Berlin
Besucheranschrift:
Reinhardtstr. 58 | 10117 Berlin

Tel. +49 (0)30 450 562171
frank.konietschke@charite.de
https://biometrie.charite.de/

Name, Vorname: Liu, Hanyang
Emailadresse: hanyang.liu@charite.de
Matrikelnummer: 4001145
PromotionsbetreuerIn: Prof. Dr. med. Frank Tacke;
Dr. rer. nat. Adrien Guillot
Promotionsinstitution / Klinik: Medizinische Klinik für Hepatologie und Gastroenterologie, CCM/CVK

Bescheinigung

Hiermit bescheinige ich, dass Herr Hanyang Liu innerhalb der Service Unit Biometrie des Instituts für Biometrie und klinische Epidemiologie (iBikE) bei mir eine statistische Beratung zu einem Promotionsvorhaben wahrgenommen hat. Folgende Beratungstermine wurden wahrgenommen:

- 11.01.2024

Folgende wesentliche Ratschläge hinsichtlich einer sinnvollen Auswertung und Interpretation der Daten wurden während der Beratung erteilt:

- T-Test- und ANOVA-Annahmen
- ANOVA mit wiederholten Messungen

Diese Bescheinigung garantiert nicht die richtige Umsetzung der in der Beratung gemachten Vorschläge, die korrekte Durchführung der empfohlenen statistischen Verfahren und die richtige Darstellung und Interpretation der Ergebnisse. Die Verantwortung hierfür obliegt allein dem Promovierenden. Das Institut für Biometrie und klinische Epidemiologie übernimmt hierfür keine Haftung.

Datum:	Name des Beraters\ der Beraterin:
11.01.2024	Camilo J. Hernandez-Toro

Camilo Jose Hernandez Toro
Digital unterschrieben von Camilo Jose Hernandez Toro
Datum: 2024.01.11 12:54:57 +01'00'

Unterschrift BeraterIn, Institutsstempel

CHARITÉ
UNIVERSITÄTSMEDIZIN BERLIN
Institut für Biometrie und Klinische Epidemiologie
Campus Charité Mitte
Charitéplatz 1 | D-10117 Berlin
Sitz: Reinhardtstr. 58